CORA Cork Open Research Archive
Cartlann Taighde Oscailte Chorcaí

Title	Rate-induced tipping in a moving habitat
Authors	MacCárthaigh, Ruaidhrí
Publication date	2021-03
Original Citation	MacCárthaigh, R. 2021. Rate-induced tipping in a moving habitat. MRes Thesis, University College Cork.
Type of publication	Masters thesis (Research)
Rights	© 2021, Ruaidhrí Mac Cárthaigh. - https://creativecommons.org/licenses/by-nc-nd/4.0/
Download date	2026-11-01 08:19:47
Item downloaded from	https://hdl.handle.net/10468/11869



UCC
University College Cork, Ireland
Coláiste na hOllscoile Corcaigh

Rate-induced Tipping in a Moving Habitat

Ruaidhrí Mac Cárthaigh



Thesis submitted for the degree of
Master of Science

UNIVERSITY COLLEGE CORK

Department of Applied Mathematics

Head of Department: Prof. Sebastian Wieczorek

Supervisors: Prof. Sebastian Wieczorek
Dr. Cris Hasan

March 2021

This is to certify that the work I am submitting is my own and has not been submitted for another degree, either at University College Cork or elsewhere. All external references and sources are clearly acknowledged and identified within the contents. I have read and understood the regulations of University College Cork concerning plagiarism.

Ruaidhrí Mac Cárthaigh

March 2021

Acknowledgements

Firstly I'd like to thank Sebastian, Cris, and Emma for the considerable amount of time they devoted to correcting and recorrecting my work, and for the guidance and patience they provided me in both physical and digital meetings throughout the abnormal and difficult past year and a half. My thesis would be a shell of what it became without their help.

Secondly I'd like to thank my family, in particular my mother and sister who delivered dinners and other food supplies to me throughout the last few weeks (including during my run in with the coronavirus in January, at their own peril), and my father who helped me with his favourite Mathematica (which in fairness led me to cut one simulation runtime down from ten days to ten seconds).

Lastly I'd like to thank my labmates, who after suffering through a few years of PhD work still held shreds of optimism as I quizzed them about research in our lunchtime conversations before the lockdown, and my housemates past and present, who may be partly responsible for slowing my progress with fun parties last year and not-so-fun coronavirus infections this year but who consistently kept me entertained, happy, and sane throughout the last eighteen months.

Abstract

As our planet's surface warms, its ecosystems are shifting to cooler and more suitable climates to survive [1]. This issue raises some important research questions. How successfully can life on earth adapt to these changes? How fast can populations be pushed to migrate before they fail to adapt and collapse to extinction? This thesis addresses the problem of species adapting to shifting habitats, using the framework of "critical transitions" or "tipping points". Specifically, it explores the persistence of a single species in a fast-moving habitat, and how the nature of its population growth affects its adaptability. The spatiotemporal evolution of the species concerned is described by partial differential equations (PDEs) in the form of nonlinear one-dimensional reaction-diffusion equations and reaction-convection-diffusion equations. Two distinct growth models are constructed and the moving habitat is incorporated into each model with the addition of a continuous non-autonomous term. The first model is a quadratic monostable model of logistic growth limited by the carrying capacity of the habitat, similar to models used in previously published work on the topic of species in a moving habitat [2, 3, 4]. The second model is made cubic and bistable by incorporating an additional limitation to population growth at low population densities, known as the Allee effect.

The spatial distribution of the populations are computed as standing wave solutions in the static habitat and travelling pulse solutions in the moving habitat, drifting at a constant habitat speed. A critical habitat speed is found for both the monostable and bistable models, above which no physical travelling pulse solution exists, meaning that the population within the habitat dies out. In the monostable Logistic Model, a transcritical bifurcation occurs between its travelling pulse solution and its zero (extinction) solution, which gives rate-induced tipping that can be reversed with a clear indication of an eventual local extinction as this critical speed is approached. In contrast, in the bistable Allee Model a saddle-node bifurcation of travelling pulses occurs, which produces an rate-induced tipping point, which typically cannot be reversed in nature, at which the population in the habitat abruptly collapses to extirpation, without any clear indication of the imminent collapse. This provides a stark ecological insight into how the increasing rate of climate change may give little to no advanced warning of extinction for some species that are observed to have an Allee effect and other complex features influencing their population dynamics.

Contents

1 Introduction **1**

1.1 Biodiversity and Shifting Habitats 3

1.2 Tipping Points 4

1.3 Population Growth Models 5

1.3.1 Linear Model 5

1.3.2 Logistic Model 7

1.3.3 Allee Model 9

2 Good and Bad Habitats **15**

2.1 Previous Work on Species Dynamics in a Habitat 16

2.2 Our Approach 18

2.2.1 Habitat Function 18

2.2.2 Habitat with Logistic Growth 20

2.2.3 Habitat with Allee Effect 23

3 The Habitat Models **27**

3.1 The Logistic Model 28

3.1.1 Nondimensionalisation 28

3.1.2 The Dimensionless Logistic Model 29

3.2 The Allee Model 30

3.2.1 Nondimensionalisation 30

3.2.2 The Dimensionless Allee Model 31

4 Static Habitat **33**

4.1 Solutions of Static Logistic Model 34

4.1.1 Time Evolution of Solutions 34

4.1.2 Existence of Stationary Solutions 35

4.1.3 Stability Analysis of Stationary Solutions 35

4.2 Solutions of Static Allee Model 36

4.2.1 Time Evolution of Solutions 36
4.2.2 Existence of Stationary Solutions 37
4.2.3 Stability Analysis of Stationary Solutions 38

5 Travelling Waves **40**
5.1 Standard Approach for Travelling Wave Solution Analysis . . . 42
5.2 Our Approach for Travelling Wave Solution Analysis 44

6 Moving Habitat **47**
6.1 The Logistic Model 48
6.1.1 Comoving Frame 48
6.1.2 Computing Travelling Pulse Solutions 50
6.1.3 Stability Analysis of Travelling Pulse Solutions 51
6.1.4 Transcritical Bifurcation of Travelling Pulses 52
6.2 The Allee Model 55
6.2.1 Comoving Frame 55
6.2.2 Computing Travelling Pulse Solutions 56
6.2.3 Stability Analysis of Travelling Pulse Solutions 57
6.2.4 Saddle-Node Bifurcation of Travelling Pulses 59

7 Solving Differential Equations **63**
7.1 Numerical Methods 63
7.1.1 IBVPs for PDEs 63
7.1.2 BVPs for ODEs 64
7.2 Existence of Solutions 65
7.2.1 Computing Stationary Solutions 65
7.2.1.1 The Logistic Model 65
7.2.1.2 The Allee Model 69
7.2.2 Computing Travelling Pulse Solutions 71
7.2.2.1 The Logistic Model 72
7.2.2.2 The Allee Model 74
7.3 Stability Analysis of Solutions 75
7.3.1 Time Evolution and Stability Analysis of Stationary Solutions 75
7.3.1.1 The Logistic Model 75
7.3.1.2 The Allee Model 75
7.3.2 Stability Analysis of Travelling Pulses 75

8 Conclusion **78**

9 Appendix **81**
9.1 Code 81
9.1.1 Python Code 81
9.1.1.1 Collocation Code for the Allee Model in the Static Habitat 82
9.1.1.2 MOL Code for the Allee Model in the Static Habitat 83
9.1.2 Mathematica Code 85
9.1.2.1 MOL Code for the Allee Model in the Moving Habitat 85

Chapter 1

Introduction

Anthropogenic climate change is an exigent threat to almost all life on earth. The frequency and intensity of some extreme weather and climate events have increased as a consequence of global warming and will continue to increase under medium and high emission scenarios [1]. Climate warming and intensifying human activities are sending many ecosystems and species scrambling to adjust their range and location, and eradicating those ecosystems which cannot adapt as quickly [5]. Those systems that can adapt may be forced to migrate polewards to colder climates, forcing the species within to attempt to keep pace with these shifts in latitude. As the rate of climate change increases year on year we will see the extirpation and even full extinction of many species that fail to keep this pace [6].

In this research project we use partial differential equation models of shifting habitats to study the spatio-temporal dynamics of species subject to slow habitat drift. Within the moving habitat, we consider two distinct population growth models to analyse effects of population growth limitations at large and small population densities. A core objective of this project is to investigate whether a species can adapt and persist as its habitat follows the shifting isotherms of climate change, and whether there exists a critical habitat speed above which its population collapses. Alternative and improved methods to those employed in previous work on this topic are used to examine various phenomena that may arise as the species approach and exceed their critical extirpation speeds. These phenomena may be studied and implemented in future ecological models such that more accurate predictions can be made of the impact climate change will have on ecosystems and biodiversity. Herein lies the

motivation for the project.

The foundation upon which our study is built is the spatially and temporally varying smooth habitat function. The habitat function defines the boundaries of the area where there are optimal conditions for population growth in the ecosystem, describes the drift of this suitable habitat in space, and is designed using bifurcation theory.

Our approach is different from the approach taken in prior research (see [2, 3, 4]), where the moving habitat is modelled with a discontinuous piecewise constant habitat function. More specifically, the population growth of the species has predominantly been characterised by a standard logistic growth model for individuals within the optimal habitat and a linear death model for those who stray outside of it, which are combined with discontinuities between the models at the boundaries of the optimal habitat. In this project, for both population systems, we consider a continuous non-autonomous partial differential equation with a continuous habitat function. One of the models we derive, which is based only on logistic growth, returns similar results to the literature. The second model, however, delivers somewhat novel results due to the inclusion of an Allee effect. The results of both models are studied in the context of tipping points, a concept which will be introduced later in this chapter.

The thesis is structured as follows: the remainder of this chapter introduces the underlying concepts of the project and its population growth models. Chapter 2 considers previous work on species dynamics, introduces our habitat model, and explains the main differences from the work in the literature. The two population models are introduced in full in Chapter 3 and their equations expressed in dimensionless form for clarity, before the evolution of the species population in a static habitat and its stationary solutions are explored in Chapter 4. In Chapter 5, travelling wave theory is studied and general equations for the moving habitat are derived which are then solved for both models in Chapter 6, leading to an analysis of travelling pulse bifurcations and tipping points. Finally Chapter 7 delves into the numerical methods utilised for solving the differential equations throughout the project before the conclusions of the study are discussed in Chapter 8.

1.1 Biodiversity and Shifting Habitats

The impact climate change is having on ecological biodiversity has been researched extensively [7, 8, 9, 6, 10]. The specific niches of various species are known to be closely linked to their local biodiversity [11]. As isotherms shift poleward due to climate warming, terrestrial and marine species have no option but to migrate to either a higher latitude (in the Northern Hemisphere; lower latitude in the Southern Hemisphere), or a higher altitude (on land; lower elevation in the ocean), to survive [12, 13, 14, 15, 16, 17, 18].

While some migratory species [12, 18] and marine species [15, 16, 17] may quickly adapt to shifting isotherms, the distributions of sedentary terrestrial species are slow to shift polewards in an ever-warming climate, not least due to their limited dispersal abilities [19].

An older, frequently cited synthesis using data collected from birds, butterflies, and alpine herbs put the average terrestrial poleward range shift at 0.61 ± 0.24 km/yr [20]. An updated paper which compiled data on marine and terrestrial species in both the Northern and Southern hemispheres studied how closely each followed shifting isotherms [21]. The results show that the range shift of marine life (7.2 ± 1.35 km/yr poleward) closely follows the isotherm shifts. On the other hand the results make it clear that the range shift of terrestrial life (1.1 ± 0.94 km/yr poleward) lags starkly behind isotherm shifts.

In a paper by Lenoir and Svenning [18], the more vagile, long-lived, and larger organisms such as birds are observed to be more likely to expand their range and shift poleward at their leading edge while also persisting locally at their trailing edge. These species would have a high critical extirpation speed and are less prone to extinction. Similarly vagile organisms that are more short-lived and smaller such as butterflies in the Northern Hemisphere studied in Parmesan et al. [12] are observed as shifting both their leading edge and trailing edge northwards to keep pace with varying isotherms, as do their corresponding marine ectotherms: expanding poleward and contracting equatorward. The models in this project will therefore be most relevant for marine species and vagile terrestrial species such as these.

The persistence of populations travelling in a moving habitat has been modelled using differential equations for a single species [3, 4], and two species [2] in a predator-prey system. In these papers, a critical speed is found at which the populations fail to keep pace with a moving habitat and succumb to extinction.

There is advanced warning of this extinction in that the populations begin to noticeably diminish at speeds approaching this critical speed. Despite variations in diffusion and death rates, the populations that are studied in these papers are generally restricted to species that follow a logistic growth model inside their "patch" or "good habitat". In Section 1.3, a more complex growth model will be introduced with the addition of the so-called Allee effect, which demonstrates some interesting and unique behaviour not found in the logistic growth models. The differences between the models will be examined later in this thesis in the context of nonlinear phenomena known as tipping points.

1.2 Tipping Points

In the fifth assessment report by the United Nations Intergovernmental Panel on Climate Change [1], a tipping point is described as:

"A level of change in system properties beyond which a system reorganizes, often abruptly, and does not return to the initial state even if the drivers of the change are abated. For the climate system, it refers to a critical threshold when global or regional climate changes from one stable state to another stable state."

Tipping points can be understood mathematically as a nonlinear phenomenon in dynamical systems at which the system may abruptly 'tip' from one state to another in a relatively short time compared to the lifetime of the system [22]. To begin exploring the concept of tipping points, the following autonomous ordinary differential equation (ODE) is introduced

$$\frac{dU}{dt} = f(U; p), \tag{1.1}$$

where $U(t)$ is an unknown function of time t, p is a parameter, and the system has at least one stable equilibrium $U^*(p)$ such that

$$f(U^*(p)) = 0, \quad \left.\frac{df}{dU}\right|_{U=U^*(p)} < 0. \tag{1.2}$$

If p becomes a time dependent input $p(t)$, (1.1) then becomes non-autonomous

$$\frac{dU}{dt} = f(U; p(t)), \tag{1.3}$$

which has a stable state $U^*(p(t))$ corresponding to the stable equilibrium of the autonomous or frozen system. Ashwin et al. [22] used the framework of one

such non-autonomous system to identify different categories of tipping points including bifurcation-induced tipping (B-tipping) and rate-induced tipping (R-tipping).

B-tipping is caused by a classical dangerous bifurcation (see [23] for the classification of bifurcations) in the non-autonomous system's corresponding frozen system, occurring at critical levels of the parameter p [24, 25], where there is a discontinuity in the branch of attractors $U^*(p)$. In contrast to the critical level that is passed through in B-tipping, R-tipping occurs when the time derivative of the input $\dot{p}(t) = \frac{dp(t)}{dt}$ exceeds a certain critical *rate* and the non-autonomous system fails to keep track of its stable state $U^*(p(t))$. In fact, the existence of a bifurcation of $U^*(p)$ in the frozen system at any value of p is not required for R-tipping to occur. We say that R-tipping can be reversed if a decrease in $\dot{p}(t)$ below this critical rate makes the non-autonomous system return to its original stable state.

B-tipping [26, 27] and R-tipping [28, 29] have been frequently observed in real world ecosystems. In the context of one such ecosystem that reaches a tipping point, it is indicative of B-tipping if the *magnitude* of environmental change is the primary factor in tipping, and of R-tipping if the *speed* at which the change in the system occurs begets tipping [24]. Regardless of characterisation, catastrophe ensues if the tipping in an ecosystem proves irreversible and thus, to mitigate damage caused to our global biodiversity, tipping must be predicted and prevented [30] wherever and whenever possible. This project aims to aid the understanding of tipping phenomena by searching for any extirpation tipping points that could appear for species following nonlinear population growth models.

1.3 Population Growth Models

1.3.1 Linear Model

The population growth model is a useful mathematical method to describe the time evolution of a species's population using differential and difference equations [31]. A simple and often relatively accurate example for certain species is what will be referred to as the Linear Model in this report - defined such that the net growth rate in the model is linearly dependent on the size of

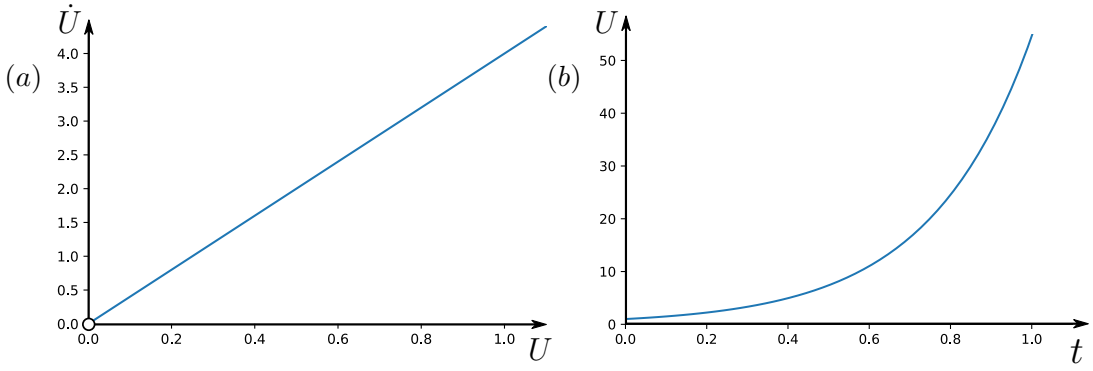


Figure 1.1: (a) Net growth rate versus population density for the Linear Model (1.5). (b) Solution to (1.5) for $U_0 = 1$, with a single unstable equilibrium (open circle in (a)) at $U^* = 0$. The parameter is set to $r = 4$.

the population. Using the intrinsic growth rate $r > 0$,

$$r = \alpha - \beta, \tag{1.4}$$

where α is the birth rate and β is the death rate of a single species population, this model can be defined using the following first order linear ODE

$$\frac{dU}{dt} = \alpha U - \beta U = rU, \tag{1.5}$$

where $U(t)$ is the population density at time t. This equation has one equilibrium

$$U^* = 0, \tag{1.6}$$

which when linearised gives a single-element Jacobian matrix with eigenvalue r, meaning this equilibrium is unstable for $r > 0\,; \alpha > \beta$ and stable for $r < 0\,; \alpha < \beta$. Equation (1.5) can be reformulated and solved for $U(t)$ through integrating by separation of variables,

$$U(t) = U_0 e^{rt}, \tag{1.7}$$

where $U_0 = U(0)$ is the initial given population density. This result reveals a perpetual exponential growth of the population density for $r > 0$, which is not possible for real populations confined within finite ecosystems in nature. Any ecosystem will have a limit of space and/or resources for its constituent species which infers that there must be a limit where the population can no longer grow and must level out at a maximum population, or "carrying capacity".

1.3.2 Logistic Model

The logistic equation and logistic growth were first formulated by Pierre-François Verhulst in a series of papers in the 19th century and used to model human populations in different nations and areas with relative degrees of success. It expanded upon the linear model with the inclusion of a carrying capacity, to curb the exponential growth of (1.7).

To impose a physical capacity on the population of an ecosystem a nonlinear density term $-\mu U^2$ is introduced to equation (1.5)

$$\begin{aligned}\frac{dU}{dt} &= \alpha U - \beta U - \mu U^2 \\ &= rU - \mu U^2,\end{aligned} \tag{1.8}$$

that can be rearranged to give

$$\frac{dU}{dt} = rU\left(1 - \frac{\mu U}{r}\right), \tag{1.9}$$

which has the same form as Verhulst's logistic equation:

$$\frac{dU}{dt} = rU\left(1 - \frac{U}{K}\right). \tag{1.10}$$

Therefore, this model is named the Logistic Model, with K being the carrying capacity. Its equilibria can be defined as

$$\begin{aligned}U_a^* &= 0, \\ U_b^* &= \frac{r}{\mu} = \frac{\alpha - \beta}{\mu} = K.\end{aligned} \tag{1.11}$$

To confirm the stabilities of these equilibria, the equation

$$\frac{dU}{dt} = f(U) = rU - \mu U^2, \tag{1.12}$$

must be linearised

$$\frac{df}{dU} = r - 2\mu U, \tag{1.13}$$

and the equilibria inserted. For U_a^*,

$$\left.\frac{df}{dU}\right|_{U=U_a^*} = r, \tag{1.14}$$

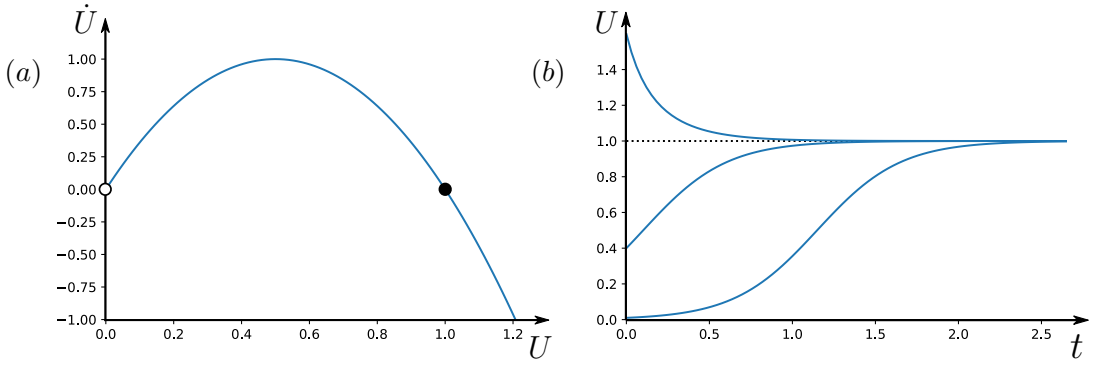


Figure 1.2: (a) Net growth rate versus population density for the Logistic Model (1.10). (b) Solutions to (1.10) for $U_0 = 0.01$, $U_0 = 0.4$, $U_0 = 1.6$, with an unstable equilibrium (open circle in (a)) at $U^* = 0$ and stable equilibrium (filled circle in (a), dotted line in (b)) at $U^* = 1$. Parameters are set to $r = 4$ and $K = 1$.

and thus U_a^* is unstable for $r > 0$; $\alpha > \beta$. For U_b^*,

$$\left.\frac{df}{dU}\right|_{U=U_b^*} = r - 2r = -r, \tag{1.15}$$

which is stable for $r > 0$; $\alpha > \beta$.

By reformulating the logistic equation into two integrals the ODE can be solved for $U(t)$ through integrating by separation of variables,

$$\int_{U(0)}^{U(t)} \frac{dU'}{U' - U'^2/K} = \int_0^t r dt', \tag{1.16}$$

$$rt = \int_{U(0)}^{U(t)} \frac{K}{KU' - U'^2} dU' = \int_{U(0)}^{U(t)} \left(\frac{1}{U'} + \frac{1}{K - U'}\right) dU', \tag{1.17}$$

$$rt = ln\left(\frac{U}{U_0}\right) - ln\left(\frac{K - U}{K - U_0}\right), \tag{1.18}$$

where $U_0 \equiv U(0)$, rearranging to give

$$U(t) = \frac{K}{1 + e^{-rt}\frac{K - U_0}{U_0}}, \tag{1.19}$$

which can be rewritten as

$$U(t) = \frac{r}{\mu + Ce^{-rt}}, \tag{1.20}$$

with constant $C = \frac{r - \mu U_0}{U_0}$.

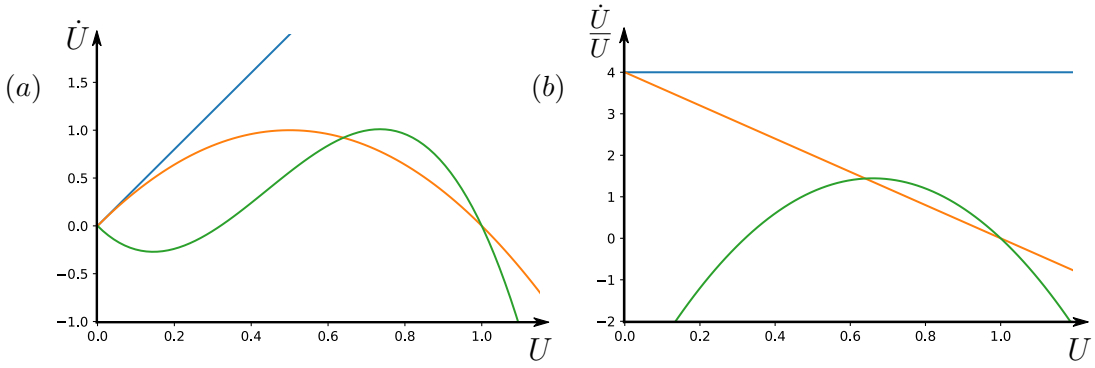


Figure 1.3: (a) Net growth rate versus population density and (b) per capita growth rate versus population density for the Linear Model (1.5) (blue), Logistic model (1.10) (orange), and Allee model (1.21) (green). Parameters are set to $r = 4$, $K = 1$, and $A = 0.32$.

This result clearly shows that for any positive initial value of the population $U_0 > 0$ and positive $r > 0$, the population grows or declines towards the stable equilibrium at $U_b^* = r/\mu = K$ as $t \to \infty$, which agrees with observations of certain species such as colonies of bacteria and yeast and other simple organisms in ideal conditions [32].

In many cases for species with more complex mating and cooperation needs, this model begins to break down, particularly in populations of some species at low densities where a reduced or even negative growth rate is observed, such as with anthropods like gypsy moths [33] and larger creatures. It follows that a more complex model is necessary to accommodate these species, along with an understanding of the so-called Allee effect.

1.3.3 Allee Model

The Allee effect describes a phenomenon where at low population densities the per capita growth rate of a species in a habitat decreases and may even become negative, heightening the likelihood that it goes extinct [34]. In his experiments in animal aggregation, W. C. Allee found that "There is danger also in overcrowding, but it is the ill effects from undercrowding that give the most generalized evidence for natural cooperation or at least for proto-cooperation among living organisms" [35]. This theory of undercrowding in addition to overcrowding being a limiting factor became Allee's principle (coined by his collaborator E.P Odum), and later became known as the Allee effect.

The effect is also described as inverse density dependence [36] and factors involved in generating this dependence generally fall into three categories:

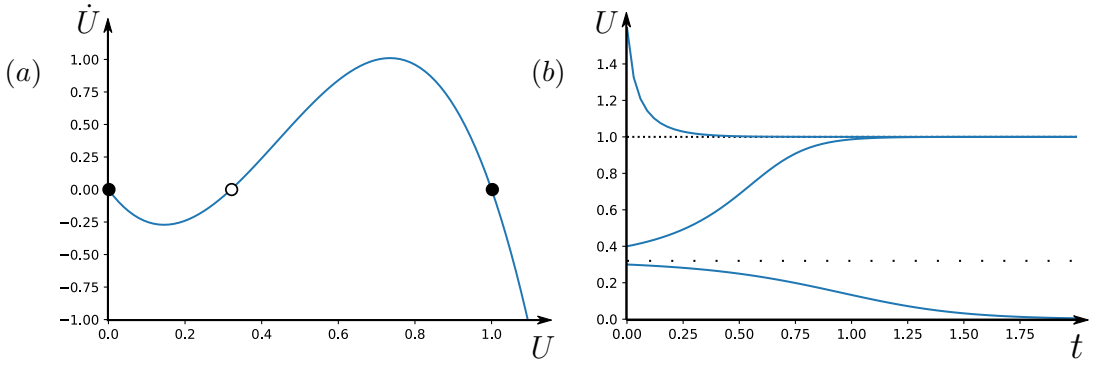


Figure 1.4: (a) Net growth rate versus population density for the Allee Model (1.21). (b) Numerically computed solutions to (1.21) for $U_0 = 0.3$, $U_0 = 0.4$, $U_0 = 1.6$, with stable equilibria (filled circles in (a), densely dotted line in (b)) at $U^* = 0$ and $U^* = 1$, and an unstable equilibrium (open circle in (a), loosely dotted line in (b)) at $U^* = 0.32$. Parameters are set to $r = 4$, $K = 1$, and $A = 0.32$.

genetic inbreeding, demographic stochasticity, and reduction in cooperative interactions at low population densities [34]. Many biological features of species can produce an Allee effect. For example, plants may have difficulty getting pollinated at low densities, or animals that rely on social defences against enemies may find these breaking down at low densities, such as small colonies of sea birds that suffer higher predation.

The existence of inverse density dependence at low densities contradicts the logic of logistic growth which holds that the sole limiting factor of a species's growth is the finite selection of resources at high population densities (see Figure 1.3). A major consequence of this phenomenon, in cases where a strong Allee effect is present (see [37] for classification of Allee effects), is the existence of a critical density below which the aggregation unit considered (e.g. population, colony, or social group) is likely to go extinct due to a negative growth rate [34].

This implies the existence of an unstable equilibrium near $U \gtrsim 0$ and a stable equilibrium at $U = 0$, necessitating the introduction of an extra term to the Logistic Model to construct an Allee effect model.

The logistic growth equation (1.10) is altered to include a critical density A, $0 < A \ll K$ [38],

$$\frac{dU}{dt} = r_A U\left(1 - \frac{U}{K}\right)\left(\frac{U}{A} - 1\right), \tag{1.21}$$

where $r_A > 0$ is the Allee intrinsic growth rate, differing from the earlier r as it denotes the rate of exponential decay at low densities, as shown in Figure 1.4,

whereas r denotes the rate of exponential growth for both the Linear Model and the Logistic Model at low densities. The equilibria of (1.21) are simply $U^* = 0$, $U^* = A$, and $U^* = K$.

Dennis [39] gives an overview of a Volterra paper [40] in which Volterra's argument gives a qualitatively similar result to (1.21) by introducing the crucial second non-zero equilibrium. At first, before including the nonlinear density term $-\mu U^2$ introduced in equation (1.8), Volterra examines the birth rate and argues that it should not be a linear function of the population density as individuals cannot procreate alone. Due to the number of encounters between males and females necessary for mating to occur (assuming a constant sex ratio), the birth rate must be proportional to U^2. The logic behind this reasoning is somewhat analogous to that of bimolecular collisions. He therefore alters equation (1.5) by setting $\alpha = 0$; $r = -\beta$, ensuring a stable equilibrium at $U^* = 0$, and by adding in the quadratic birth term λU^2,

$$\frac{dU}{dt} = -\beta U + \lambda U^2, \tag{1.22}$$

where λ is a positive parameter. This gives the desired stable equilibrium at $U^* = 0$ and unstable equilibrium at $U^* = \beta/\lambda$, whereby any population density below this critical density of β/λ falls to extinction. This equation gives a simple mathematical argument for the inclusion of the Allee Effect but falls short in its accuracy without the inclusion of the logistic term, resulting in unbounded growth for any population beginning at $U(t = 0) > \beta/\lambda$.

If the quadratic logistic term $-\mu U^2$ from earlier is included, the system qualitatively remains the same for $\lambda > \mu$ and flips to the logistic equation (1.8) for $\mu > \lambda$. Therefore, Volterra argued that the ratio between births and encounters (which originally led him to include the quadratic birth term) is not constant. He believed that a term that linearly decreases this ratio with population should be included due to the fact that at higher populations an increase in encounters is inevitable and shouldn't proportionally increase births. This term is cubic in population density and negative. It produces another stable equilibrium that acts as the new carrying capacity, transforming the birth term introduced in equation (1.22) into a birth expression $(\lambda - \gamma U)U^2$, where γ is a positive parameter. It can also be argued that this cubic term accounts for the rate of death for large populations in the absence of mating encounters due

to limited resources. With its inclusion the ODE now becomes,

$$\frac{dU}{dt} = -\beta U + \lambda U^2 - \gamma U^3. \tag{1.23}$$

which will henceforth be referred to as the Allee Model. This equation differs in form from equation (1.21) but remains qualitatively equivalent.

The two non-zero equilibria in (1.23) are equivalent to the carrying capacity K and critical density A from (1.21). The three equilibrium points for $\dot{U} = \frac{dU}{dt} = 0$ are calculated to be,

$$\begin{aligned} U_1^* &= 0, \\ U_2^* &= A = \frac{\lambda - \sqrt{\lambda^2 - 4\gamma\beta}}{2\gamma}, \\ U_3^* &= K = \frac{\lambda + \sqrt{\lambda^2 - 4\gamma\beta}}{2\gamma}, \end{aligned} \tag{1.24}$$

and thus (1.23) can be expressed in a similar form to (1.21),

$$\begin{aligned} \frac{dU}{dt} &= \beta U\left(1 - \frac{U}{\frac{\lambda+\sqrt{\lambda^2-4\gamma\beta}}{2\gamma}}\right)\left(\frac{U}{\frac{\lambda-\sqrt{\lambda^2-4\gamma\beta}}{2\gamma}} - 1\right), \\ &= \beta U\left(1 - \frac{2\gamma U}{\lambda + \sqrt{\lambda^2 - 4\gamma\beta}}\right)\left(\frac{2\gamma U}{\lambda - \sqrt{\lambda^2 - 4\gamma\beta}} - 1\right), \end{aligned} \tag{1.25}$$

where β is analogous to r_A for $\alpha = 0$ as the magnitude of negative growth at low densities. β can therefore be expressed, along with λ and γ, in terms of the parameters of (1.21) as follows

$$\begin{aligned} \beta &= r_A, \\ \lambda &= \frac{r_A}{A} + \frac{r_A}{K}, \\ \gamma &= \frac{r_A}{AK}. \end{aligned} \tag{1.26}$$

These equations infer that r_A, A, and K are interdependent due to the fact the birth and death rates β, λ, and γ must be independent of each other. For this reason Volterra's formulation (1.23) will be kept for the Allee Model in this thesis.

To confirm the stability of the model's equilibria, the right hand side of equation (1.23),

$$f(U) = -\beta U + \lambda U^2 - \gamma U^3. \tag{1.27}$$

is linearised,

$$\frac{df}{dU} = -\beta + 2\lambda U - 3\gamma U^2, \tag{1.28}$$

and the equilibrium U_1^* is inserted,

$$\left.\frac{df}{dU}\right|_{U=U_1^*} = -\beta, \tag{1.29}$$

which is negative as $\beta > 0$, therefore U_1^* is stable. Similarly for U_2^*,

$$\begin{aligned}
\left.\frac{df}{dU}\right|_{U=U_2^*} &= -\beta + 2\lambda\frac{\lambda - \sqrt{\lambda^2 - 4\gamma\beta}}{2\gamma} - 3\gamma\frac{\lambda^2 - 2\lambda\sqrt{\lambda^2 - 4\gamma\beta} + (\lambda^2 - 4\gamma\beta)}{4\gamma^2}, \\
&= -\beta + \frac{2\lambda^2 - 2\lambda\sqrt{\lambda^2 - 4\gamma\beta}}{2\gamma} - \frac{3\lambda^2 - 3\lambda\sqrt{\lambda^2 - 4\gamma\beta}}{2\gamma} + 3\beta, \\
&= 2\beta + \frac{-\lambda^2 + \lambda\sqrt{\lambda^2 - 4\gamma\beta}}{2\gamma} = 2\beta - \lambda\left(\frac{\lambda - \sqrt{\lambda^2 - 4\gamma\beta}}{2\gamma}\right),
\end{aligned} \tag{1.30}$$

which must be negative to be stable,

$$\begin{aligned}
2\beta - \lambda\left(\frac{\lambda - \sqrt{\lambda^2 - 4\gamma\beta}}{2\gamma}\right) &< 0, \\
\frac{4\gamma\beta}{\lambda} - \lambda + \sqrt{\lambda^2 - 4\gamma\beta} &< 0, \\
\sqrt{1 - \frac{4\gamma\beta}{\lambda^2}} &< 1 - \frac{4\gamma\beta}{\lambda^2}.
\end{aligned} \tag{1.31}$$

Taking $x = 1 - 4\gamma\beta/\lambda^2$ this relation becomes $\sqrt{x} < x$ which is true only for $x > 1$. If the roots are assumed to be real then $4\gamma\beta/\lambda^2 < 1$ and thus $0 < 1 - 4\gamma\beta/\lambda^2 < 1$. Therefore, U_2^* can never be stable and so it must be

unstable for all real values of U_2^*. For U_3^*,

$$\begin{aligned}\left.\frac{df}{dU}\right|_{U=U_3^*} &= -\beta + 2\lambda\frac{\lambda+\sqrt{\lambda^2-4\gamma\beta}}{2\gamma} - 3\gamma\frac{\lambda^2+2\lambda\sqrt{\lambda^2-4\gamma\beta}+(\lambda^2-4\gamma\beta)}{4\gamma^2},\\ &= -\beta + \frac{2\lambda^2+2\lambda\sqrt{\lambda^2-4\gamma\beta}}{2\gamma} - \frac{3\lambda^2+3\lambda\sqrt{\lambda^2-4\gamma\beta}}{2\gamma} + 3\beta,\\ &= 2\beta + \frac{-\lambda^2-\lambda\sqrt{\lambda^2-4\gamma\beta}}{2\gamma} = 2\beta - \lambda\left(\frac{\lambda+\sqrt{\lambda^2-4\gamma\beta}}{2\gamma}\right),\end{aligned} \tag{1.32}$$

which again must be negative,

$$\begin{aligned}2\beta - \lambda\left(\frac{\lambda+\sqrt{\lambda^2-4\gamma\beta}}{2\gamma}\right) &< 0,\\ \frac{4\gamma\beta}{\lambda} &< \lambda + \sqrt{\lambda^2-4\gamma\beta},\\ \frac{4\gamma\beta}{\lambda^2} &< 1 + \sqrt{1-\frac{4\gamma\beta}{\lambda^2}}.\end{aligned} \tag{1.33}$$

Assuming the roots are real, $4\gamma\beta/\lambda^2 < 1$ for all positive values of the parameters, then (1.33) is true and therefore U_3^* is stable for all real values of U_3^*. These results confirm that the Allee Model is bistable and therefore that at least two basins of attraction exist in the Allee Model system. This bistability becomes crucial later in this thesis as the possibility of potential tipping points being reversed is studied.

Chapter 2

Good and Bad Habitats

In Berestycki et al. [3], the concepts of a "good habitat" and a "bad habitat" spanning a spatial domain within which a given species lives are introduced. A piecewise function governs the growth or decline of its population: operating as a bounded growth function within the confines of the good habitat - where food is plentiful and population growth is only limited by logistic model's carrying capacity - and as a decay function affecting individuals that stray outside into the bad habitat - where food is scarce and the population declines exponentially.

This chapter uses a form of parabolic PDE called a reaction-diffusion equation (RDE) as its foundation

$$\frac{\partial U}{\partial t} = D\frac{\partial^2 U}{\partial x^2} + f(U, x - ct), \tag{2.1}$$

where D is a diffusion coefficient, f is the reaction term that describes population growth dynamics, and ct is a function of speed c and time t that describes the constant drift of the habitat in one-dimensional space $x \in \mathbb{R}$, with the initial condition

$$U(x, 0) = U_0(x), \tag{2.2}$$

and the Dirichlet boundary conditions

$$\lim_{x \to \pm\infty} U(x, t) = 0. \tag{2.3}$$

For the models in this study, the function $f(U, x - ct)$ is made continuous across the entire spatial domain by using a spatially and temporally dependent smooth habitat function (in contrast to the equivalent piecewise function in

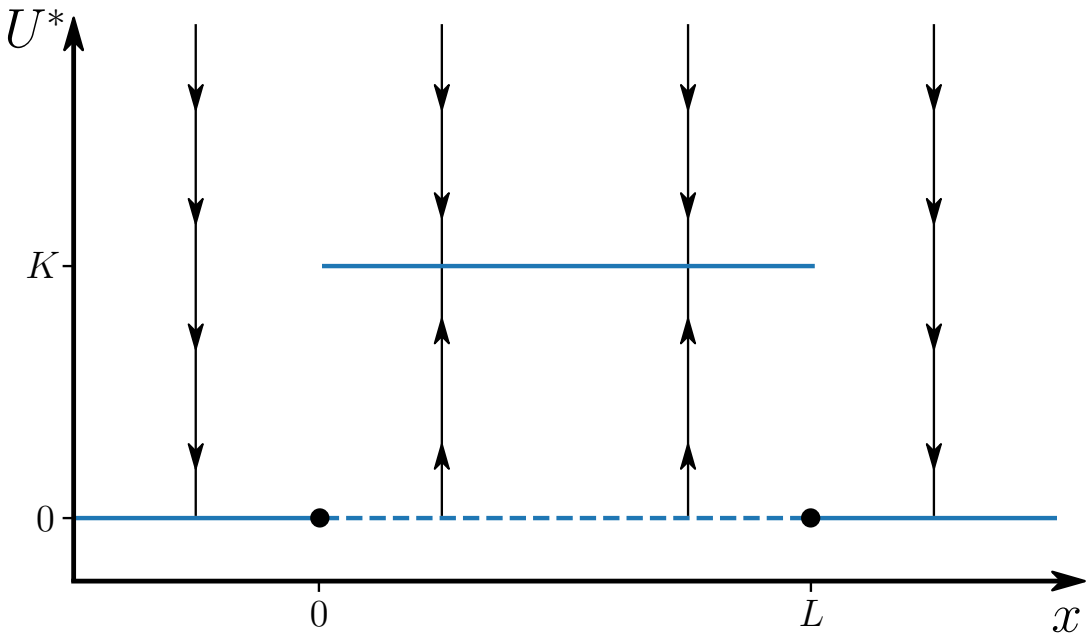


Figure 2.1: Bifurcation diagram for (2.5) with bifurcations at the filled circles, where solid lines indicate stability, dashed lines indicate instability, and arrows indicate flow.

Berestycki et al.) to help define the good and bad habitats.

2.1 Previous Work on Species Dynamics in a Habitat

Berestycki et al. [3] begin with (2.1)

$$\frac{\partial U}{\partial t} = D\frac{\partial^2 U}{\partial x^2} + f(U, x - ct), \tag{2.4}$$

where f describes the net effect of reproduction and mortality in this paper. Their growth rate at $c = 0$, for given positive parameters $\tilde{r}$, r, K, and L, is defined as

$$f(U,x) = \begin{cases} -\tilde{r}\,U & x < 0 \text{ and } x > L \\ r\,U\left(1 - \frac{U}{K}\right) & 0 \le x \le L, \end{cases} \tag{2.5}$$

making a direct distinction between the good habitat defined in $x \in [0, L]$ where the authors use the logistic growth function (1.10), and the bad habitat within which the authors impose an exponential population decline. This creates a discontinuity at the edge of the good habitat (which we would like to avoid in our study) that is evident in its bifurcation diagram in Figure 2.1 at $x = 0$ and

$x = L$.

This paper continues by normalising the variables to reduce the number of parameters in (2.4)–(2.5) and transforming it into a new comoving frame with new variables $\xi = x - ct$, $V(\xi) = U(x - ct)$, and $W(\xi) = dV/d\xi$, such that the bad habitat is described for $\xi < 0$ and $\xi > L$ by the first order system:

$$\begin{aligned} V_\xi &= W, \\ W_\xi &= V - cW, \end{aligned} \tag{2.6}$$

and the good habitat is described for $0 \leq \xi \leq L$ by the first order system:

$$\begin{aligned} V_\xi &= W, \\ W_\xi &= -rV(1 - V) - cW. \end{aligned} \tag{2.7}$$

The bad habitat has an equilibrium at $\mathbf{Y}_B^* = (V^*, W^*) = (0, 0)$ and linearisation at this point gives opposite-sign eigenvalues, meaning the equilibrium is a saddle point. In the physical $V \geq 0$ half-plane of (V, W)-space, there exists a linear spatially unstable manifold of the saddle for $-\infty < \xi < 0$ and a linear spatially stable manifold for $L < \xi < \infty$. The phase portrait of the good habitat is combined with the phase portrait of the bad habitat to find a connection between these manifolds for $0 \leq \xi \leq L$.

The good habitat has equilibria at $\mathbf{Y}_G^* = (V_1^*, W_1^*) = (0, 0)$ and $\bar{\mathbf{Y}}_G^* = (V_2^*, W_2^*) = (1, 0)$. Linearisation at $\mathbf{Y}_G^*$ gives a stable node when $r < (\frac{c}{2})^2$, and a stable spiral when $r > (c/2)^2$, while linearisation at $\bar{\mathbf{Y}}_G^*$ gives another saddle point for all r.

To avoid an obstruction forming between the stable and unstable manifolds of saddle $\mathbf{Y}_B^*$ via an orbit connecting saddle $\bar{\mathbf{Y}}_G^*$ to stable node $\mathbf{Y}_G^*$, a condition $r > (c/2)^2$ (or $0 < c < 2\sqrt{r}$ as we consider positive speed) is imposed to ensure that $\mathbf{Y}_G^*$ is a stable spiral. This allows a piece of orbit that evolves for a ξ-interval of exactly length L to be be used to connect the stable and unstable manifolds of the bad habitat's saddle $\mathbf{Y}_B^*$. These two phase portraits are stitched together to obtain solution to the full problem, including a trajectory that moves along the unstable manifold from the origin up to an orbit that it follows for length L until it meets the stable manifold of the origin and continues back to the origin.

The paper finds that the condition $0 < c < 2\sqrt{r}$ gives the invasion speed $c_{inv} = 2\sqrt{r}$ and goes on to find a formula for a critical length of the good habitat

L_{crit} in terms of r and c below which the population in its habitat collapses.

2.2 Our Approach

Our approach to the problem refines the logistic growth approach used in Berestycki et al. into the Logistic Model before expanding upon it by introducing the Allee effect and developing the Allee Model. It initially differs from the previous paper by incorporating both the good and bad habitat into a single continuous equation in each model for all space. The distinction between the habitats will thus be uniquely defined using bifurcations of the equilibria present in both the good and the bad, which will be situated at the boundaries $x = 0$ and $x = L$. These bifurcations separate the bad habitat, where a single stable equilibrium exists at $U = 0$, from the good habitat, where at least one non-zero stable equilibrium exists. Therefore, the piecewise approach to defining the reaction function f in Berestycki et al. can be avoided and a continuous transition at the boundaries of the good habitat can be established using a spatially and temporally dependent smooth habitat function.

2.2.1 Habitat Function

The reaction term $f(U, x - ct)$ from equation (2.1) can be defined using the terms from each of our models combined with the spatially and temporally dependent habitat function $H(\xi; a, L)$, where $\xi = x - ct$. This function can be conveniently defined as,

$$\begin{aligned} H(\xi; a, L) &= \frac{\tanh(a\xi) - \tanh(a(\xi - L))}{2\tanh(aL)} \\ &= \frac{1 + e^{-2aL}}{1 - e^{-2aL}} \left(\frac{1}{1 + e^{-2a\xi}} - \frac{1}{1 + e^{-2a(\xi - L)}} \right), \end{aligned} \tag{2.8}$$

where a is a positive parameter that gives the slope of the habitat boundary at the edge of the good habitat and L is the spatial extent of the good habitat.

To simplify the problem while the habitat function is incorporated into the models we set the speed to $c = 0$, and from equation (2.1) set the diffusion term $D\frac{\partial^2 U}{\partial x^2} = 0$ as the important preliminary information about the habitats in both models can be obtained using a non-diffuse static habitat. The spatial variable x can now be considered as an additional parameter while the equation contains

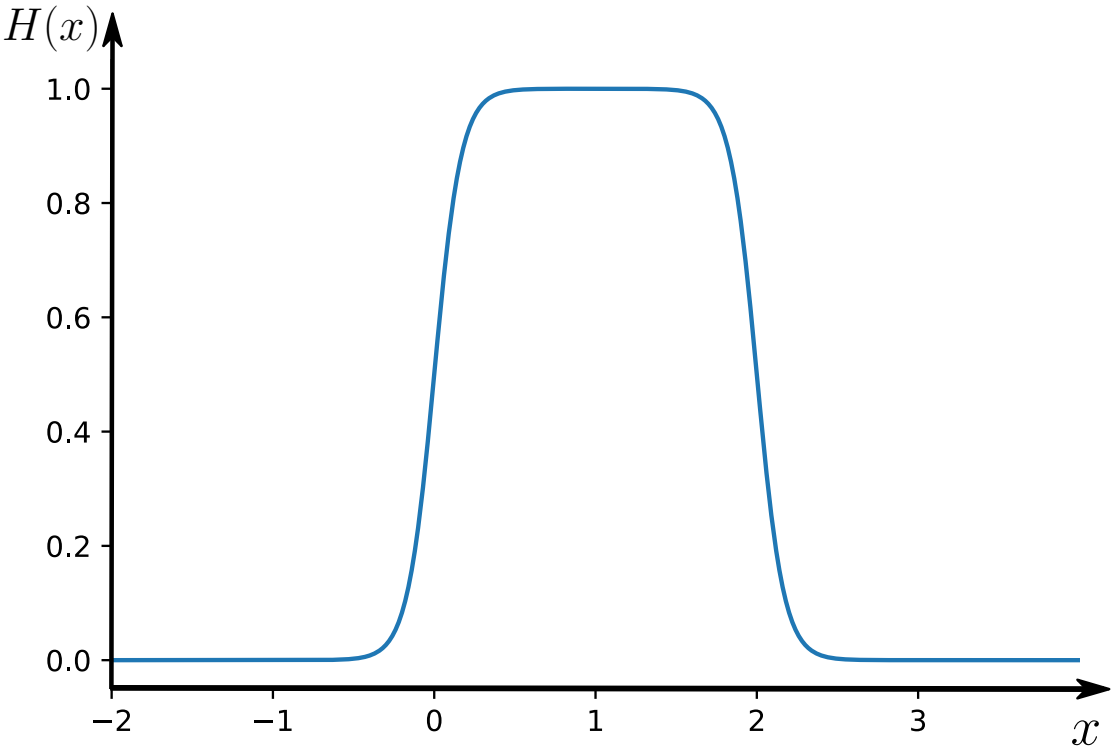


Figure 2.2: Habitat function $H(x; a, L)$ defined in (2.10) with parameters set to $a = 6$ and $L = 2$.

no spatial derivatives. This simplifies the RDE (2.1) to an ODE,

$$\frac{dU}{dt} = f(U, x). \tag{2.9}$$

and the habitat function becomes time independent,

$$H(x; a, L) = \frac{\tanh(ax) - \tanh(a(x - L))}{2\tanh(aL)}, \tag{2.10}$$

The habitat function is defined as such in order to create a good habitat with a large flat peak density and a sharp drop-off as it nears the bad habitat at its boundaries, which is clearly visible in Figure 2.2, and so that at the explicitly defined boundaries of the habitat $x = 0$ and $x = L$,

$$H(x = 0) = H(x = L) = \frac{1}{2}. \tag{2.11}$$

To maintain the flat topped peak seen in this figure we impose that $a\,L \geq 12$, which also give us a maximum value in the middle of the habitat at $x = \frac{L}{2}$ of,

$$H(L/2; a, L) = \frac{\tanh\left(\frac{a\,L}{2}\right)}{\tanh(aL)}, \tag{2.12}$$

where,

$$0.9999 < \frac{\tanh\left(\frac{a\,L}{2}\right)}{\tanh\left(aL\right)} < 1 \quad \text{if} \quad a\,L \geq 12. \tag{2.13}$$

2.2.2 Habitat with Logistic Growth

To introduce the habitat function into the Logistic Model, such that a stable equilibrium remains for a positive physical population, it must be incorporated into the growth rate r from equation (1.8). This alters equation (1.4)

$$r(x;\alpha,\beta,a,L) = \alpha\,H(x;a,L) - \beta, \tag{2.14}$$

which allows the reaction term $f(U,x)$ from equation (2.9) for the Logistic model to become

$$\begin{aligned} f(U,x) &= r(x;\alpha,\beta,a,L)\,U - \mu U^2 \\ &= \alpha\,H(x;a,L)\,U - \beta U - \mu U^2 \\ &= \alpha\,\frac{\tanh\left(ax\right) - \tanh\left(a(x-L)\right)}{2\tanh\left(aL\right)}\,U - \beta U - \mu U^2 \\ f(U,x=\frac{L}{2}) &\approx (\alpha-\beta)U - \mu U^2. \end{aligned} \tag{2.15}$$

Filling this in to equation (2.9) gives a differential equation

$$\frac{dU}{dt} = \alpha\,\frac{\tanh\left(ax\right) - \tanh\left(a(x-L)\right)}{2\tanh\left(aL\right)}\,U - \beta U - \mu U^2, \tag{2.16}$$

which has the following two equilibria:

$$\begin{aligned} U_a^* &= 0, \\ U_b^* &= \alpha\,\frac{\tanh\left(ax\right) - \tanh\left(a(x-L)\right)}{2\mu\tanh\left(aL\right)} - \frac{\beta}{\mu}. \end{aligned} \tag{2.17}$$

The next objective is to define the boundaries of the good habitat using transcritical bifurcations imposed at $x = 0$ and $x = L$. This is achieved by choosing parameter β such that the equilibria become degenerate via transverse crossing and a single physical stable equilibrium at $U_a^* = 0$ emerges in the bad habitat, where U_b^* becomes negative and thus unphysical. If we fix β as follows, using (2.11), two transcritical bifurcations occur at $x = 0$ and $x = L$,

$$\beta = \alpha\,H(x=0) = \alpha\,H(x=L) = \frac{\alpha}{2}, \tag{2.18}$$

which when filled in to (2.16) gives the non-autonomous Logistic Model

$$\begin{aligned}\frac{dU}{dt} &= \alpha \frac{\tanh(ax) - \tanh(a(x-L))}{2\tanh(aL)} U - \frac{\alpha}{2}U - \mu U^2, \\ &= \alpha \left(H(x;a,L) - \frac{1}{2} \right) U - \mu U^2, \end{aligned} \tag{2.19}$$

with equilibria

$$\begin{aligned} U_a^* &= 0, \\ U_b^* &= \alpha \frac{\tanh(ax) - \tanh(a(x-L))}{2\mu\tanh(aL)} - \frac{\alpha}{2\mu}, \\ &= \frac{\alpha}{\mu}\left(H(x;a,L) - \frac{1}{2} \right) \end{aligned} \tag{2.20}$$

which results in an equilibrium U_b^* shaped like a scaled top half of the habitat function $H(x;a,L)$ from Figure 2.2 present physically within the good habitat only.

To plot the bifurcation diagram with these equilibria and x as a parameter their stabilities must be examined. These can be calculated by linearising equation (2.19) and finding its single-element Jacobian matrix,

$$\begin{aligned} f(U,x) &= \alpha \left(H(x;a,L) - \frac{1}{2} \right) U - \mu U^2 \\ \frac{\partial f}{\partial U} &= \alpha \left(H(x;a,L) - \frac{1}{2} \right) - 2\mu U. \end{aligned} \tag{2.21}$$

Substituting in the equilibria, U_a^*

$$\left. \frac{\partial f}{\partial U} \right|_{U=U_a^*} = \alpha \left(H(x;a,L) - \frac{1}{2} \right), \tag{2.22}$$

and U_b^*

$$\begin{aligned} \left. \frac{\partial f}{\partial U} \right|_{U=U_b^*} &= \alpha \left(H(x;a,L) - \frac{1}{2} \right) - 2\mu \left(\frac{\alpha}{\mu} \left(H(x;a,L) - \frac{1}{2} \right) \right), \\ &= -\alpha \left(H(x;a,L) - \frac{1}{2} \right), \end{aligned} \tag{2.23}$$

it follows that U_a^* is stable and U_b^* is unstable while,

$$H(x;a,L) < \frac{1}{2}, \tag{2.24}$$

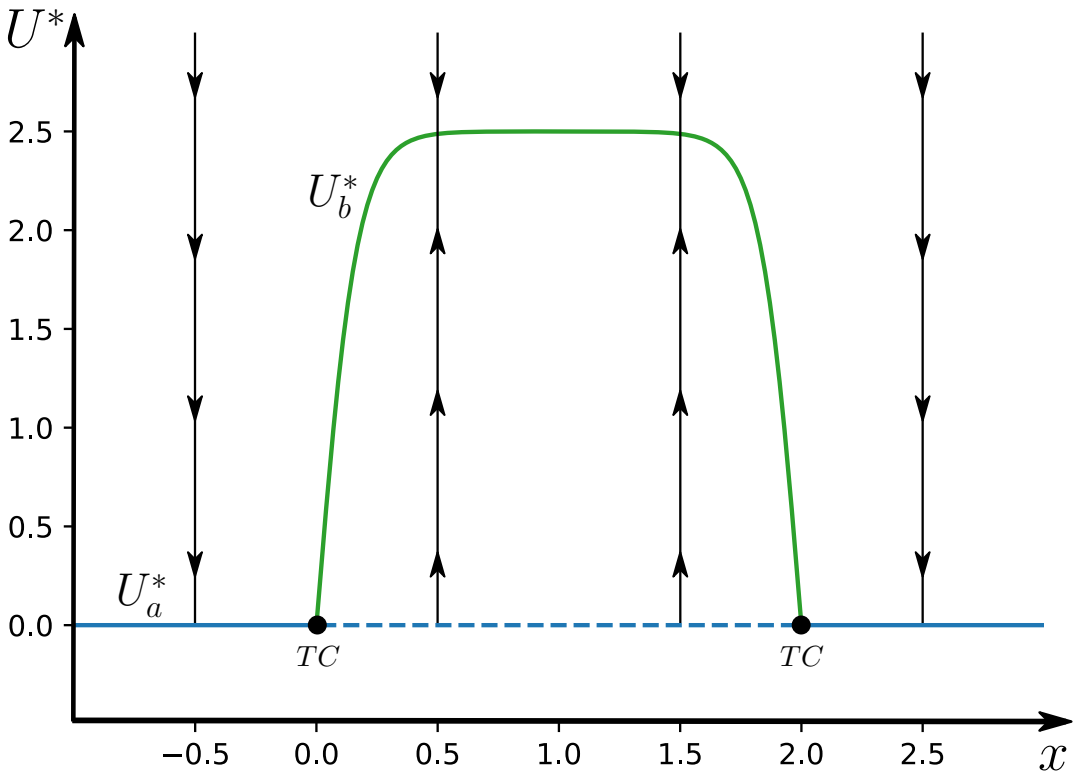


Figure 2.3: Bifurcation diagram of the stationary solutions of (2.19), given by (2.20), with two transcritical (TC) bifurcation points at (0,0) and (2,0). Model parameters are set to $\alpha = 5$, $\mu = 1$, $a = 6$, and $L = 2$. Solid lines indicate stability, dashed lines indicate instability, arrows indicate flow, and the lower branches are cut off as they are unphysical.

which is the case only in the bad habitat, and U_a^* is unstable and U_b^* is stable while,

$$H(x; a, L) > \frac{1}{2}. \tag{2.25}$$

which is true within the good habitat. This result infers that the physical portion of U_b^* within the good habitat remains stable while U_a^* switches stability at the transcritical bifurcation points on the boundaries. This is clearly evident in the bifurcation diagram in Figure 2.3 where the equilibria (2.20) are plotted against parameter x, displaying only the physical non-negative densities.

The Logistic Model results in accurate conditions for the bad habitat. The conditions within the good habitat could be made more realistic at low densities, however, as the population always rises to the stable equilibrium U_b^*, even if only a single individual remains in it. This prompts the addition of the Allee effect into the system with the Allee Model.

2.2.3 Habitat with Allee Effect

The habitat function is incorporated into the nonlinear birth term λU^2 in the Allee Model (1.23) such that the non-zero equilibria remain positive and physical within the good habitat and a continuous stable equilibrium exists at $U^* = 0$ for the entire spatial domain.

The reaction term $f(U, x)$ of equation (2.9) for the Allee model becomes

$$f(U,x) = -\beta\, U + \lambda\, \frac{\tanh(ax) - \tanh(a(x-L))}{2\tanh(aL)}\, U^2 - \gamma\, U^3, \tag{2.26}$$

which, filling in to equation (2.9), gives a differential equation

$$\begin{aligned} \frac{dU}{dt} &= -\beta\, U + \lambda \frac{\tanh(ax) - \tanh(a(x-L))}{2\tanh(aL)}\, U^2 - \gamma\, U^3, \\ &= -\beta\, U + \lambda\, H(x;a,L)\, U^2 - \gamma\, U^3, \end{aligned} \tag{2.27}$$

with the following equilibria:

$$\begin{aligned} U_1^* &= 0, \\ U_2^* &= \frac{\lambda\, H(x;a,L) - \sqrt{(\lambda\, H(x;a,L))^2 - 4\gamma\beta}}{2\gamma}, \\ U_3^* &= \frac{\lambda\, H(x;a,L) + \sqrt{(\lambda\, H(x;a,L))^2 - 4\gamma\beta}}{2\gamma}. \end{aligned} \tag{2.28}$$

It follows that the equilibria become degenerate when

$$4\gamma\beta \geq (\lambda\, H(x;a,L))^2 \quad \text{or} \quad 2\sqrt{\gamma\beta} \geq \lambda\, H(x;a,L), \tag{2.29}$$

and thus two saddle node bifurcations can be imposed at $x = 0$ and $x = L$ to define the good habitat such that only U_1^* exists in the bad habitat.

From equation (2.11), the right hand side of the inequality in (2.29) at the boundaries of the good habitat can be expressed as follows:

$$\lambda\, H(x=0;a,L) = \lambda\, H(x=L;a,L) = \frac{\lambda}{2}, \tag{2.30}$$

and can be set equal to $2\sqrt{\gamma\beta}$, thereby allowing the nonlinear birth parameter λ to be chosen as

$$\lambda = 4\sqrt{\gamma\beta}. \tag{2.31}$$

Filling this into (2.27) gives the non-autonomous Allee Model

$$\begin{aligned}\frac{dU}{dt} &= -\beta\, U + 4\sqrt{\gamma\beta}\frac{\tanh\left(ax\right) - \tanh\left(a(x-L)\right)}{2\tanh\left(aL\right)}\, U^2 - \gamma\, U^3,\\ &= -\beta\, U + 4\sqrt{\gamma\beta}\, H(x;a,L)\, U^2 - \gamma\, U^3,\end{aligned} \tag{2.32}$$

with equilibria

$$\begin{aligned}U_1^* &= 0,\\ U_2^* &= \frac{2\, H(x;a,L) - \sqrt{4\left(H(x;a,L)\right)^2 - 1}}{\sqrt{\gamma/\beta}},\\ U_3^* &= \frac{2\, H(x;a,L) + \sqrt{4\left(H(x;a,L)\right)^2 - 1}}{\sqrt{\gamma/\beta}}.\end{aligned} \tag{2.33}$$

The stability of these equilibria can now be investigated with the help of the stability analysis performed previously in Section 1.3.3. Just as with the Logistic Model, the Allee Model's finalised ODE (2.32) is linearised, giving its single-element Jacobian matrix

$$\begin{aligned}f(U,x) &= -\beta\, U + 4\sqrt{\gamma\beta}\, H(x;a,L)\, U^2 - \gamma\, U^3\\ \frac{\partial f}{\partial U} &= -\beta + 8\sqrt{\gamma\beta}\, H(x;a,L)\, U - 3\gamma\, U^2.\end{aligned} \tag{2.34}$$

and the zero equilibrium is substituted in

$$\left.\frac{\partial f}{\partial U}\right|_{U=U_1^*} = -\beta, \tag{2.35}$$

giving the same result as (1.29) in Section 1.3.3. With the substitution of U_2^*

$$\begin{aligned}\left.\frac{\partial f}{\partial U}\right|_{U=U_2^*} &= -\beta + 8\sqrt{\gamma\beta}\, H(x;a,L)\, \left(\frac{2\, H(x;a,L) - \sqrt{4\left(H(x;a,L)\right)^2 - 1}}{\sqrt{\gamma/\beta}}\right)\\ &\quad - 3\gamma\, \left(\frac{2\, H(x;a,L) - \sqrt{4\left(H(x;a,L)\right)^2 - 1}}{\sqrt{\gamma/\beta}}\right)^2,\end{aligned} \tag{2.36}$$

equations (1.30) and (1.31) are borrowed, giving a shortcut for an inequality

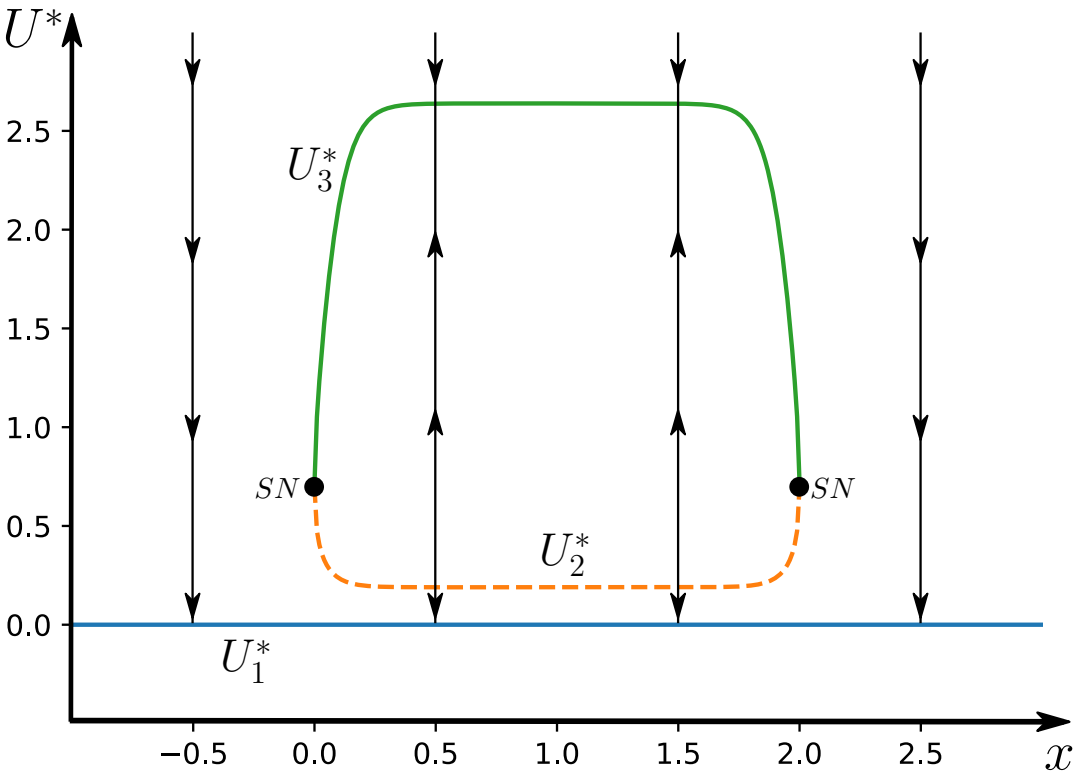


Figure 2.4: Bifurcation diagram of the stationary solutions of (2.32), given by (2.33), with the two saddle-node (SN) bifurcation points at $(0, \frac{1}{\sqrt{2}})$ and $(2, \frac{1}{\sqrt{2}})$. Model parameters are set to $\beta = 0.5$, $\gamma = 1$, $a = 8$, and $L = 2$. Solid lines indicate stability, dashed lines indicate instability, and the arrows indicate flow.

that determines stability by substituting the λ in (1.31) for $4\sqrt{\gamma\beta}H(x;a,L)$

$$\sqrt{1 - \frac{1}{4\left(H(x;a,L)\right)^2}} < 1 - \frac{1}{4\left(H(x;a,L)\right)^2}, \tag{2.37}$$

which, just as in Section 1.3.3, is false for all real values of the left hand side of the inequality (i.e. within the good habitat). Therefore, U_2^* is unstable. Similarly for U_3^*,

$$\begin{aligned}\left.\frac{\partial f}{\partial U}\right|_{U=U_3^*} &= -\beta + 8\sqrt{\gamma\beta}\, H(x;a,L)\left(\frac{2\,H(x;a,L) + \sqrt{4\left(H(x;a,L)\right)^2 - 1}}{\sqrt{\gamma/\beta}}\right) \\ &\quad - 3\gamma\left(\frac{2\,H(x;a,L) + \sqrt{4\left(H(x;a,L)\right)^2 - 1}}{\sqrt{\gamma/\beta}}\right)^2,\end{aligned} \tag{2.38}$$

equations (1.32) and (1.33) are borrowed, giving a shortcut for an inequality

using the same substitution,

$$\frac{1}{4\left(H(x;a,L)\right)^2} < 1 + \sqrt{1 - \frac{1}{4\left(H(x;a,L)\right)^2}} \tag{2.39}$$

which again is true for all real values and therefore U_3^* is stable.

These equilibria are plotted in a bifurcation diagram with parameter x in Figure 2.4, displaying the imposed saddle-node bifurcations on either boundary of the good habitat at $x = 0$ and $x = L$, and a continuous stable equilibrium at $U_1^* = 0$. This creates a more realistic situation in which the threat of extinction is possible throughout the spatial domain but the probability of survival within the confines of the good habitat for a self-sustained and fit population is also present.

The survival of the species can be studied further again in the following chapter with the reintroduction of the diffusion term $D\frac{\partial^2 U}{\partial x^2}$ into the models and an examination of the dynamics of the population in time from initial conditions within a static habitat.

Chapter 3

The Habitat Models

The diffusion term $D\frac{\partial^2 U}{\partial x^2}$ and habitat speed c are reincorporated into the differential equations of each model, turning these equations back into nonlinear non-autonomous parabolic PDEs that are non-autonomous in both independent variables x and t. Equation (2.1) is re-expressed

$$\frac{\partial U}{\partial t} = D\frac{\partial^2 U}{\partial x^2} + f(U, x - ct). \tag{3.1}$$

with the initial condition

$$U(x, 0) = U_0(x). \tag{3.2}$$

and the Dirichlet boundary conditions

$$\lim_{x \to \pm\infty} U(x, t) = 0. \tag{3.3}$$

Equation (3.1) can be written for the Logistic Model as follows

$$\frac{\partial U}{\partial t} = D\frac{\partial^2 U}{\partial x^2} + \alpha \left(H(x - ct; a, L) - \frac{1}{2} \right) U - \mu U^2, \tag{3.4}$$

and for the Allee Model as follows

$$\frac{\partial U}{\partial t} = D\frac{\partial^2 U}{\partial x^2} - \beta\, U + 4\sqrt{\gamma\beta}\, H(x - ct; a, L)\, U^2 - \gamma\, U^3, \tag{3.5}$$

with the initial condition

$$U(x, 0) = U_0(x), \tag{3.6}$$

and Dirichlet boundary conditions

$$\lim_{x\to\pm\infty} U(x,t) = 0, \tag{3.7}$$

where the habitat function again becomes

$$H(x-ct;a,L) = \frac{\tanh\left(a(x-ct)\right) - \tanh\left(a(x-ct-L)\right)}{2\tanh\left(aL\right)}. \tag{3.8}$$

In the two habitat models there are four shared model parameters D, a, L and c; two unique parameters to the Logistic Model, α and μ; and two unique parameters to the Allee Model, β and γ. By rescaling U, x, and t in each model, two shared parameters and a unique parameter from each model can be excluded, reducing the total number of parameters in each model from six to three. From there solutions may be numerically computed using these simplified nondimensionalised models.

3.1 The Logistic Model

3.1.1 Nondimensionalisation

The following rescaled dimensionless variables are introduced,

$$\tilde{U} = \frac{U}{\upsilon}, \quad \tilde{x} = \frac{x}{\chi}, \quad \tilde{t} = \frac{t}{\tau}, \tag{3.9}$$

where υ is in units of inverse length, χ is in units of length, and τ is in units of time. Equation (3.4) can now be expressed as,

$$\frac{\upsilon}{\tau}\frac{\partial\tilde{U}}{\partial\tilde{t}} = D\left(\frac{\upsilon}{\chi^2}\frac{\partial^2\tilde{U}}{\partial\tilde{x}^2}\right) + \alpha\left(H(\chi\tilde{x}-c\tau\tilde{t};a,L) - \frac{1}{2}\right)\upsilon\tilde{U} - \mu\left(\upsilon\tilde{U}\right)^2,$$

$$\frac{\partial\tilde{U}}{\partial\tilde{t}} = \frac{\tau D}{\chi^2}\frac{\partial^2\tilde{U}}{\partial\tilde{x}^2} + \tau\alpha\left(H(\chi\tilde{x}-c\tau\tilde{t};a,L) - \frac{1}{2}\right)\tilde{U} - \upsilon\tau\mu\tilde{U}^2, \tag{3.10}$$

and the habitat function becomes

$$H(\chi\tilde{x}-c\tau\tilde{t};a,L) = \frac{\tanh\left(a(\chi\tilde{x}-c\tau\tilde{t})\right) - \tanh\left(a(\chi\tilde{x}-c\tau\tilde{t}-L)\right)}{2\tanh\left(aL\right)}, \tag{3.11}$$

such that the RDE is now dimensionless. The coefficient of the spatial derivative can be normalised by choosing τ

$$\tau = \frac{L^2}{D}. \tag{3.12}$$

By choosing to define χ, and rescaling a and c

$$\chi = L, \quad \tilde{a} = aL, \quad \tilde{c} = \frac{L}{D}c, \tag{3.13}$$

and thus

$$\tanh\left(a(\chi\tilde{x} - c\tau\tilde{t})\right) = \tanh\left(\frac{\tilde{a}}{L}\left(L\tilde{x} - \frac{D}{L}\tilde{c}\frac{L^2}{D}\tilde{t}\right)\right) = \tanh\left(\tilde{a}(\tilde{x} - \tilde{c}\tilde{t})\right), \tag{3.14}$$

the habitat function can be defined as

$$H(\tilde{x} - \tilde{c}\tilde{t}; \tilde{a}) = \frac{\tanh\left(\tilde{a}(\tilde{x} - \tilde{c}\tilde{t})\right) - \tanh\left(\tilde{a}(\tilde{x} - \tilde{c}\tilde{t} - 1)\right)}{2\tanh\tilde{a}}. \tag{3.15}$$

The nonlinear term is now normalised by choosing υ, and α rescaled

$$\upsilon = \frac{D}{\mu L^2}, \quad \tilde{\alpha} = \frac{\alpha L^2}{D}, \tag{3.16}$$

such that the RDE simplifies to

$$\frac{\partial \tilde{U}}{\partial \tilde{t}} = \frac{\partial^2 \tilde{U}}{\partial \tilde{x}^2} + \tilde{\alpha}\left(H(\tilde{x} - \tilde{c}\tilde{t}; \tilde{a}) - \frac{1}{2}\right)\tilde{U} - \tilde{U}^2, \tag{3.17}$$

effectively eliminating D, L, and μ in this rescaled model.

3.1.2 The Dimensionless Logistic Model

The dimensionless model for the static case of the Logistic Model is as follows; the nonlinear non-autonomous one-dimensional RDE

$$\frac{\partial \tilde{U}}{\partial \tilde{t}} = \frac{\partial^2 \tilde{U}}{\partial \tilde{x}^2} + \tilde{\alpha}\left(H(\tilde{x} - \tilde{c}\tilde{t}; \tilde{a}) - \frac{1}{2}\right)\tilde{U} - \tilde{U}^2, \tag{3.18}$$

with the initial condition

$$\tilde{U}(\tilde{x}, 0) = \tilde{U}_0(\tilde{x}), \tag{3.19}$$

and boundary conditions

$$\lim_{\tilde{x}\to\pm\infty} \tilde{U}(\tilde{x}, \tilde{t}) = 0, \tag{3.20}$$

Table 3.1: Upper: Examples of the original parameter values.
Lower: The values of the scaled parameters defined in (3.22).

Symbol	Description	Typical value	Units
α	Approximate peak birth rate	5	s^{-1}
$\beta = \alpha/2$	Linear death rate	2.5	s^{-1}
μ	Nonlinear death rate	1	ms^{-1}
L	Spatial extent of good habitat	2	m
a	Slope of habitat boundary	6	m^{-1}
D	Diffusion constant	0.02	m^2s^{-1}
c	Habitat propagation speed	0	ms^{-1}
$\tilde{\alpha}$	Defined in (3.22)	1000	
$\tilde{a}$	Defined in (3.22)	12	
$\tilde{c}$	Defined in (3.22)	0	

where the rescaled habitat function is

$$H(\tilde{x} - \tilde{c}\tilde{t}; \tilde{a}) = \frac{\tanh\left(\tilde{a}(\tilde{x} - \tilde{c}\tilde{t})\right) - \tanh\left(\tilde{a}(\tilde{x} - \tilde{c}\tilde{t} - 1)\right)}{2\tanh\tilde{a}}, \tag{3.21}$$

and the new rescaled variables and parameters are defined as

$$\tilde{U} = \frac{\mu L^2}{D}U, \quad \tilde{t} = \frac{D}{L^2}t, \quad \tilde{x} = \frac{x}{L}, \quad \tilde{a} = aL, \quad \tilde{\alpha} = \frac{L^2}{D}\alpha, \quad \tilde{c} = \frac{L}{D}c. \tag{3.22}$$

3.2 The Allee Model

3.2.1 Nondimensionalisation

Rescaled dimensionless variables are introduced again

$$\tilde{U} = \frac{U}{\upsilon}, \quad \tilde{x} = \frac{x}{\chi}, \quad \tilde{t} = \frac{t}{\tau}, \tag{3.23}$$

and (3.5) can now be expressed as,

$$\frac{\upsilon}{\tau}\frac{\partial\tilde{U}}{\partial\tilde{t}} = D\left(\frac{\upsilon}{\chi^2}\frac{\partial^2\tilde{U}}{\partial\tilde{x}^2}\right) - \beta\left(\upsilon\tilde{U}\right) + 4\sqrt{\gamma\beta}\,H(\chi\tilde{x} - c\tau\tilde{t}; a, L)\left(\upsilon\tilde{U}\right)^2 - \gamma\left(\upsilon\tilde{U}\right)^3,$$

$$\frac{\partial\tilde{U}}{\partial\tilde{t}} = \frac{\tau D}{\chi^2}\frac{\partial^2\tilde{U}}{\partial\tilde{x}^2} - \tau\beta\tilde{U} + \upsilon\tau\,4\sqrt{\gamma\beta}\,H(\chi\tilde{x} - c\tau\tilde{t}; a, L)\,\tilde{U}^2 - \upsilon^2\tau\gamma\tilde{U}^3. \tag{3.24}$$

The habitat function becomes

$$H(\chi\tilde{x} - c\tau\tilde{t}; a, L) = \frac{\tanh\left(a(\chi\tilde{x} - c\tau\tilde{t})\right) - \tanh\left(a(\chi\tilde{x} - c\tau\tilde{t} - L)\right)}{2\tanh(aL)}, \tag{3.25}$$

such that the RDE is now dimensionless. As before, the coefficient of the spatial derivative can be normalised by choosing τ

$$\tau = \frac{L^2}{D}. \tag{3.26}$$

and by choosing to define χ, and rescaling a and c

$$\chi = L, \quad \tilde{a} = aL, \quad \tilde{c} = \frac{L}{D}c, \tag{3.27}$$

the habitat function can be defined as

$$H(\tilde{x} - \tilde{c}\tilde{t}; \tilde{a}) = \frac{\tanh(\tilde{a}(\tilde{x} - \tilde{c}\tilde{t})) - \tanh(\tilde{a}(\tilde{x} - \tilde{c}\tilde{t} - 1))}{2\tanh\tilde{a}}. \tag{3.28}$$

The nonlinear death term coefficient is normalised by choosing υ

$$\upsilon = \frac{1}{L}\sqrt{\frac{D}{\gamma}}, \tag{3.29}$$

and finally by choosing $\tilde{\beta}$ to simplify the remaining coefficients

$$\tilde{\beta} = L\sqrt{\frac{\beta}{D}}, \quad \tilde{\beta}^2 = \frac{L^2\beta}{D}, \tag{3.30}$$

the RDE for $\tilde{c} = 0$ simplifies to

$$\frac{\partial\tilde{U}}{\partial\tilde{t}} = \frac{\partial^2\tilde{U}}{\partial\tilde{x}^2} - \tilde{\beta}^2\tilde{U} + 4\tilde{\beta}\,H(\tilde{x} - \tilde{c}\tilde{t}; \tilde{a})\,\tilde{U}^2 - \tilde{U}^3, \tag{3.31}$$

effectively eliminating D, L, and γ for this rescaled model.

3.2.2 The Dimensionless Allee Model

The dimensionless model for the static case of the Allee Model is as follows; the nonlinear non-autonomous one-dimensional RDE

$$\frac{\partial\tilde{U}}{\partial\tilde{t}} = \frac{\partial^2\tilde{U}}{\partial\tilde{x}^2} - \tilde{\beta}^2\tilde{U} + 4\tilde{\beta}\,H(\tilde{x} - \tilde{c}\tilde{t}; \tilde{a})\,\tilde{U}^2 - \tilde{U}^3, \tag{3.32}$$

Table 3.2: Upper: Examples of the original parameter values.
Lower: The values of the scaled parameters defined in (3.36).

Symbol	Description	Typical value	Units
β	Linear death rate	0.5	s^{-1}
$\lambda = 4\sqrt{\gamma\beta}$	Approximate peak birth rate	2.83	ms^{-1}
γ	Nonlinear death rate	1	m^2s^{-1}
L	Spatial extent of good habitat	2	m
a	Slope of habitat boundary	6	m^{-1}
D	Diffusion constant	0.02	m^2s^{-1}
c	Habitat propagation speed	0	ms^{-1}
$\tilde{\beta}$	Defined in (3.36)	10	
$\tilde{a}$	Defined in (3.36)	12	
$\tilde{c}$	Defined in (3.36)	0	

with the initial condition

$$\tilde{U}(\tilde{x}, 0) = \tilde{U}_0(\tilde{x}), \tag{3.33}$$

and boundary conditions

$$\lim_{\tilde{x}\to\pm\infty} \tilde{U}(\tilde{x}, \tilde{t}) = 0, \tag{3.34}$$

where the rescaled habitat function is

$$H(\tilde{x} - \tilde{c}\tilde{t}; \tilde{a}) = \frac{\tanh\left(\tilde{a}(\tilde{x} - \tilde{c}\tilde{t})\right) - \tanh\left(\tilde{a}(\tilde{x} - \tilde{c}\tilde{t} - 1)\right)}{2\tanh\tilde{a}}, \tag{3.35}$$

and the new rescaled variables and parameters are defined as

$$\tilde{U} = L\sqrt{\frac{\gamma}{D}}U, \quad \tilde{t} = \frac{D}{L^2}t, \quad \tilde{x} = \frac{x}{L}, \quad \tilde{a} = aL, \quad \tilde{\beta} = L\sqrt{\frac{\beta}{D}}, \quad \tilde{c} = \frac{L}{D}c. \tag{3.36}$$

Chapter 4

Static Habitat

For the study of the static habitat the habitat speed $\tilde{c}$ is set to zero, meaning the nonlinear non-autonomous one-dimensional RDE is now non-autonomous only in the spatial independent variable $\tilde{x}$. A dimensionless form of (3.1) is expressed with habitat speed set to $\tilde{c} = 0$

$$\frac{\partial \tilde{U}}{\partial \tilde{t}} = \frac{\partial^2 \tilde{U}}{\partial \tilde{x}^2} + \tilde{f}(\tilde{U}, \tilde{x}), \tag{4.1}$$

where $\tilde{f}$ is a dimensionless form of the reaction function f. Equation (4.1) can be written for the Logistic Model as follows

$$\frac{\partial \tilde{U}}{\partial \tilde{t}} = \frac{\partial^2 \tilde{U}}{\partial \tilde{x}^2} + \tilde{\alpha}\left(H(\tilde{x};\tilde{a}) - \frac{1}{2}\right)\tilde{U} - \tilde{U}^2, \tag{4.2}$$

and for the Allee Model as follows

$$\frac{\partial \tilde{U}}{\partial \tilde{t}} = \frac{\partial^2 \tilde{U}}{\partial \tilde{x}^2} - \tilde{\beta}^2\tilde{U} + 4\tilde{\beta}\,H(\tilde{x};\tilde{a})\,\tilde{U}^2 - \tilde{U}^3, \tag{4.3}$$

with the initial condition,

$$\tilde{U}(\tilde{x}, 0) = \tilde{U}_0(\tilde{x}), \tag{4.4}$$

and Dirichlet boundary conditions,

$$\lim_{\tilde{x}\to\pm\infty} \tilde{U}(\tilde{x}, \tilde{t}) = 0, \tag{4.5}$$

where the habitat function is expressed as

$$H(\tilde{x};\tilde{a}) = \frac{\tanh(\tilde{a}\tilde{x}) - \tanh(\tilde{a}(\tilde{x}-1))}{2\tanh\tilde{a}}. \tag{4.6}$$

The equilibria for the Logistic Model from (2.20) become,

$$\tilde{U}_a^*(\tilde{x}) = 0,$$

$$\begin{aligned} \tilde{U}_b^*(\tilde{x}) &= \tilde{\alpha}\left(H(\tilde{x};\tilde{a}) - \frac{1}{2}\right), \\ \tilde{U}_b^*(\tilde{x} = \frac{1}{2}) &\approx \frac{\tilde{\alpha}}{2} \end{aligned} \tag{4.7}$$

and equilibria for the Allee Model from (2.33) now become,

$$\tilde{U}_1^*(\tilde{x}) = 0,$$

$$\begin{aligned} \tilde{U}_2^*(\tilde{x}) &= \tilde{\beta}\left(2H(\tilde{x};\tilde{a}) - \sqrt{4H(\tilde{x};\tilde{a})^2 - 1}\right) \\ \tilde{U}_2^*(\tilde{x} = \frac{1}{2}) &\approx \tilde{\beta}\,(2 - \sqrt{3}) \end{aligned}$$

$$\begin{aligned} \tilde{U}_3^*(\tilde{x}) &= \tilde{\beta}\left(2H(\tilde{x};\tilde{a}) + \sqrt{4H(\tilde{x};\tilde{a})^2 - 1}\right) \\ \tilde{U}_3^*(\tilde{x} = \frac{1}{2}) &\approx \tilde{\beta}\,(2 + \sqrt{3}). \end{aligned} \tag{4.8}$$

4.1 Solutions of Static Logistic Model

4.1.1 Time Evolution of Solutions

Numerical solutions $\tilde{U}(\tilde{x}, \tilde{t})$ to the static habitat Logistic Model initial-boundary value problem (IBVP) (4.2), (4.4)–(4.5) can be numerically integrated using the method of lines (MOL) IBVP solver (see Section 7.2). A unique look at the evolution of the population in time for a variety of initial conditions (4.4) can be found with this method. A specific, relatively low-density initial condition is chosen for the figures, given by rectangular function

$$\tilde{U}_0(\tilde{x}) = \begin{cases} 0 & \tilde{x} < -1 \text{ and } \tilde{x} > 2 \\ 1 & -1 \leq \tilde{x} \leq 2, \end{cases} \tag{4.9}$$

and the IBVP (4.2), (4.4)–(4.5) is solved using parameter values set in Table 3.1. The results are shown in Figure 4.1(a), where the population density evolves in time from this initial condition in blue to a long-term solution in brown.

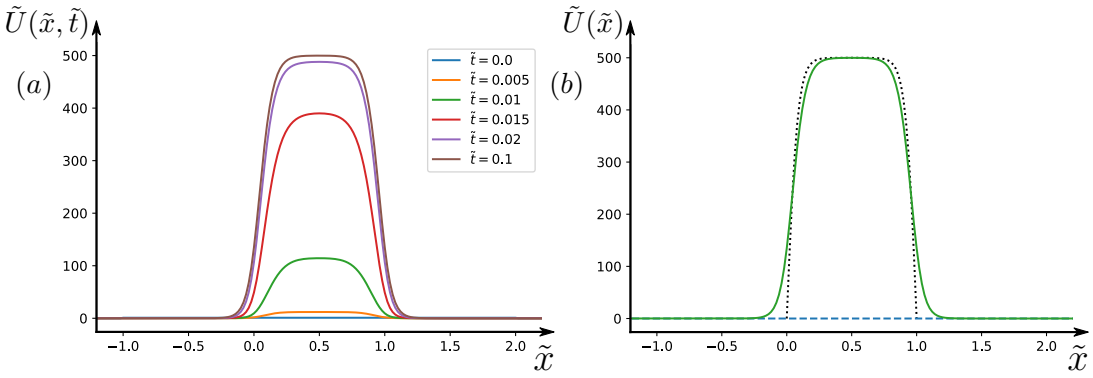


Figure 4.1: (a) Numerical solutions to the IBVP (4.2), (4.4)–(4.5) computed using the MOL (shown in Section 7.2.1.1) at various values of $\tilde{t}$ all satisfying boundary conditions (4.5), for initial condition (4.9) shown in blue. (b) Stationary solutions of (4.2) with trivial unstable zero solution (blue dashed line), and stable non-zero solution (green solid line) found using MOL as the long-term numerical solution to the IBVP (4.2), (4.4)–(4.5). Both are plotted over $\tilde{U}_b^*(\tilde{x})$ (black dotted line) from (4.7). Model parameters are set to $\tilde{\alpha} = 1000$ and $\tilde{a} = 12$ for both figures.

4.1.2 Existence of Stationary Solutions

Stationary solutions $\tilde{U}(\tilde{x})$ of the IBVP (4.2), (4.4)–(4.5) are solutions of the problem that satisfy

$$\frac{\partial \tilde{U}}{\partial \tilde{t}} = 0. \tag{4.10}$$

The trivial stationary solution of (4.2), (4.4)–(4.5) is $\tilde{U} \equiv 0$, which corresponds to the unstable equilibrium $\tilde{U}_a^*(\tilde{x})$ from (4.7). The non-trivial stationary solution, which corresponds to the stable equilibrium $\tilde{U}_b^*(\tilde{x})$ from (4.7), can not be solved analytically but can be numerically integrated using the MOL.

It appears that an identical long-term solution which remains constant in time (4.10), satisfying boundary conditions (4.5), is converged to for every physical non-zero initial condition $\tilde{U}_0(\tilde{x}) > 0$ in the form of (4.9). The results are shown in Figure 4.1(b), where this long-term solution is displayed in green and is plotted alongside the trivial solution $\tilde{U} \equiv 0$ in blue and $\tilde{U}_b^*(\tilde{x})$ from (4.7) in black.

4.1.3 Stability Analysis of Stationary Solutions

No analytic stability analysis is performed but it appears from the MOL computations that for all physical non-zero initial conditions $\tilde{U}_0(\tilde{x}) > 0$ in the form of (4.9) the population density converges to the non-zero stationary solution as $\tilde{t} \to \infty$, inferring that it is asymptotically stable. The opposite is

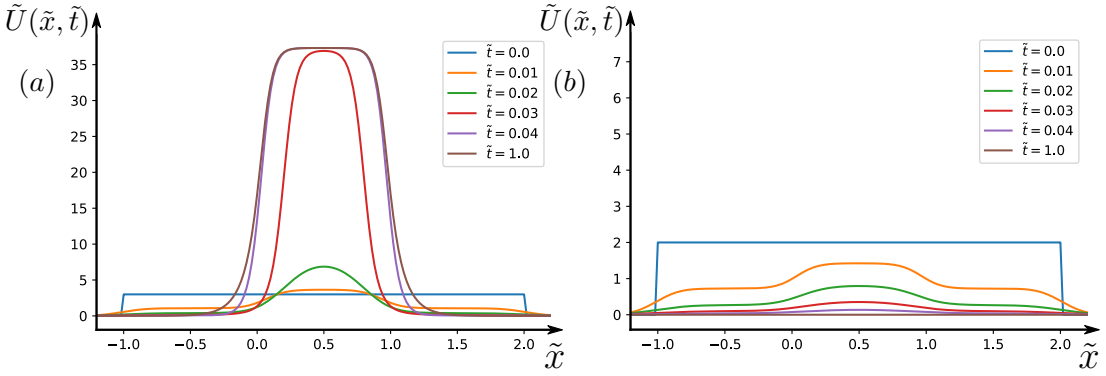


Figure 4.2: Numerical solutions to the IBVP (4.3)–(4.5) computed using the MOL (explained in Section 7.3.1.2) at various values of $\tilde{t}$ all satisfying boundary conditions (4.5), for initial conditions (a) (4.11) and (b) (4.12) shown in blue. Model parameters are set to $\tilde{\beta} = 10$ and $\tilde{a} = 12$ for both figures.

true of the trivial stationary solution $\tilde{U} \equiv 0$ which is unstable. As is evident in Figure 4.1(a) for a low-density initial condition (4.9) the solutions are repelled from extinction in forward-time. These stabilities match those of their corresponding equilibria $\tilde{U}_b^*(\tilde{x})$ and $\tilde{U}_a^*(\tilde{x})$ from (4.7).

4.2 Solutions of Static Allee Model

4.2.1 Time Evolution of Solutions

Numerical solutions $\tilde{U}(\tilde{x},\tilde{t})$ to the static habitat Allee Model IBVP (4.3)–(4.5) can be numerically integrated using the MOL IBVP solver (see Section 7.2). A unique look at the evolution of the population in time for a variety of initial conditions (4.4) can be found once again with this method. Two different initial conditions are chosen for the figures, given by rectangular functions

$$\tilde{U}_0(\tilde{x}) = \begin{cases} 0 & \tilde{x} < -1 \text{ and } \tilde{x} > 2 \\ 3 & -1 \leq \tilde{x} \leq 2, \end{cases} \tag{4.11}$$

and,

$$\tilde{U}_0(\tilde{x}) = \begin{cases} 0 & \tilde{x} < -1 \text{ and } \tilde{x} > 2 \\ 2 & -1 \leq \tilde{x} \leq 2. \end{cases} \tag{4.12}$$

The IBVP (4.3)–(4.5) is then solved with (4.11) and (4.12) using parameter values set in Table 3.2. The results are shown in Figures 4.1(a) and 4.1(b) where the population density evolves in time from initial conditions (4.11) and (4.12) respectively in blue to long-term solutions in brown.

4.2.2 Existence of Stationary Solutions

Stationary solutions $\tilde{U}(\tilde{x})$ of the IBVP (4.3)–(4.5) are solutions of the problem that satisfy

$$\frac{\partial \tilde{U}}{\partial \tilde{t}} = 0. \tag{4.13}$$

The trivial stationary solution of (4.3)–(4.5) is $\tilde{U} \equiv 0$ as before, which now corresponds to the stable equilibrium $\tilde{U}_1^*(\tilde{x})$ from (4.8). In Figure 4.2(a), the population density clearly converges to a non-trivial stationary solution as $\tilde{t} \to +\infty$ (along with the trivial solution in Figure 4.2(b)), corresponding to the stable equilibrium $\tilde{U}_3^*(\tilde{x})$ from (4.8). Any existing non-trivial unstable stationary solutions could not be computed through the forward-time approach used with the MOL, however, and convergence would only be reached by reversing time. Unfortunately time cannot simply be reversed in this problem, or reversed in any RDE, as the odd-ordered time derivative in (4.1) would change sign

$$\frac{\partial \tilde{U}}{\partial(-\tilde{t})} - \frac{\partial^2 \tilde{U}}{\partial \tilde{x}^2} + \tilde{f}(\tilde{U}, \tilde{x}) = -\frac{\partial \tilde{U}}{\partial \tilde{t}} - \frac{\partial^2 \tilde{U}}{\partial \tilde{x}^2} + \tilde{f}(\tilde{U}, \tilde{x}), \tag{4.14}$$

which would qualitatively change the equation, indicating that $\tilde{U}(\tilde{x}, \tilde{t})$ and $\tilde{U}(\tilde{x}, -\tilde{t})$ are not interchangeable solutions for (4.3).

The static Allee Model RDE (4.3) must therefore be reformulated to study the existence of all stationary solutions of the Allee Model IBVP (4.3)–(4.5) by imposing (4.13). The problem changes from an IBVP for a nonlinear non-autonomous parabolic PDE to a boundary value problem (BVP) for a second order nonlinear non-autonomous ODE

$$\frac{d^2 \tilde{U}}{d\tilde{x}^2} = \tilde{\beta}^2 \tilde{U} - 4\tilde{\beta}\, H(\tilde{x}; \tilde{a})\, \tilde{U}^2 + \tilde{U}^3, \tag{4.15}$$

with the Dirichlet boundary conditions

$$\lim_{\tilde{x} \to \pm\infty} \tilde{U}(\tilde{x}) = 0. \tag{4.16}$$

Three solutions to this BVP, including the trivial solution $\tilde{U} \equiv 0$, are expected as there are three equivalent equilibria in (4.8), although a proof for this is not provided. The non-trivial solutions must be computed using a different type of numerical method to a standard IBVP solver like the MOL, which uses direct numerical integration. A collocation method is utilised instead (which is elaborated upon in Section 7.1.2).

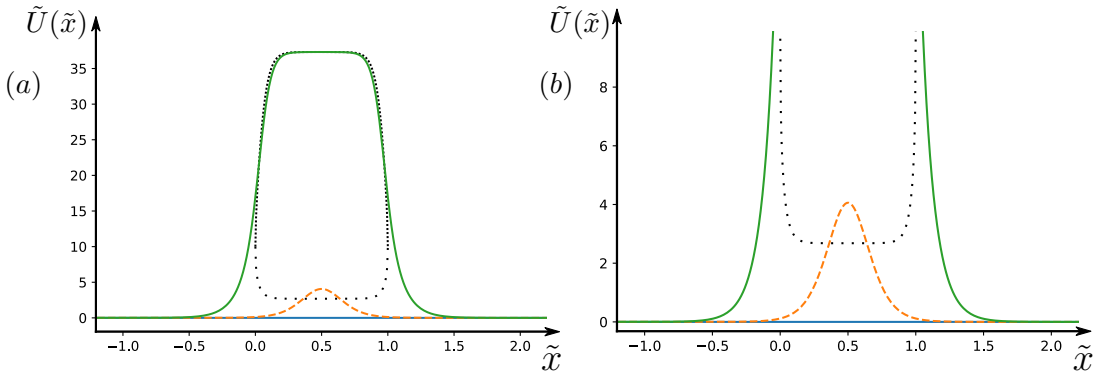


Figure 4.3: Three solutions to BVP (4.15)–(4.16) numerically computed using the collocation method (shown in Section 7.2.1.2). These are also stationary solutions of IBVP (4.3)–(4.5) with stability indicated by solid lines and instability indicated by dashed lines. (a) Full view of non-zero stable stationary solution (solid green line) corresponding to equilibrium $\tilde{U}_3^*(\tilde{x})$ (densely dotted line) from (4.8), non-zero unstable stationary solution (dashed orange line) corresponding to $\tilde{U}_2^*(\tilde{x})$ (sparsely dotted line), and zero stable stationary solution (solid blue line) corresponding to $\tilde{U}_1^*(\tilde{x}) \equiv 0$. (b) Close-up of stationary solutions and equilibria displayed between $\tilde{U} = 0$ and $\tilde{U} = 10$. Model parameters are set to $\tilde{\beta} = 10$ and $\tilde{a} = 12$ for both figures.

The two non-trivial solutions to the BVP (4.15)–(4.16) are numerically computed and shown in Figure 4.3 alongside the trivial solution $\tilde{U} \equiv 0$ and equilibria (4.8). These are the three stationary solutions of the static habitat Allee Model RDE (4.3) satisfying identical boundary conditions (4.5).

4.2.3 Stability Analysis of Stationary Solutions

Again, no analytic stability analysis is performed, but it appears from the MOL computations and in Figure 4.2(a) that non-zero initial solutions $\tilde{U}_0(\tilde{x})$ close to, but greater than, the stationary solution shown in orange in Figure 4.3 converge to the stationary solution shown in green as $\tilde{t} \to \infty$. It also appears in Figure 4.2(b) that non-zero initial solutions $\tilde{U}_0(\tilde{x})$ defined close to, but less than, the stationary solution shown in orange converge to the trivial zero solution shown in blue in Figure 4.3.

This infers that the non-zero stationary solution corresponding to $\tilde{U}_3^*$ shown in green in Figure 4.3 and the zero stationary solution corresponding to $\tilde{U}_1^*$ shown in blue in Figure 4.3 are asymptotically stable, as forward-time numerical integration converges to one or the other for all physical non-zero initial solutions. Conversely, the non-zero stationary solution shown in orange in Figure 4.3, which corresponds to equilibrium $\tilde{U}_2^*$, is unstable as it repels all

initial solutions defined in its proximity. The stabilities of these stationary solutions match the stabilities of their corresponding equilibria from (4.8).

These results become foundational to the work in the following chapters as the habitat speed $\tilde{c}$ is reintroduced into the habitat models.

Chapter 5

Travelling Waves

After exploring the static habitat and its stationary solutions the next step is to set the habitat in motion and to study some non-stationary solutions, such as travelling wave solutions. The population is said to be keeping pace with a moving habitat drifting at speed $\tilde{c}$ if a stable non-zero travelling wave solution $\tilde{U}(\tilde{x} - \tilde{c}\tilde{t})$ exists. This stable non-zero travelling wave may cease to exist when the speed exceeds a certain critical value. Consequently, the trivial solution $\tilde{U} \equiv 0$ would become the only stable solution and the species in the habitat would then be destined for extinction, independently of the initial condition.

The speed $\tilde{c}$, defined in (3.22) and (3.36), is reintroduced and (4.1) now becomes

$$\frac{\partial \tilde{U}}{\partial \tilde{t}} = \frac{\partial^2 \tilde{U}}{\partial \tilde{x}^2} + \tilde{f}(\tilde{U}, \tilde{x} - \tilde{c}\tilde{t}). \tag{5.1}$$

with initial condition

$$\tilde{U}(\tilde{x}, 0) = \tilde{U}_0(\tilde{x}), \tag{5.2}$$

and boundary conditions

$$\lim_{\tilde{x} \to \pm\infty} \tilde{U}(\tilde{x}, \tilde{t}) = 0. \tag{5.3}$$

The drift of the habitat represented by non-trivial travelling wave solutions may be more easily studied by converting (5.1) into a comoving frame [4, 41, 42]. A coordinate change is made and variables $\tilde{x}$, $\tilde{t}$, and $\tilde{U}$ are transformed into three new variables ξ, s, and V

$$\xi = \tilde{x} - \tilde{c}\tilde{t}, \quad s = \tilde{t}, \quad V(\xi, s) = \tilde{U}(\tilde{x}, \tilde{t}). \tag{5.4}$$

The old derivatives within (5.1) are therefore also transformed due to this

coordinate change (5.4) into new derivatives:

$$\frac{\partial V}{\partial \tilde{x}} = \frac{\partial \xi}{\partial \tilde{x}}\frac{\partial V}{\partial \xi} + \frac{\partial s}{\partial \tilde{x}}\frac{\partial V}{\partial s} = \frac{\partial V}{\partial \xi}, \tag{5.5}$$

$$\frac{\partial^2 V}{\partial \tilde{x}^2} = \frac{\partial^2 V}{\partial \xi^2}, \tag{5.6}$$

$$\begin{aligned}\frac{\partial V}{\partial \tilde{t}} &= \frac{\partial \xi}{\partial \tilde{t}}\frac{\partial V}{\partial \xi} + \frac{\partial s}{\partial \tilde{t}}\frac{\partial V}{\partial s} \\ &= -\tilde{c}\frac{\partial V}{\partial \xi} + \frac{\partial V}{\partial s}.\end{aligned} \tag{5.7}$$

Under this transformation (5.4)–(5.7) the RDE (5.1) becomes the following reaction-convection-diffusion equation (RCDE):

$$\frac{\partial V}{\partial s} = \frac{\partial^2 V}{\partial \xi^2} + \tilde{c}\,\frac{\partial V}{\partial \xi} + \tilde{f}(V, \xi), \tag{5.8}$$

with its initial condition (5.2) becoming

$$V(\xi, 0) = V_0(\xi), \tag{5.9}$$

and boundary conditions (5.3) becoming

$$\lim_{\xi \to \pm\infty} V(\xi, s) = 0. \tag{5.10}$$

The stationary solutions $V(\xi)$ of this new transformed IBVP (5.8)–(5.10) correspond to travelling wave solutions $\tilde{U}(\tilde{x} - \tilde{c}\tilde{t})$ of the original IBVP (5.1)–(5.3) [41]. Therefore, to investigate the existence of these travelling waves, the time derivative in (5.8) is set to zero

$$\frac{\partial V}{\partial s} = 0, \tag{5.11}$$

and the IBVP for a nonlinear non-autonomous hyperbolic-parabolic PDE (5.8)–(5.10) is simplified to a BVP for a second-order nonlinear non-autonomous ODE

$$\frac{d^2 V}{d\xi^2} + \tilde{c}\,\frac{dV}{d\xi} + \tilde{f}(V, \xi) = 0, \tag{5.12}$$

with Dirichlet boundary conditions

$$\lim_{\xi \to \pm\infty} V(\xi) = 0. \tag{5.13}$$

The existence of travelling wave solutions $\tilde{U}(\tilde{x} - \tilde{c}\tilde{t})$ of (5.1)–(5.3) can now be easily studied by solving the BVP (5.12)–(5.13).

The stability of travelling wave solutions $\tilde{U}(\tilde{x} - \tilde{c}\tilde{t})$ of (5.1)–(5.3) can be investigated numerically via direct integration of the comoving IBVP (5.8)–(5.10). In Section 7.2 it will be shown that this is significantly more computationally efficient than investigating the stability using the original IBVP (5.1)–(5.3).

5.1 Standard Approach for Travelling Wave Solution Analysis

In Kuehn's textbook on PDE Dynamics [43], a standard approach to investigating the existence of travelling wave solutions is illustrated. A one dimensional autonomous RDE

$$\frac{\partial \tilde{U}}{\partial \tilde{t}} = \frac{\partial^2 \tilde{U}}{\partial \tilde{x}^2} + h(\tilde{U}), \tag{5.14}$$

is discussed and transformed into an ODE in a comoving frame using the coordinate change (5.4)–(5.7) with (5.11)

$$\frac{d^2V}{d\xi^2} + \tilde{c}\,\frac{dV}{d\xi} + h(V) = 0. \tag{5.15}$$

A new variable is introduced $W = dV/d\xi$ such that an equivalent first-order autonomous system of coupled ODEs to (5.15) can be expressed

$$\begin{aligned} \frac{dV}{d\xi} &= W, \\ \frac{dW}{d\xi} &= -\tilde{c}\,W - h(V). \end{aligned} \tag{5.16}$$

Phase plane analysis can be used for this system to find travelling wave solutions of the original PDE (5.14). Let $\mathbf{Y}^*$ and $\bar{\mathbf{Y}}^*$ be two different steady states of the system (5.16), with general solutions denoted $\mathbf{Y}(\xi) = (\mathrm{V}(\xi),\mathrm{W}(\xi))$. Three types of solutions of (5.16) are defined as follows:

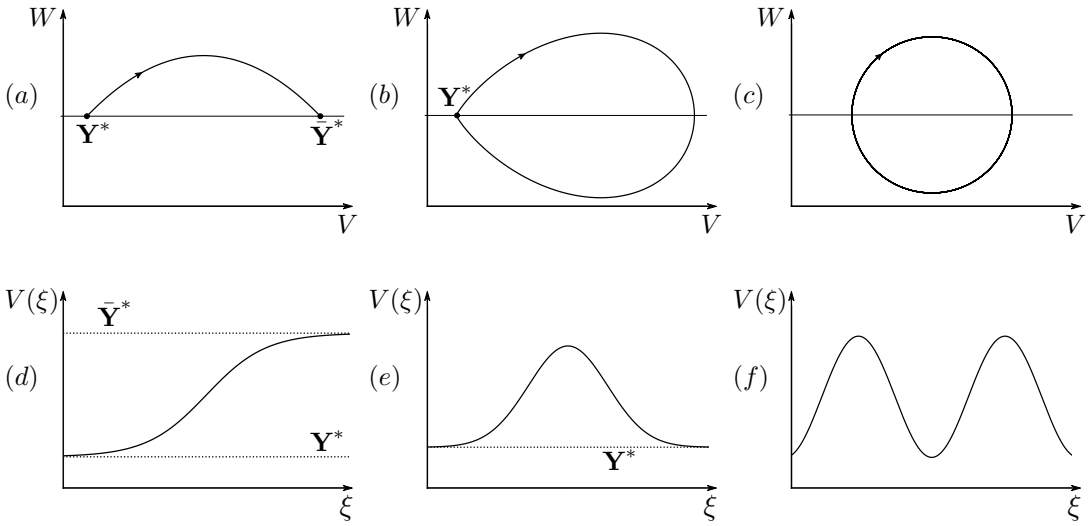


Figure 5.1: Correspondence between phase portraits of (5.16) (upper row), and solutions to (5.15) (i.e. travelling wave solutions of (5.14) in the comoving frame) (lower row) for the (a) heteroclinic connection (5.17), (b) homoclinic connection (5.18), and (c) periodic orbit (5.19), representing a (d) travelling front, (e) travelling pulse, (f) travelling wave train respectively.

A solution $\mathbf{Y}(\xi)$ is called a heteroclinic orbit or connection between $\mathbf{Y}^*$ and $\bar{\mathbf{Y}}^*$ (see Figure 5.1(a)) if

$$\lim_{\xi\to-\infty}\mathbf{Y}(\xi)=\mathbf{Y}^*,\quad \lim_{\xi\to+\infty}\mathbf{Y}(\xi)=\bar{\mathbf{Y}}^*. \tag{5.17}$$

A solution $\mathbf{Y}(\xi)$ is called a homoclinic orbit or connection to $\mathbf{Y}^*$ (see Figure 5.1(b)) if

$$\lim_{\xi\to-\infty}\mathbf{Y}(\xi)=\mathbf{Y}^*=\lim_{\xi\to+\infty}\mathbf{Y}(\xi). \tag{5.18}$$

A solution $\mathbf{Y}(\xi)$ is called a periodic orbit of minimal period $\xi_T>0$ (see Figure 5.1(c)) if there exists a $\xi_T>0$ such that

$$\mathbf{Y}(\xi)=\mathbf{Y}(\xi+\xi_T) \tag{5.19}$$

for all $\xi\in\mathbb{R}$ and there is no smaller ξ_T such that (5.19) holds.

Any periodic orbits or heteroclinic and homoclinic bounded solutions connecting steady states in (5.16) correspond to unique travelling wave solutions in (5.14) according to Kuehn. From equations (5.17)-(5.19) the following observations are clear:

If there is a solution $\mathbf{Y}(\xi)$ which is a heteroclinic orbit in the (V,W) phase space of (5.16), then this solution corresponds to a travelling front solution of

the associated PDE (5.14) (see Figure 5.1(d)).

If there is a solution $\mathbf{Y}(\xi)$ which is a homoclinic orbit in the (V, W) phase space of (5.16), then this solution corresponds to a travelling pulse solution of the associated PDE (5.14) (see Figure 5.1(e)).

If there is a solution $\mathbf{Y}(\xi)$ which is a periodic orbit in the (V, W) phase space of (5.16), then this solution corresponds to a travelling wave train solution of the associated PDE (5.14) (see Figure 5.1(f)).

5.2 Our Approach for Travelling Wave Solution Analysis

In this thesis, the main difference from the standard approach discussed by [43] is that both the Logistic Model RDE (3.18) and Allee Model RDE (3.32) are non-autonomous. These are then transformed into non-autonomous travelling wave ODEs like (5.12) in the comoving frame when investigating the existence of travelling pulse solutions. This means that our problem differs from the standard approach in two ways. First, the non-autonomous travelling wave ODE must be expressed as an autonomous system of ODEs to compare it with (5.16), which can be done at the expense of adding an extra dimension [31] making it a three-dimensional autonomous system. Second, this three-dimensional autonomous system cannot have any equilibrium solutions. To obtain a travelling pulse solution the standard approach would find where in (V,W) phase space the unstable manifold of a steady state of (5.16) intersects non-transversely with its stable manifold. This would define a homoclinic connection that corresponds to a travelling pulse of the associated PDE. In the absence of any steady states, as in our problem, this approach cannot be reproduced. Therefore, to obtain the travelling pulse solutions of the non-autonomous RDE (5.1), and later the RDEs of both models (3.18), (3.32), a comoving frame BVP such as (5.12)-(5.13) is numerically solved to find isolated trajectories between $\xi = -\infty$ and $\xi = \infty$ that can be displayed in a three-dimensional phase portrait.

A similar approach to the standard approach is initially taken, where (5.12) can

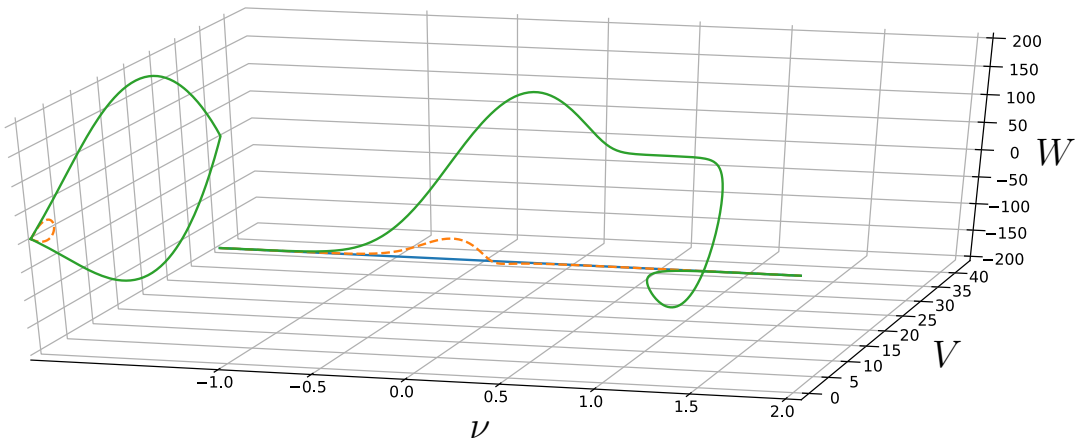


Figure 5.2: Phase portrait of (5.22)–(5.24), where trajectories were numerically computed using the collocation method. The trajectories are plotted between $\nu \in [-1, 2]$ in three-dimensional phase space and a projection on a two-dimensional plane of V vs. W is displayed on the left hand side of the figure, with the trivial solution in blue and the non-trivial solutions in orange and green. Model parameters set at $\tilde{\beta} = 10$, $\tilde{a} = 12$, and $\tilde{c} = 1$.

be reformulated into two first-order non-autonomous ODEs,

$$\begin{aligned} \frac{dV}{d\xi} &= W, \\ \frac{dW}{d\xi} &= -\tilde{c}\,W - \tilde{f}(V, \xi), \end{aligned} \tag{5.20}$$

with the same boundary conditions (5.10)

$$\lim_{\xi \to \pm\infty} V(\xi) = 0. \tag{5.21}$$

To make the system autonomous like in the standard approach another dependent variable must be defined, $\nu(\xi) = \xi$, allowing it to be expressed as three first-order autonomous coupled ODEs

$$\begin{aligned} \frac{dV}{d\xi} &= W, \\ \frac{dW}{d\xi} &= -\tilde{c}\,W - \tilde{f}(V, \nu), \\ \frac{d\nu}{d\xi} &= 1. \end{aligned} \tag{5.22}$$

with (5.21) and an additional condition for ν

$$\lim_{\xi \to \pm\infty} V(\xi) = 0, \quad \nu(\xi = 0) = 0. \tag{5.23}$$

No steady states exist in this transformed autonomous system as there is no point in (V, W, ν) phase space at which all derivatives in (5.22) equal zero. To visualise the three-dimensional phase portrait of this system (shown in Figure 5.2), $\tilde{f}$ from equation (3.32) is borrowed (the phase portraits of the Allee Model will be explored in full in the next chapter), with coordinate changes and new variables, (5.4) and $\nu(\xi) = \xi$,

$$\tilde{f}(V, \nu) = -\tilde{\beta}^2 V + 4\tilde{\beta}\, H(\nu; \tilde{a})\, V^2 - V^3. \tag{5.24}$$

This is substituted into (5.22) and numerically solved using collocation (see Section 7.1.2), where the habitat function is expressed as

$$H(\nu; \tilde{a}) = \frac{\tanh\left(\tilde{a}(\nu)\right) - \tanh\left(\tilde{a}(\nu - 1)\right)}{2 \tanh \tilde{a}}. \tag{5.25}$$

In the two-dimensional projection of the trajectories on the left-hand side of Figure 5.2, both of the two non-trivial trajectories (shown in orange and green) give the appearance of being homoclinic connections to (V,W) = (0,0), as one might expect from travelling pulse solutions in a two-dimensional autonomous system. In the three-dimensional phase portrait plotted between $\nu = -1$ and $\nu = 2$, however, the non-trivial trajectories are clearly not closed loops. Each trajectory in fact becomes bi-asymptotically constant in both negative and positive ξ, and therefore also in ν, tending towards $\nu = -\infty$ and $\nu = +\infty$ respectively. These results highlight the unique properties of the non-autonomous systems in this thesis, which will be explored further for both models in the following chapter as the value of the habitat speed parameter $\tilde{c}$ is varied.

Chapter 6

Moving Habitat

The effect that a moving habitat has on a species which adheres to the dynamics of the Logistic or Allee Model may now be studied and a few questions are to be considered. Can the species keep pace with a rapidly moving habitat? If so, is there a limit to the speed of the habitat above which the population may succumb to extinction? As the habitat speed increases, would there be any advanced warning of this extinction or would the collapse of the population appear to be abrupt and spontaneous? Can the collapse to extinction be characterised as a bifurcation of travelling pulse solutions? These questions will be addressed for both models using numerical computations[1] and bifurcation analysis.

With the reintroduction of the habitat speed $\tilde{c}$, the RDEs of the models are now non-autonomous in both independent variables $\tilde{x}$ and $\tilde{t}$ once again. The RDE of the Logistic Model (4.2) becomes

$$\frac{\partial \tilde{U}}{\partial \tilde{t}} = \frac{\partial^2 \tilde{U}}{\partial \tilde{x}^2} + \tilde{\alpha}\left(H(\tilde{x} - \tilde{c}\tilde{t}; \tilde{a}) - \frac{1}{2}\right)\tilde{U} - \tilde{U}^2, \tag{6.1}$$

and the RDE of the Allee Model (4.3) becomes

$$\frac{\partial \tilde{U}}{\partial \tilde{t}} = \frac{\partial^2 \tilde{U}}{\partial \tilde{x}^2} - \tilde{\beta}^2\tilde{U} + 4\tilde{\beta}\, H(\tilde{x} - \tilde{c}\tilde{t}; \tilde{a})\,\tilde{U}^2 - \tilde{U}^3, \tag{6.2}$$

with the initial condition

$$\tilde{U}(\tilde{x}, 0) = \tilde{U}_0(\tilde{x}), \tag{6.3}$$

[1] The numerical methods used are given in Chapter 7.

boundary conditions

$$\lim_{\tilde{x}\to\pm\infty} \tilde{U}(\tilde{x},\tilde{t}) = 0, \tag{6.4}$$

and habitat function

$$H(\tilde{x}-\tilde{c}\tilde{t};\tilde{a}) = \frac{\tanh\left(\tilde{a}(\tilde{x}-\tilde{c}\tilde{t})\right) - \tanh\left(\tilde{a}(\tilde{x}-\tilde{c}\tilde{t}-1)\right)}{2\tanh\tilde{a}}, \tag{6.5}$$

for both.

6.1 The Logistic Model

6.1.1 Comoving Frame

In order to study the existence of travelling pulse solutions in the Logistic Model, the same approach from Chapter 5 is taken and a comoving frame PDE is derived. Using the comoving frame transformation (5.4)–(5.7), the RDE (6.1) becomes the following RCDE:

$$\frac{\partial V}{\partial s} = \frac{\partial^2 V}{\partial \xi^2} + \tilde{c}\,\frac{\partial V}{\partial \xi} + \tilde{\alpha}\left(H(\xi;\tilde{a}) - \frac{1}{2}\right)V - V^2, \tag{6.6}$$

with its initial condition (6.3) becoming

$$V(\xi,0) = V_0(\xi), \tag{6.7}$$

boundary conditions (6.4) becoming

$$\lim_{\xi\to\pm\infty} V(\xi) = 0, \tag{6.8}$$

and habitat function expressed as

$$H(\xi;\tilde{a}) = \frac{\tanh\left(\tilde{a}\,\xi\right) - \tanh\left(\tilde{a}(\xi-1)\right)}{2\tanh\tilde{a}}. \tag{6.9}$$

The non-trivial stationary solutions $V(\xi)$ of this new transformed IBVP (6.6)–(6.8) correspond to travelling pulse solutions in the form $\tilde{U}(\tilde{x}-\tilde{c}\tilde{t})$ of the original Logistic Model IBVP (6.1),(6.3)–(6.4) [41]. Therefore, to investigate the existence of the travelling pulses in the Logistic Model, the time derivative in (6.6) is set to zero

$$\frac{\partial V}{\partial s} = 0, \tag{6.10}$$

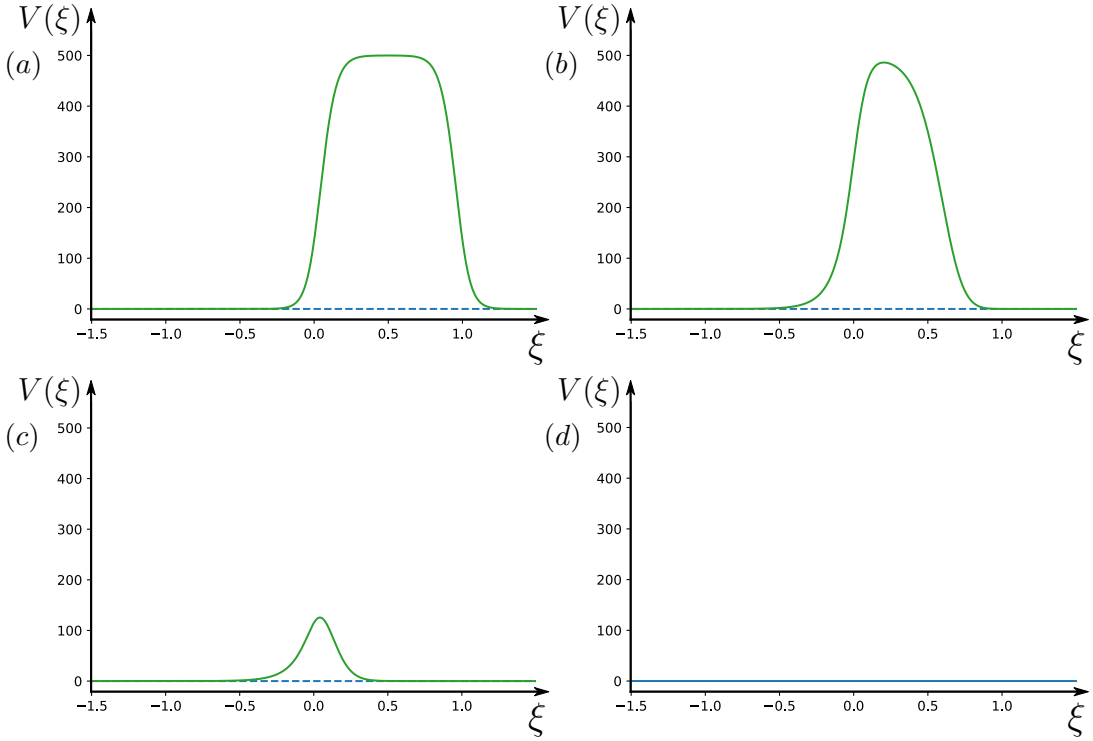


Figure 6.1: Stable (solid lines) and unstable (dashed lines) solutions to (6.11)–(6.12) computed using collocation and plotted in the comoving frame for (a) $\tilde{c} = 0$, (b) $\tilde{c} = 40$, (c) $\tilde{c} = 44$, and (d) $\tilde{c} = 44.14$. The remaining model parameters are set at $\tilde{\alpha} = 1000$ and $\tilde{a} = 12$.

and the IBVP for an RCDE (6.6)–(6.8) is simplified to a BVP for the following ODE

$$\frac{d^2V}{d\xi^2} + \tilde{c}\,\frac{dV}{d\xi} + \tilde{\alpha}\left(H(\xi;\tilde{a}) - \frac{1}{2}\right)V - V^2 = 0, \tag{6.11}$$

with Dirichlet boundary conditions

$$\lim_{\xi\to\pm\infty} V(\xi) = 0. \tag{6.12}$$

It would be instructive to also study the phase portrait of the Logistic Model. To visualise the full phase portrait of the non-autonomous system, (6.11) is turned into an equivalent system of three first-order autonomous coupled ODEs, as in (5.22), by introducing the dependent variables $W = dV/d\xi$ and $\nu(\xi) = \xi$:

$$\begin{aligned}
\frac{dV}{d\xi} &= W,\\
\frac{dW}{d\xi} &= -\tilde{c}\,W - \tilde{\alpha}\left(H(\nu;\tilde{a}) - \frac{1}{2}\right)V + V^2,\\
\frac{d\nu}{d\xi} &= 1,
\end{aligned} \tag{6.13}$$

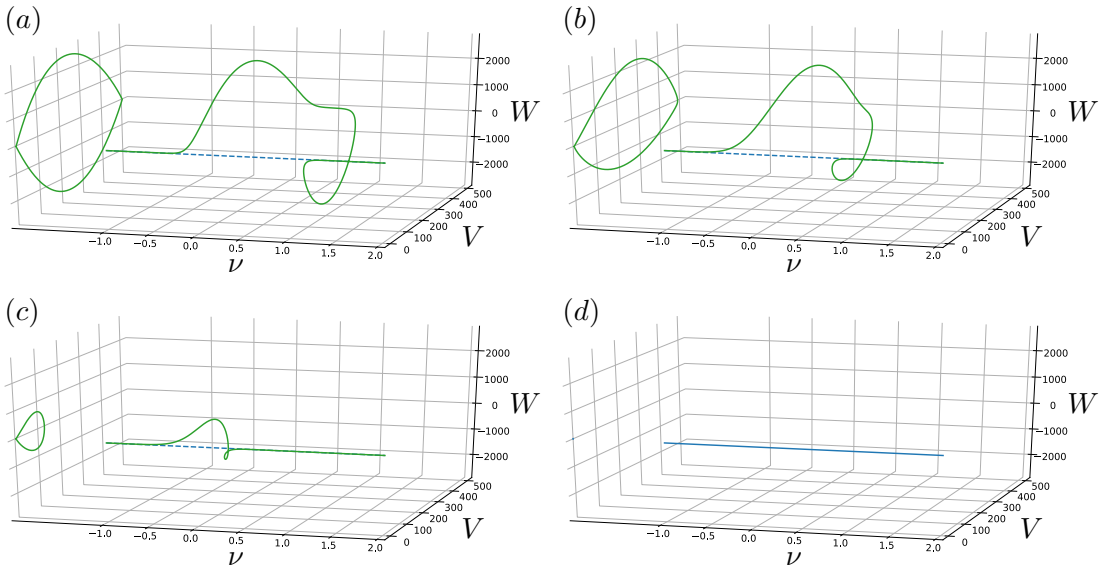


Figure 6.2: Phase portraits of (6.13)–(6.14), where trajectories were numerically computed using collocation. Stable (solid lines) and unstable (dashed lines) solutions are plotted between $\nu \in [-1, 2]$ in three-dimensional phase space and a projection onto the (V, W) plane is displayed on the left hand side of the figure for (a) $\tilde{c} = 0$, (b) $\tilde{c} = 40$, (c) $\tilde{c} = 44$, and (d) $\tilde{c} = 44.14$. The remaining model parameters are set at $\tilde{\alpha} = 1000$ and $\tilde{a} = 12$.

together with (6.12), and an additional condition for ν,

$$\lim_{\xi \to \pm\infty} V(\xi) = 0, \quad \nu(\xi = 0) = 0. \tag{6.14}$$

6.1.2 Computing Travelling Pulse Solutions

In the Logistic Model up to two travelling pulse solutions $\tilde{U}(\tilde{x} - \tilde{c}\tilde{t})$ of the moving habitat IBVP (6.1),(6.3)–(6.4) are expected for all values of $\tilde{c}$ as two stationary solutions $\tilde{U}(\tilde{x})$ were found to the static habitat IBVP (4.2), (4.4)–(4.5) (although a proof for this is not provided). Therefore, up to two equivalent solutions $V(\xi)$ of the BVP (6.11)–(6.12) are expected, including the trivial solution $V \equiv 0$. A collocation method (see Section 7.1.2) is utilised to numerically solve the BVP (6.11)–(6.12) for non-trivial solutions $V(\xi)$ at a range of values of $\tilde{c}$. The approach used is explained in full in Section 7.2.2.1.

The results are displayed in Figure 6.1. A travelling pulse solution is found for each of value of $\tilde{c}$ up to a critical speed $\tilde{c} = \tilde{c}_{crit}$, above which it ceases to exist. The trivial solution (shown in blue) remains unchanged for all $\tilde{c} < \tilde{c}_{crit}$. The travelling pulse solutions (shown in green) become narrower and begin falling towards the trivial solution as $\tilde{c}$ approaches $\tilde{c}_{crit}$. The travelling pulse solutions

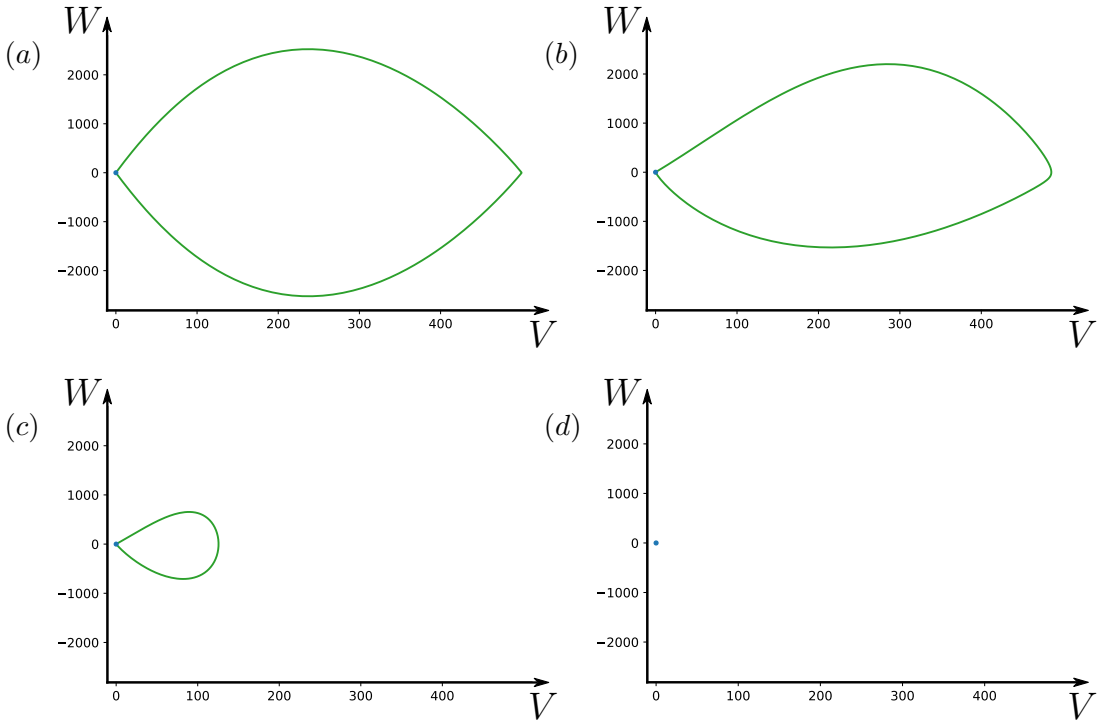


Figure 6.3: Projection of the phase portraits of (6.13)–(6.14) on a two-dimensional plane of V vs. W, where trajectories were numerically computed using collocation. Solutions are plotted for (a) $\tilde{c} = 0$, (b) $\tilde{c} = 40$, (c) $\tilde{c} = 44$, and (d) $\tilde{c} = 44.14$. The remaining model parameters are set at $\tilde{\alpha} = 1000$ and $\tilde{a} = 12$.

then collide with trivial solution at $\tilde{c} = \tilde{c}_{crit}$, making the trivial solution the only remaining physical solution for $\tilde{c} > \tilde{c}_{crit}$.

The corresponding phase portraits for (6.13)–(6.14) are shown in Figure 6.2 with two-dimensional projections of the trajectories displayed on the left-hand side of each plot and in Figure 6.3. Under the parameter variation of $\tilde{c}$, two topologically nonequivalent phase portraits appear to emerge for $\tilde{c} \leq 44$ and for $\tilde{c} \geq 44.14$. Therefore, a bifurcation occurs at a point between $44 < \tilde{c}_{crit} < 44.14$.

6.1.3 Stability Analysis of Travelling Pulse Solutions

Similarly to the stability analysis conducted in Chapter 4, no analytical stability analysis can be performed on the solutions to (6.11)–(6.12) but the MOL is utilised again to analyse the stability numerically. The IBVP in the comoving frame (6.6)–(6.8) is solved for a range of values of $\tilde{c}$ using an initial solution given by the following rectangular function

$$V_0(\xi) = \begin{cases} 0 & \xi < -1 \text{ and } \xi > 2 \\ 1 & -1 \leq \xi \leq 2. \end{cases} \tag{6.15}$$

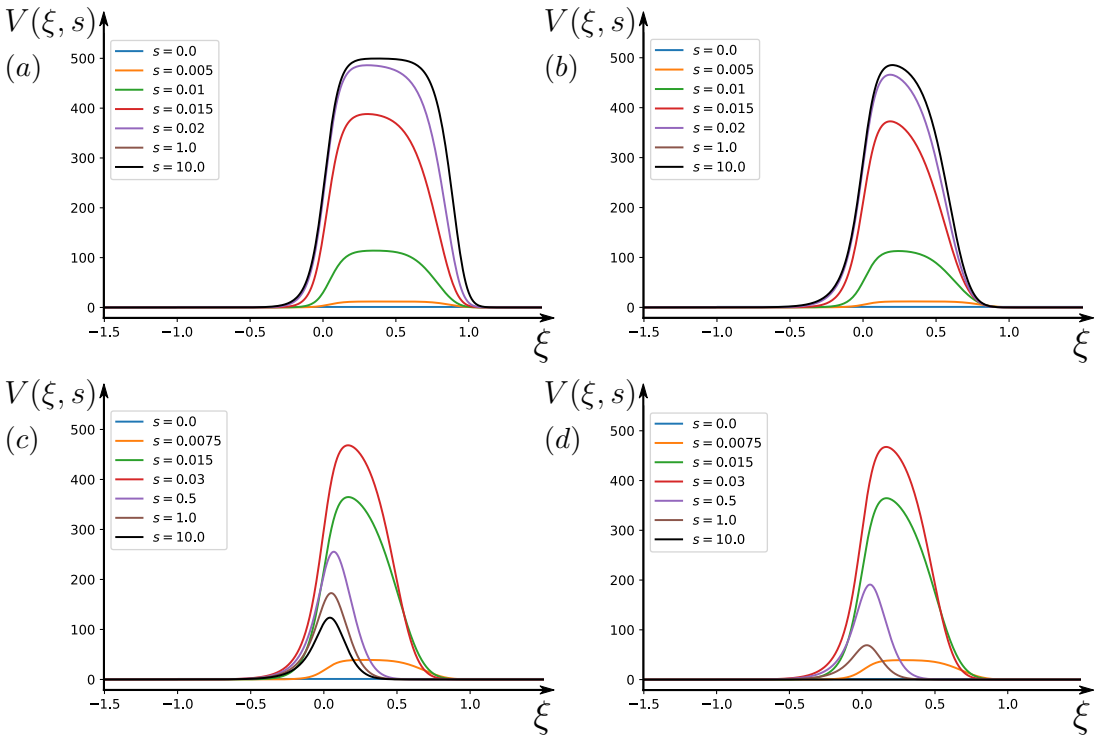


Figure 6.4: Numerical solutions to the IBVP (6.6)–(6.8) computed using the MOL at various values of s with initial solution (6.15) shown in blue and the long-term solution shown in black for (a) $\tilde{c} = 20$, (b) $\tilde{c} = 40$, (c) $\tilde{c} = 44$, and (d) $\tilde{c} = 44.14$. The remaining model parameters are set at $\tilde{\alpha} = 1000$ and $\tilde{a} = 12$.

The results are displayed in Figure 6.4 for $\tilde{c} = 20$, $\tilde{c} = 40$, $\tilde{c} = 44$, and $\tilde{c} = 44.14$. In Figure 6.4(a) and 6.4(b), as time s evolves, the solutions rise up to their long-term shapes shown in black, equal to the travelling pulse solution of the BVP (6.11)–(6.12) at their respective speeds. In Figure 6.4(c) and 6.4(d)), the intermediate-time solutions appear to rise up again before very slowly falling to their respective long-term shapes shown in black as $s \to \infty$.

The forward-time numerical integration results suggest that the travelling pulse solutions are always stable while they exist for $\tilde{c} < \tilde{c}_{crit}$. The trivial solution remains unstable up to this bifurcation point before becoming stable for $\tilde{c} > \tilde{c}_{crit}$ as shown in Figure 6.4(d).

6.1.4 Transcritical Bifurcation of Travelling Pulses

In Figures 6.1, 6.2, 6.3, and 6.4, it is clear a bifurcation occurs at the critical speed $44 < \tilde{c}_{crit} < 44.14$. Bifurcation analysis is performed which finds the bifurcation point to be $\tilde{c}_{crit} = 44.1370$, above which only a stable solution at zero remains and the population dies out. This can be seen in the bifurcation

diagrams of Figure 6.5 for the total populations

$$P_{tot}(\tilde{c}) = \int_{-\infty}^{\infty} V(\xi;\tilde{c})\, d\xi, \tag{6.16}$$

L^2 norms

$$\|V(\xi;\tilde{c})\| = \sqrt{\int_{-\infty}^{\infty} V^2(\xi;\tilde{c})\, d\xi}, \tag{6.17}$$

maximum values

$$V_{max}(\tilde{c}) = \max_{\xi\in\mathbb{R}} V(\xi;\tilde{c}), \tag{6.18}$$

and full width at half maximum (FWHM) values

$$FWHM(\tilde{c}) = |\xi_2(\tilde{c}) - \xi_1(\tilde{c})|, \tag{6.19}$$

of the solutions to (6.11)–(6.12), where $\xi_1(\tilde{c})$ and $\xi_2(\tilde{c})$ are defined implicitly as the two values of ξ at which $V(\xi;\tilde{c})$ equals half of its maximum value

$$V(\xi_1;\tilde{c}) = V(\xi_2;\tilde{c}) = \frac{V_{max}(\tilde{c})}{2}. \tag{6.20}$$

As is evident in Figure 6.5(a)–(c), there is a transverse crossing at the bifurcation point $\tilde{c}_{crit} = 44.1370$ where the stable travelling pulse solutions (shown in green) fall and collide with the unstable trivial solution (shown in blue) before disappearing from the physical plots. At this juncture the trivial solution switches stability and becomes stable for $\tilde{c} > \tilde{c}_{crit}$. This infers that a transcritical bifurcation occurs at $\tilde{c} = \tilde{c}_{crit}$.

In the limit as L goes to infinity, the habitat function (2.8) become homogeneous, that is, $H(\xi) = 1$. In this setting, there exists a travelling front from $(V, W) = (1, 0)$ to $(V, W) = (0, 0)$ when the habitat speed is above a certain threshold $\tilde{c} = \tilde{c}_{inv} = \sqrt{2\tilde{\alpha}} \approx 44.7214$, which is known as the invasion speed. This calculation is done in the spirit of [3], as shown in Section 2.1. The result implies that a species cannot track a moving habitat that moves faster than the invasion speed of the species into the habitat [3]. It is expected that if the good habitat were to extend through all space that the values of $\tilde{c}_{inv}$ and $\tilde{c}_{crit}$ would converge.

From the point of view of an observer the population of the moving habitat (shown in Figure 6.5(a)) would appear to fall steadily at first as the speed of the habitat increased before experiencing a noticeably steep decline in its final quarter between $\frac{3}{4}\tilde{c}_{crit} < \tilde{c} < \tilde{c}_{crit}$. The spread of the population would appear

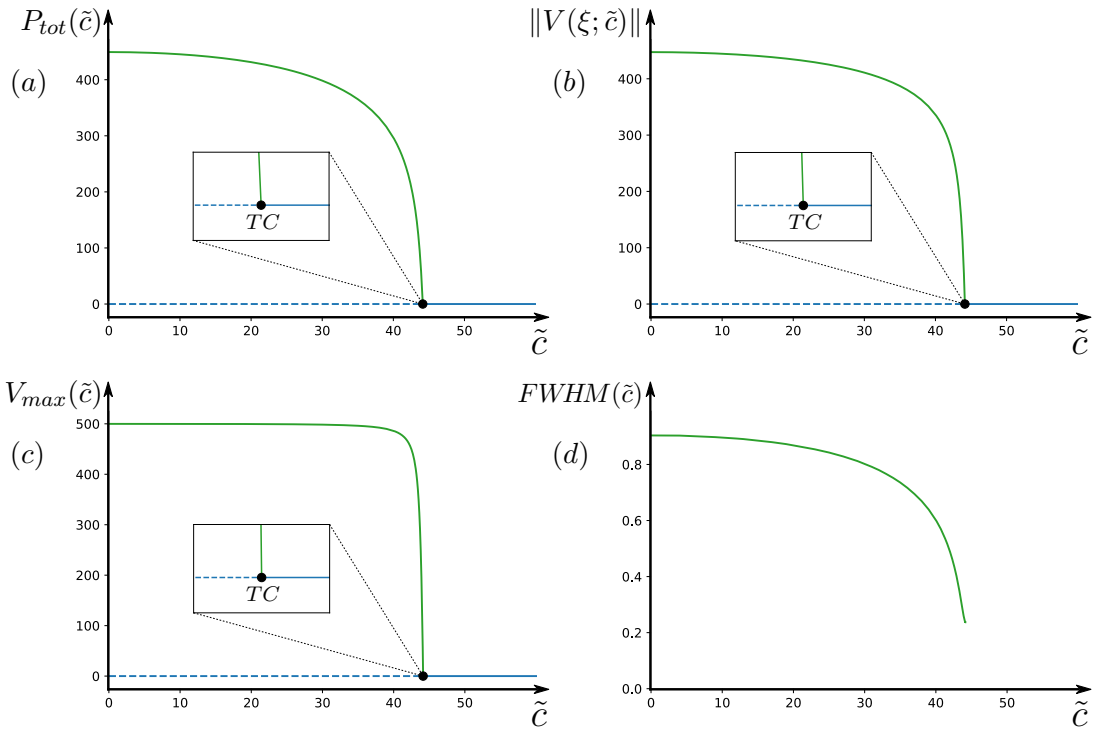


Figure 6.5: One-parameter bifurcation diagrams with speed parameter $\tilde{c}$ for the (a) total population (6.16), (b) L^2 norm (6.17), (c) maximum value (6.18), and (d) FWHM (6.19) of the stable (solid lines) and unstable (dashed lines) solutions to (6.11)–(6.12) computed using collocation. A transcritical (TC) bifurcation point appears at $\tilde{c} = 44.1370$ in (a)–(c) as the solutions become degenerate via a non-perpendicular tranverse crossing. The remaining model parameters are set at $\tilde{\alpha} = 1000$ and $\tilde{a} = 12$.

as well to become increasingly narrow (shown in Figure 6.5(d)) before collapsing relatively swiftly (depending on the acceleration of the habitat towards the critical speed) as $\tilde{c}$ approached $\tilde{c}_{crit}$ and its maximum density (shown in Figure 6.5(c)) plummeted. For a species that follows the dynamics of the Logistic Model this would mean there would be an evident warning of the possibility of extinction for the population as the habitat advanced towards the critical speed.

This bifurcation point can be understood as a tipping point of the system, where the population tips towards extirpation. Despite the presence of the bifurcation, this tipping point is indicative of rate-induced tipping (R-tipping) rather than bifurcation-induced tipping (B-tipping), with $\tilde{c}_{crit}$ representing the critical rate. Ashwin et al. [22] show that an R-tipping problem with a steady drift can be reduced to a bifurcation problem in another coordinate system. For our Logistic Model, the R-tipping is a non-autonomous bifurcation in (6.1) that is reduced to a transcritical bifurcation in the comoving frame in (6.6). This R-tipping can be reversed if the speed $\tilde{c}$ decreases below $\tilde{c}_{crit}$ to return to the

non-zero stable state, provided it is reversed when a few individuals still remain to repopulate the habitat.

6.2 The Allee Model

6.2.1 Comoving Frame

In order to study the existence of travelling pulse solutions in the Allee Model, the same approach from Chapter 5 and Section 6.1.1 is taken and an RCDE is derived. Using the comoving frame transformation (5.4)–(5.7), the RDE (6.2) becomes

$$\frac{\partial V}{\partial s} = \frac{\partial^2 V}{\partial \xi^2} + \tilde{c}\,\frac{\partial V}{\partial \xi} - \tilde{\beta}^2 V + 4\tilde{\beta}\,H(\xi;\tilde{a})\,V^2 - V^3, \tag{6.21}$$

with its initial condition (6.3) becoming

$$V(\xi, 0) = V_0(\xi), \tag{6.22}$$

boundary conditions (6.4) becoming

$$\lim_{\xi \to \pm\infty} V(\xi) = 0, \tag{6.23}$$

and habitat function expressed as

$$H(\xi;\tilde{a}) = \frac{\tanh(\tilde{a}\,\xi) - \tanh(\tilde{a}(\xi - 1))}{2\tanh\tilde{a}}. \tag{6.24}$$

The non-trivial stationary solutions $V(\xi)$ of this new transformed IBVP (6.21)–(6.23) correspond to travelling pulse solutions in the form $\tilde{U}(\tilde{x} - \tilde{c}\tilde{t})$ of the original Allee Model IBVP (6.2)–(6.4) [41]. Therefore, to investigate the existence of the travelling pulses in the Allee Model, the time derivative in (6.21) is set to zero

$$\frac{\partial V}{\partial s} = 0, \tag{6.25}$$

and the IBVP for an RCDE (6.21)–(6.23) is simplified to a BVP for the following ODE

$$\frac{d^2 V}{d\xi^2} + \tilde{c}\,\frac{dV}{d\xi} - \tilde{\beta}^2 V + 4\tilde{\beta}\,H(\xi;\tilde{a})\,V^2 - V^3 = 0, \tag{6.26}$$

with Dirichlet boundary conditions

$$\lim_{\xi\to\pm\infty} V(\xi) = 0. \tag{6.27}$$

When $\tilde{c} = 0$, the BVP (6.26)–(6.27) becomes qualitatively identical to (4.15)–(4.16). Thus the solutions found in Section 4.2.2 can be thought of as standing wave solutions to (6.26)–(6.27).

It is instructive to study the phase portrait of the Allee Model, as was done for the Logistic Model in Section 6.1.1. The calculations required to find the invasion speed for the Allee Model are nontrivial, however, and beyond the scope of this thesis. To visualise the full phase portrait of the non-autonomous system, (6.26) is turned into an equivalent system of three first-order autonomous coupled ODEs, as in (5.22) and (7.40), by introducing the dependent variables $W = dV/d\xi$ and $\nu(\xi) = \xi$:

$$\begin{aligned} \frac{dV}{d\xi} &= W, \\ \frac{dW}{d\xi} &= -\tilde{c}\,W + \tilde{\beta}^2 V - 4\tilde{\beta}\,H(\nu;\tilde{a})\,V^2 + V^3, \\ \frac{d\nu}{d\xi} &= 1, \end{aligned} \tag{6.28}$$

together with (6.27), and an additional condition for ν,

$$\lim_{\xi\to\pm\infty} V(\xi) = 0, \quad \nu(\xi = 0) = 0. \tag{6.29}$$

6.2.2 Computing Travelling Pulse Solutions

In the Allee Model up to three travelling pulse solutions $\tilde{U}(\tilde{x} - \tilde{c}\tilde{t})$ of the moving habitat IBVP (6.2)–(6.4) are expected for all values of $\tilde{c}$ as three stationary solutions $\tilde{U}(\tilde{x})$ were found to the static habitat IBVP (4.3)–(4.5) (although a proof for this is not provided). Therefore, up to three equivalent solutions $V(\xi)$ of the BVP (6.26)–(6.27) are expected, including the trivial solution $V \equiv 0$. A collocation method (see Section 7.1.2) is utilised to numerically solve the BVP (6.26)–(6.27) for non-trivial solutions $V(\xi)$ at a range of values of $\tilde{c}$. The approach used is explained in full in Section 7.2.2.2.

The results are displayed in Figure 6.6. Two travelling pulse solutions are obtained for each value of $\tilde{c}$ up to a critical speed $\tilde{c} = \tilde{c}_{crit}$, above which they

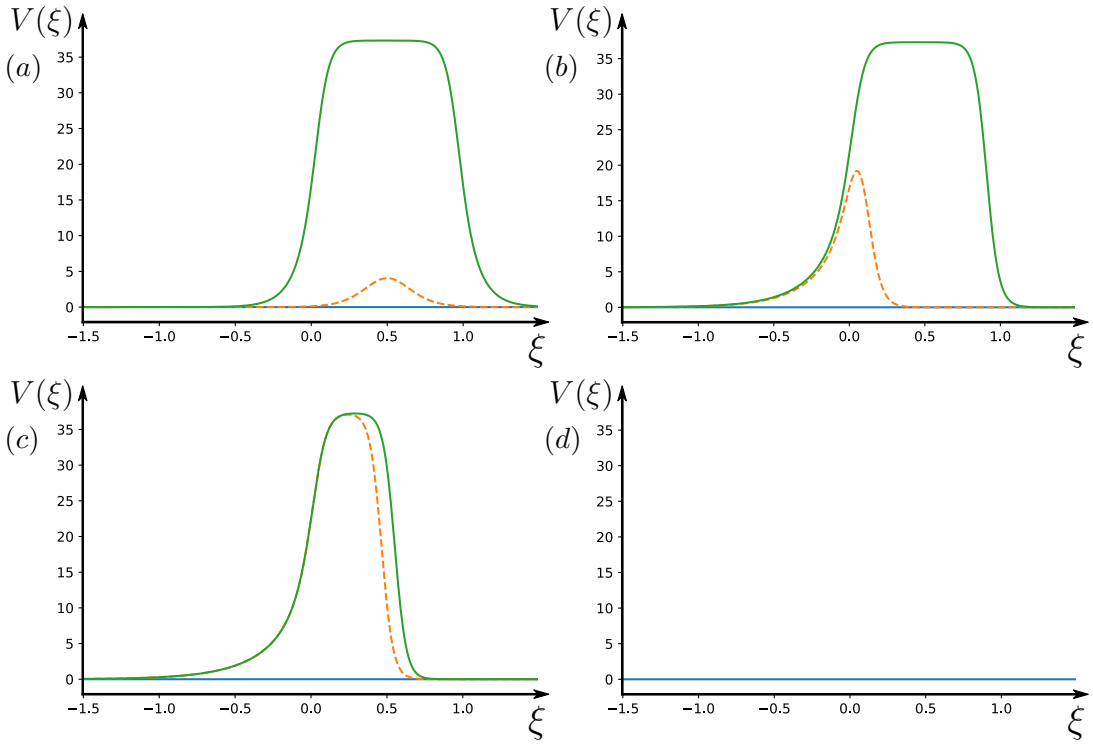


Figure 6.6: Stable (solid lines) and unstable (dashed lines) solutions to (6.26)–(6.27) computed using collocation and plotted in the comoving frame for (a) $\tilde{c} = 0$, (b) $\tilde{c} = 18$, (c) $\tilde{c} = 22.599$, and (d) $\tilde{c} = 22.6$. The remaining model parameters are set at $\tilde{\beta} = 10$ and $\tilde{a} = 12$.

vanish. It is clear the trivial solution (shown in blue) remains unchanged for all $\tilde{c}$. The larger travelling pulse solutions (shown in green) maintain a relatively constant maximum value, and acquire a steep front in the direction of motion and an elongated tail in the opposite direction at higher speeds. The smaller travelling pulse solutions (shown in orange) rise up and collide with the larger travelling pulses, annihilating one another at $\tilde{c} = \tilde{c}_{crit}$. This leaves the trivial solution as the only remaining physical solution for $\tilde{c} > \tilde{c}_{crit}$.

The corresponding phase portraits for (6.28)–(6.29) are shown in Figure 6.7, with two-dimensional projections of the trajectories displayed on the left-hand side of each plot and in Figure 6.8. Under the parameter variation of $\tilde{c}$ two topologically nonequivalent phase portraits appear to emerge for $\tilde{c} \leq 22.599$ and for $\tilde{c} \geq 22.6$. Therefore, a bifurcation occurs at a point between $22.599 < \tilde{c}_{crit} < 22.6$.

6.2.3 Stability Analysis of Travelling Pulse Solutions

Similar to the stability analysis conducted in Chapter 4, no analytical stability analysis can be performed on the solutions to (6.26)–(6.27) but the MOL is

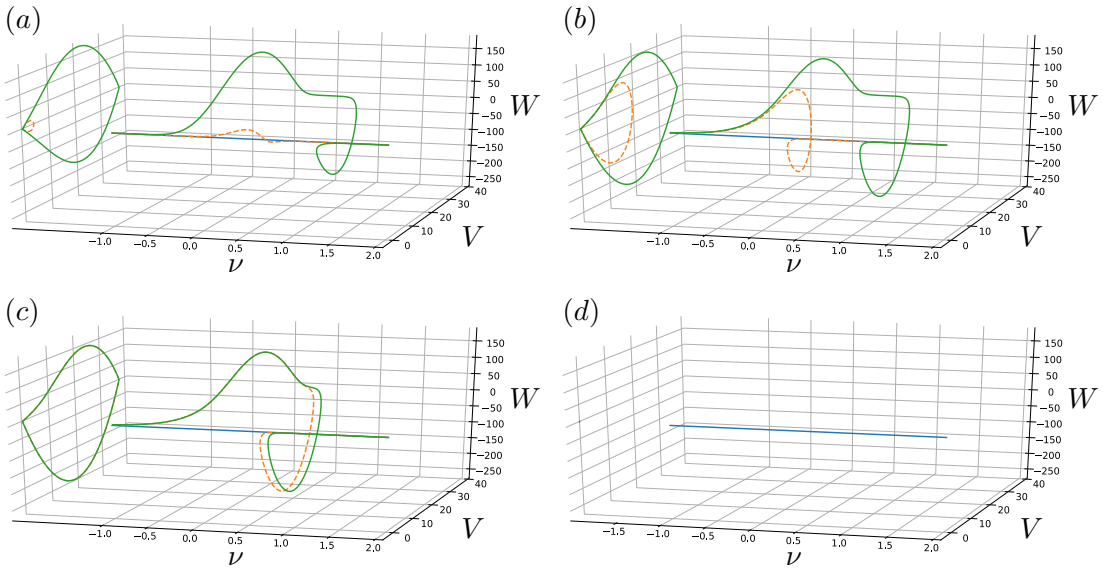


Figure 6.7: Phase portraits of (6.28)–(6.29), where trajectories were numerically computed using collocation. Stable (solid lines) and unstable (dashed lines) solutions are plotted between $\nu \in [-1, 2]$ in three-dimensional phase space and a projection on a two-dimensional plane of V vs. W is displayed on the left hand side of the figure for (a) $\tilde{c} = 0$, (b) $\tilde{c} = 18$, (c) $\tilde{c} = 22.599$, and (d) $\tilde{c} = 22.6$. The remaining model parameters are set at $\tilde{\beta} = 10$ and $\tilde{a} = 12$.

utilised again to analyse the stability numerically. The IBVP in the comoving frame (6.21)–(6.23) is solved for a range of values of $\tilde{c}$ using an initial solutions given by the following rectangular functions

$$V_0(\xi) = \begin{cases} 0 & \xi < -1 \text{ and } \xi > 2 \\ 2 & -1 \leq \xi \leq 2, \end{cases} \tag{6.30}$$

and,

$$V_0(\xi) = \begin{cases} 0 & \xi < -1 \text{ and } \xi > 2 \\ 5 & -1 \leq \xi \leq 2. \end{cases} \tag{6.31}$$

The results using initial solution (6.30) (shown in blue) are displayed in Figure 6.9(a_1) with $\tilde{c} = 18$ taken as an example. For all values of $\tilde{c}$ with this initial solution, a long-term solution (shown in black) given by the trivial solution $V \equiv 0$ is converged to as $s \to \infty$, suggesting it is always locally stable. For initial solution (6.31) (again shown in blue) results are displayed in Figures 6.9(a_2), 6.9(b), and 6.9(c) for $\tilde{c} = 18$, $\tilde{c} = 22.599$, and $\tilde{c} = 22.6$ respectively. In Figures 6.9(a_2) and 6.9(b), the intermediate-time solutions quickly rise up to their long-term shapes (again shown in black) given by the larger travelling pulse solution of BVP (6.26)–(6.27), which is shown in green in Figures 6.6(b)

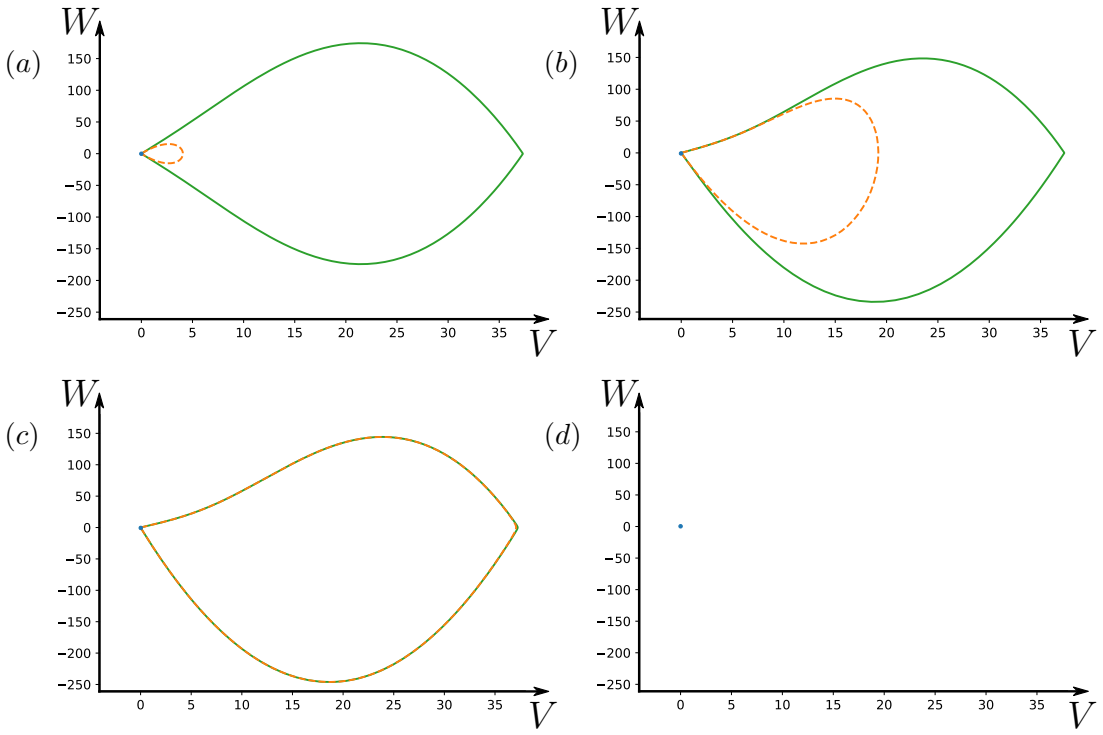


Figure 6.8: Projection of the phase portraits of (6.28)–(6.29) on a two-dimensional plane of V vs. W, where trajectories were numerically computed using collocation. Stable (solid lines) and unstable (dashed lines) solutions are plotted for (a) $\tilde{c} = 0$, (b) $\tilde{c} = 18$, (c) $\tilde{c} = 22.599$, and (d) $\tilde{c} = 22.6$. The remaining model parameters are set at $\tilde{\beta} = 10$ and $\tilde{a} = 12$.

and 6.6(c) for $\tilde{c} = 18$ and $\tilde{c} = 22.599$ respectively. Finally in Figure 6.9(c) the solution is attracted towards the location of the long-term solutions seen in the previous two subplots 6.6(b) and 6.6(c). It remains closeby for an extended period before swiftly falling to $V \equiv 0$, the only remaining stationary solution of IBVP (6.21)–(6.23) for $\tilde{c} > \tilde{c}_{crit}$.

The forward-time numerical integration results suggest that the larger travelling pulse solutions, shown in green in Figure 6.6, are always locally stable while they exist for $\tilde{c} < \tilde{c}_{crit}$. The smaller travelling pulse solutions appear to repel solutions towards one of the other stationary solutions of (6.21)–(6.23), implying they are unstable. The trivial solution remains locally stable up to the bifurcation point before becoming globally stable for $\tilde{c} > \tilde{c}_{crit}$ after the bifurcation of the travelling pulses.

6.2.4 Saddle-Node Bifurcation of Travelling Pulses

In Figures 6.6, 6.7, 6.8, and 6.9, it is clear a bifurcation occurs at the critical speed $22.599 < \tilde{c}_{crit} < 22.6$. Bifurcation analysis is performed which finds the

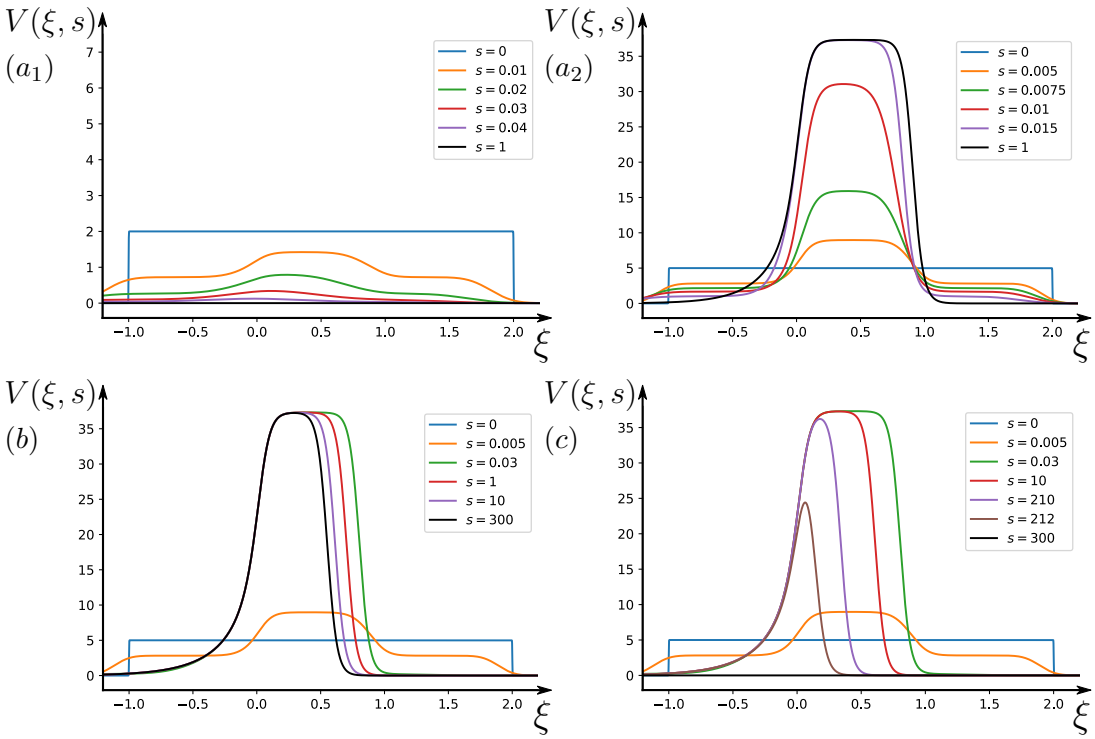


Figure 6.9: Numerical solutions to the IBVP (6.21)–(6.23) computed using the MOL at various values of s using initial solution (6.30) shown in blue and the long-term solution shown in black for (a_1) $\tilde{c} = 18$, and using initial solution (6.31) shown in blue for (a_2) $\tilde{c} = 18$, (b) $\tilde{c} = 22.599$, and (c) $\tilde{c} = 22.6$. The remaining model parameters are set at $\tilde{\beta} = 10$ and $\tilde{a} = 12$.

bifurcation point to be $\tilde{c}_{crit} = 22.5995$, above which, similar to the Logistic Model in Section 6.1.4, only a stable solution at zero remains and the population dies out. This can be seen in the bifurcation diagrams of Figure 6.10 for the total populations

$$P_{tot}(\tilde{c}) = \int_{-\infty}^{\infty} V(\xi; \tilde{c})\, d\xi, \tag{6.32}$$

L^2 norms

$$\|V(\xi; \tilde{c})\| = \sqrt{\int_{-\infty}^{\infty} V^2(\xi; \tilde{c})\, d\xi}, \tag{6.33}$$

maximum values

$$V_{max}(\tilde{c}) = \max_{\xi \in \mathbb{R}} V(\xi; \tilde{c}), \tag{6.34}$$

and FWHM values

$$FWHM(\tilde{c}) = |\xi_2(\tilde{c}) - \xi_1(\tilde{c})|, \tag{6.35}$$

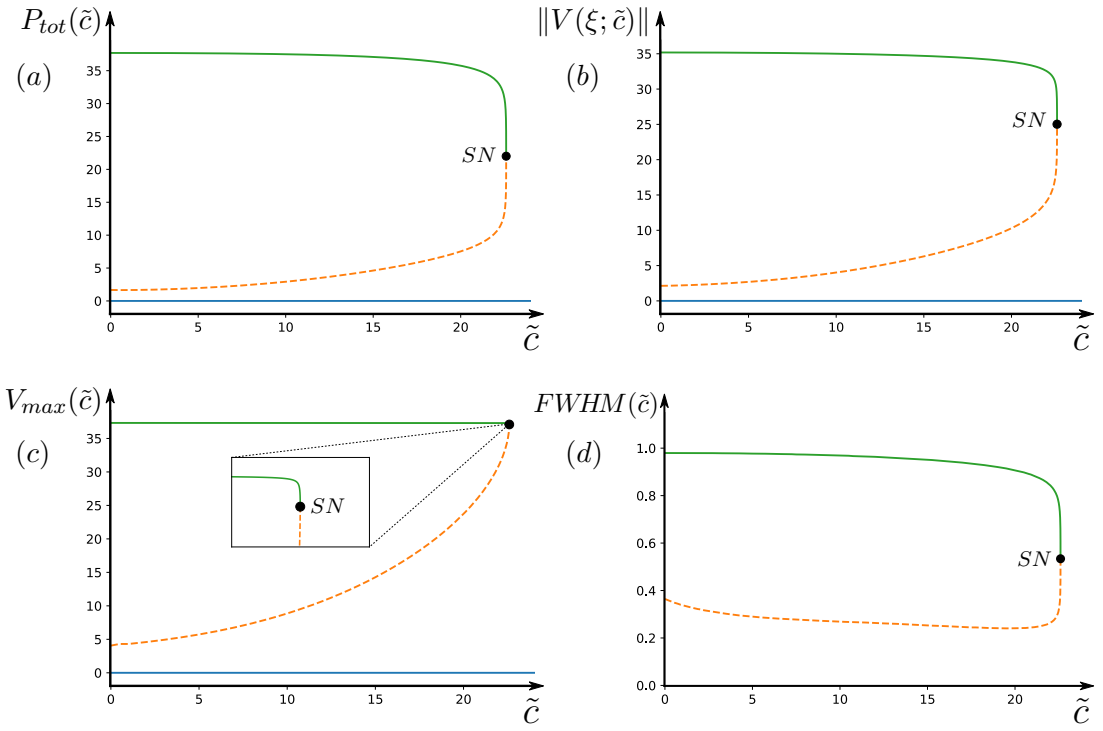


Figure 6.10: One-parameter bifurcation diagrams with speed parameter $\tilde{c}$ for the (a) total population (6.32), (b) L^2 norm (6.33), (c) maximum value (6.34), and (d) FWHM (6.35) of the stable (solid lines) and unstable (dashed lines) solutions to (6.26)–(6.27) computed using collocation. A saddle-node (SN) bifurcation appears at $\tilde{c} = 22.5995$ for all. The remaining model parameters are set at $\tilde{\beta} = 10$ and $\tilde{a} = 12$.

of the solutions to (6.26)–(6.27), where $\xi_1(\tilde{c})$ and $\xi_2(\tilde{c})$ are defined implicitly as the two values of ξ at which $V(\xi;\tilde{c})$ equals half of its maximum value

$$V(\xi_1;\tilde{c}) = V(\xi_2;\tilde{c}) = \frac{V_{max}(\tilde{c})}{2}. \tag{6.36}$$

As is evident in Figure 6.10, the Allee Model differs from the Logistic Model as the trivial solution (shown in blue) is not involved in the bifurcation. Instead its unstable travelling pulse solutions (shown in orange) and stable travelling pulse solutions (shown in green) collide at $\tilde{c}_{crit} \approx 22.5995$ and annihilate each other. This infers that a saddle-node bifurcation occurs at $\tilde{c} = \tilde{c}_{crit}$.

From the point of view of an observer the species would appear to keep pace with the moving habitat. The population (shown in Figure 6.10(a)) remains almost static with no advanced warning of collapse while the habitat accelerates towards the critical speed $\tilde{c}_{crit}$ and its maximum density (shown in Figure 6.10(c)) remains constant. In nature, the unstable travelling pulse solutions would not be detectable and thus, as this critical speed is reached, the species

population would suddenly drop before inexplicably dying out from the perspective of the observer at the saddle-node bifurcation point.

This contrasts with the Logistic Model, since a species following the dynamics of that model appears to be able to sustain itself at a largely reduced population (as is evident in Figure 6.1(c) and Figure 6.5) when at higher speeds just below its own critical speed. A species following the Allee Model does not appear to share this attribute. In fact, a relatively healthy population profile is maintained up to the critical speed, as shown in green in Figure 6.6(c), before the population quite suddenly dips and collapses in Figures 6.10(a) and 6.10(b). A R-tipping point exists at this bifurcation point $\tilde{c}_{crit}$ for the Allee Model which may cause the species in this habitat to spontaneously collapse to extinction.

Similarly to the Logistic Model, this R-tipping is a non-autonomous bifurcation in (6.2) reduced to a saddle-node bifurcation in (6.21). It is also possible to reverse R-tipping in the Allee Model if a decrease in the speed $\tilde{c}$ makes the system return to the non-zero stable state (provided once again that the entire population hasn't yet perished). However, this may require a very fast decrease in $\tilde{c}$ and therefore R-tipping will typically not be reversed under decreasing speed in the Allee Model.

Chapter 7

Solving Differential Equations

In this chapter, the numerical methods used to solve the IBVPs and BVPs in Chapters 4–6 are explored. Code snippets from all methods will be included in the appendix.

7.1 Numerical Methods

7.1.1 IBVPs for PDEs

Finite difference methods (FDMs) are a popular means of solving differential equations and are especially useful in solving PDEs. A FDM may require discretising all or some of the independent variables in a given differential equation and substituting in a finite difference approximation in place of at least one of the derivatives. These approximate derivatives allow the PDE to be transformed into a system of algebraic equations, using methods such as the forward-time centered-space method [44, 45] or the Crank-Nicholson method [46, 45]. For this project, however, a different approach is used with the method of lines (MOL).

The MOL can be seen as a refinement of standard explicit and implicit PDE FDMs. Instead of discretising both time and space and using finite differences to transform the PDE into a system of algebraic equations it requires space alone to be discretised to create a system of initial value problems (IVPs) with coupled ODEs defined at each discrete value in space. This allows the MOL to make use of existing and quite well established numerical methods for IVPs such as Runge-Kutta methods or backward differentiation formula (BDF) methods.

For the majority of the numerical integration in this project Python was utilised to create a system of ODEs which could be solved with the inbuilt IVP solver from Python's SciPy library "integrate.solve_ivp" [47] (see Section 9.1.1.2). Within this solver the BDF integration method was selected, which is an implicit variable-order (1 to 5) method and among the most popular multistep methods for stiff problems [48].

Towards the end of the project an MOL solver was discovered within Mathematica's inbuilt "NDSolve" [49], which created and solved the system of IVPs all within the one function (see Section 9.1.2.1). This proved to significantly decrease computational runtime in comparison to the Python method, particularly in the moving habitat as the problems became more stiff at values of $\tilde{c}$ near the bifurcation point $\tilde{c}_{crit}$ of each model. Within NDSolve the BDF option was once again selected with default precision used. The resulting data was then imported back into Python.

7.1.2 BVPs for ODEs

Standard numerical methods for solving a two-point BVP for an ODE include shooting methods, FDMs, and collocation methods. Shooting methods turn the BVP into an IVP by choosing an appropriate boundary as the initial value and using an IVP solver to "shoot" for the other boundary and iteratively converge to the solution of the original BVP. Due to the stiffness of the ODEs that appear throughout this thesis, however, a more robust method is necessary to solve them. Any explicit FDM or Runge-Kutta methods also prove to frequently cause numerical instabilities in the solutions for this reason, therefore an implicit method must be employed.

Python was utilised once again and an inbuilt BVP solver from Python's SciPy library "integrate.solve_bvp" [50] was selected (see Section 9.1.1.1). This function solves a first-order system of ODEs by implementing an optimised fourth order collocation algorithm (which is equivalent to the 3-stage Lobatto IIIA implicit Runge-Kutta formula [51]).

In its simplest form, collocation involves choosing a continuous function (typically a polynomial), a set of collocation points, and requires that the function satisfies the given problem at the collocation points [48]. This can be made much more accurate by dividing the domain within which the solution exists into a mesh of subintervals, then constructing a piecewise function that is continuous up to a certain degree and which satisfies the problem at a number

of collocation points within each subinterval.

SciPy's "solve_bvp" function constructs a C^1 piecewise cubic polynomial function that collocates at the midpoint and boundaries of each subinterval [51]. It then measures the residuals over each subinterval and may repeat the same process again with more nodes added each time until it either fails when the maximum number of nodes is exceeded or succeeds in converging to a solution when the residuals fall below a certain tolerance.

7.2 Existence of Solutions

7.2.1 Computing Stationary Solutions

7.2.1.1 The Logistic Model

For the Logistic Model in the static habitat the RDE (4.2) is reintroduced

$$\frac{\partial \tilde{U}}{\partial \tilde{t}} = \frac{\partial^2 \tilde{U}}{\partial \tilde{x}^2} + \tilde{\alpha}\left(H(\tilde{x};\tilde{a}) - \frac{1}{2}\right)\tilde{U} - \tilde{U}^2, \tag{7.1}$$

with its initial condition (4.4)

$$\tilde{U}(\tilde{x},0) = \tilde{U}_0(\tilde{x}), \tag{7.2}$$

Dirichlet boundary conditions (4.5)

$$\lim_{\tilde{x}\to\pm\infty} \tilde{U}(\tilde{x},\tilde{t}) = 0, \tag{7.3}$$

where the habitat function is expressed as

$$H(\tilde{x};\tilde{a}) = \frac{\tanh(\tilde{a}\tilde{x}) - \tanh(\tilde{a}(\tilde{x}-1))}{2\tanh\tilde{a}}. \tag{7.4}$$

There are two stationary solutions to the IBVP (7.1)–(7.3): the trivial solution of $\tilde{U} \equiv 0$ and a non-zero solution. As the non-zero solution is expected to be stable, the MOL is chosen to find this non-zero solution.

To implement the MOL a fixed spatial increment is first introduced

$$k = \Delta\tilde{x}, \tag{7.5}$$

which can be used to expand $\tilde{U}(\tilde{x}+k,\tilde{t})$ and $\tilde{U}(\tilde{x}-k,\tilde{t})$ in a Taylor Series

about $\tilde{x}$,

$$\tilde{U}(\tilde{x}+k) = \tilde{U}(\tilde{x}) + k\tilde{U}_{\tilde{x}}(\tilde{x}) + \frac{k^2}{2}\tilde{U}_{\tilde{x}\tilde{x}}(\tilde{x}) + \frac{k^3}{6}\tilde{U}_{\tilde{x}\tilde{x}\tilde{x}}(\tilde{x}) + O(k^4), \tag{7.6}$$

$$\tilde{U}(\tilde{x}-k) = \tilde{U}(\tilde{x}) - k\tilde{U}_{\tilde{x}}(\tilde{x}) + \frac{k^2}{2}\tilde{U}_{\tilde{x}\tilde{x}}(\tilde{x}) - \frac{k^3}{6}\tilde{U}_{\tilde{x}\tilde{x}\tilde{x}}(\tilde{x}) + O(k^4), \tag{7.7}$$

where $\tilde{U}_{\tilde{x}} = \frac{\partial \tilde{U}}{\partial \tilde{x}}$, $\tilde{U}_{\tilde{x}\tilde{x}} = \frac{\partial^2 \tilde{U}}{\partial \tilde{x}^2}$,..., and the second argument of $\tilde{U}$ is dropped for convenience. These can be subtracted to give

$$\tilde{U}(\tilde{x}+k) - \tilde{U}(\tilde{x}-k) = 2k\tilde{U}_{\tilde{x}}(\tilde{x}) + O(k^3), \tag{7.8}$$

which can be rearranged to obtain a central difference approximation for $\tilde{U}_{\tilde{x}}$

$$\frac{\partial \tilde{U}}{\partial \tilde{x}} = \tilde{U}_{\tilde{x}}(\tilde{x}) = \frac{1}{2k}\Big(\tilde{U}(\tilde{x}+k) - \tilde{U}(\tilde{x}-k)\Big) + O(k^2), \tag{7.9}$$

or added together to give,

$$\tilde{U}(\tilde{x}+k) + \tilde{U}(\tilde{x}-k) = 2\tilde{U}(\tilde{x}) + k^2\tilde{U}_{\tilde{x}\tilde{x}}(\tilde{x}) + O(k^4), \tag{7.10}$$

which can be rearranged to obtain a central difference approximation for $\tilde{U}_{\tilde{x}\tilde{x}}$

$$\frac{\partial^2 \tilde{U}}{\partial \tilde{x}^2} = \tilde{U}_{\tilde{x}\tilde{x}}(\tilde{x}) = \frac{1}{k^2}\Big(\tilde{U}(\tilde{x}+k) - 2\tilde{U}(\tilde{x}) + \tilde{U}(\tilde{x}-k)\Big) + O(k^2). \tag{7.11}$$

Before discretising the IBVP, the spatial domain must be truncated. The boundary conditions (7.3) are defined on an infinite domain $\tilde{x} \in (-\infty, \infty)$ and cannot be practically imposed in these numerical computations so they must be approximated with a sufficiently large finite ones. The finite domain $\tilde{x} \in [-\tilde{B}, \tilde{B}+1\,]$ is introduced for a large enough integer $\tilde{B}$, where $\tilde{B}$ becomes the shortest distance from each edge of the good habitat at $\tilde{x}=0$ and $\tilde{x}=1$ to the left and right boundaries of the domain respectively, such that the boundary conditions (7.3) can be approximated as

$$\tilde{U}(\tilde{x} = -\tilde{B}, \tilde{t}) = \tilde{U}(\tilde{x} = \tilde{B}+1, \tilde{t}) = 0. \tag{7.12}$$

The spatial variable can then be discretised as follows

$$\tilde{x}_i = ik - \tilde{B} \quad (i = 0, 1, 2, ...N), \tag{7.13}$$

where $Nk = 2\tilde{B} + 1$, and the dependent variable can thus be expressed as

$$\tilde{U}_i(t) = \tilde{U}(\tilde{x}_i, \tilde{t}). \tag{7.14}$$

These discretised variables, along with equation (7.11), are substituted into (7.1), such that for $i \in \{1, 2, ...N-1\}$,

$$\frac{d\tilde{U}_i}{d\tilde{t}} = \frac{\tilde{U}_{i+1} - 2\tilde{U}_i + \tilde{U}_{i-1}}{k^2} + \tilde{\alpha}\left(H(\tilde{x}_i; \tilde{a}) - \frac{1}{2}\right)\tilde{U}_i - \tilde{U}_i^2, \tag{7.15}$$

with initial condition (7.2) becoming

$$\tilde{U}_i(0) = \tilde{U}_{i\,0} = \tilde{U}_0(\tilde{x}_i), \tag{7.16}$$

and finite boundary conditions (7.12) becoming

$$\tilde{U}_{i=0}(\tilde{t}) = \tilde{U}_{i=N}(\tilde{t}) = 0. \tag{7.17}$$

such that the ODEs at $i = 0$ and $i = N$ are not required. To incorporate these Dirichlet boundary conditions (7.17) into the MOL two unique ODEs are defined for $i = 1$ and $i = N-1$ such that a simple set of $N-1$ IVPs approximating the IBVP (7.1)–(7.3) for the MOL can be inserted into the IVP solver. The full system is defined as follows:

for $i = 1$ the ODE is

$$\frac{d\tilde{U}_i}{d\tilde{t}} = \frac{\tilde{U}_{i+1} - 2\tilde{U}_i}{k^2} + \tilde{\alpha}\left(H(\tilde{x}_i; \tilde{a}) - \frac{1}{2}\right)\tilde{U}_i - \tilde{U}_i^2, \tag{7.18}$$

for $i = N-1$ the ODE is

$$\frac{d\tilde{U}_i}{d\tilde{t}} = \frac{-2\tilde{U}_i + \tilde{U}_{i-1}}{k^2} + \tilde{\alpha}\left(H(\tilde{x}_i; \tilde{a}) - \frac{1}{2}\right)\tilde{U}_i - \tilde{U}_i^2, \tag{7.19}$$

and for $i = 2, 3, ..., N-2$ the ODE is

$$\frac{d\tilde{U}_i}{d\tilde{t}} = \frac{\tilde{U}_{i+1} - 2\tilde{U}_i + \tilde{U}_{i-1}}{k^2} + \tilde{\alpha}\left(H(\tilde{x}_i; \tilde{a}) - \frac{1}{2}\right)\tilde{U}_i - \tilde{U}_i^2, \tag{7.20}$$

with initial condition for $i = 1, 2, ..., N-1$

$$\tilde{U}_i(0) = \tilde{U}_{i\,0} = \tilde{U}_0(\tilde{x}_i), \tag{7.21}$$

and the habitat function expressed as

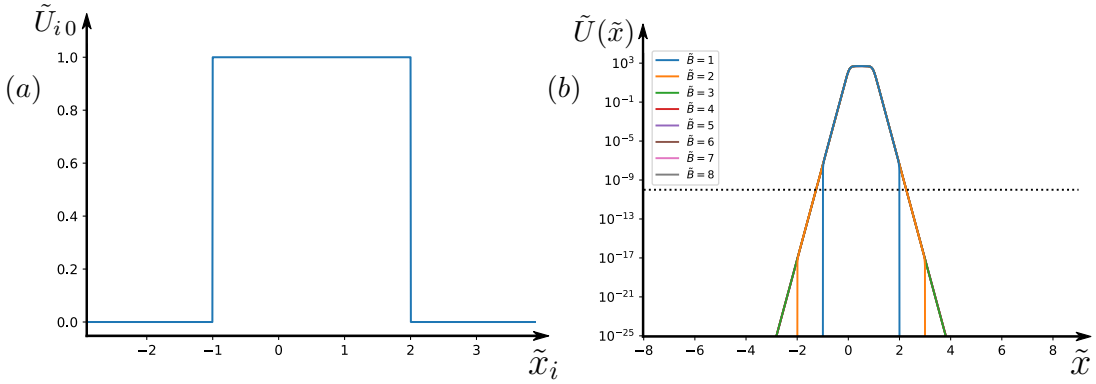


Figure 7.1: (a) Rectangular function (7.23) used as an initial solution for (7.25) with a plateau at $\tilde{u} = 1.0$. (b) Long-term solutions to the system of IVPs (7.18)–(7.21), found using initial solution (7.23) with a plateau at $\tilde{u} = 1.0$, integration time $\tilde{t} = 1$, and plotted logarithmically for various values of $\tilde{B}$. The dotted black line represents the threshold of $\varepsilon = 10^{-10}$ below which the value of $\tilde{U}(\tilde{x}, \tilde{t})$ can jump to zero. The remaining parameters are set at $\tilde{\alpha} = 1000$, $\tilde{a} = 12$, and $k = 0.005$.

$$H(\tilde{x}_i; \tilde{a}) = \frac{\tanh(\tilde{a}\tilde{x}_i) - \tanh(\tilde{a}(\tilde{x}_i - 1))}{2\tanh\tilde{a}}. \tag{7.22}$$

For the initial condition (7.21) a simple rectangular initial solution is chosen with a non-zero constant $\tilde{u}$ in the centre of the domain and a zero value everywhere else:

$$\tilde{U}_{i\,0} = \tilde{U}_0(\tilde{x}_i) = \begin{cases} 0 & \tilde{x}_i < -1 \text{ and } \tilde{x}_i > 2 \\ \tilde{u} & -1 \leq \tilde{x}_i \leq 2. \end{cases} \tag{7.23}$$

This function is displayed in Figure 7.1(a).

An appropriate value of $\tilde{B}$ for the finite domain $\tilde{x}_i \in [-\tilde{B}, \tilde{B} + 1]$ is one minimised for computational efficiency but large enough such that the boundary conditions (7.17) can be imposed without adversely affecting the final solution. As the solutions only tend towards zero as $\tilde{x} \to \pm\infty$, an artificial jump will exist between the imposed zero values at $\tilde{U}_{i=0}(\tilde{t})$ and $\tilde{U}_{i=N}(\tilde{t})$, and the non-zero values at $\tilde{U}_{i=1}(\tilde{t})$ and $\tilde{U}_{i=N-1}(\tilde{t})$ respectively, regardless of how large the finite $\tilde{B}$ is. To mitigate this a finite threshold value of $\varepsilon = 10^{-10}$ is chosen and a value of $\tilde{B}$ must therefore be found such that this jump is smaller than ε; i.e., $\tilde{U}_{i=1}(\tilde{t})$ and $\tilde{U}_{i=N-1}(\tilde{t})$ remain below this threshold value for all $\tilde{t}$.

To find this suitable value of $\tilde{B}$ SciPy's "solve_ivp" function is used to solve the set of IVPs (7.18)–(7.21) using $k = 0.005$ and an integration time of $\tilde{t} = 1$ for a range of integer values of $\tilde{B}$. These results can be seen in Figure 7.1(b) in

logarithmic plots. It's clear that for $\tilde{B} \gtrsim 1.2$ the solutions naturally fall below $\varepsilon = 10^{-10}$ before reaching the imposed zero boundary values at $\tilde{x} = -\tilde{B}$ and $\tilde{x} = \tilde{B} + 1$. Therefore, the lowest integer value $\tilde{B} = 2$ is chosen for computational efficiency.

7.2.1.2 The Allee Model

For the Allee Model in the static habitat the RDE (4.3) is reintroduced

$$\frac{\partial \tilde{U}}{\partial \tilde{t}} = \frac{\partial^2 \tilde{U}}{\partial \tilde{x}^2} - \tilde{\beta}^2 \tilde{U} + 4\tilde{\beta}\, H(\tilde{x}; \tilde{a})\, \tilde{U}^2 - \tilde{U}^3, \tag{7.24}$$

with its initial condition (4.4)

$$\tilde{U}(\tilde{x}, 0) = \tilde{U}_0(\tilde{x}), \tag{7.25}$$

Dirichlet boundary conditions (4.5)

$$\lim_{\tilde{x} \to \pm\infty} \tilde{U}(\tilde{x}, \tilde{t}) = 0, \tag{7.26}$$

where the habitat function is expressed as

$$H(\tilde{x}; \tilde{a}) = \frac{\tanh(\tilde{a}\tilde{x}) - \tanh(\tilde{a}(\tilde{x} - 1))}{2 \tanh \tilde{a}}. \tag{7.27}$$

The trivial solution is once again $\tilde{U} \equiv 0$ but there are now two non-zero stationary solutions to this IBVP (7.24)–(7.26). Following the approach taken in Section 7.2.1.1 the MOL only recovered stable solutions, however, and an unstable non-zero solution remained missing. This motivated the search for an alternative method that could recover any unstable solutions which culminated in setting the time derivative in the RDE (7.24) to zero, thus turning the IBVP (7.24)–(7.26) into the BVP (4.15)–(4.16) repeated here for convenience:

$$\frac{d^2 \tilde{U}}{d\tilde{x}^2} = \tilde{\beta}^2 \tilde{U} - 4\tilde{\beta}\, H(\tilde{x}; \tilde{a})\, \tilde{U}^2 + \tilde{U}^3, \tag{7.28}$$

with the Dirichlet boundary conditions,

$$\lim_{\tilde{x} \to \pm\infty} \tilde{U}(\tilde{x}) = 0, \tag{7.29}$$

and choosing a collocation method to solve the BVP.

The SciPy library in Python includes the "solve_bvp" function that solves

first-order BVP systems. The second-order ODE (7.28) is therefore turned into an equivalent system of first-order coupled ODEs where $\tilde{U}_{\mathrm{I}}(\tilde{x}) = \tilde{U}(\tilde{x})$ and $\tilde{U}_{\mathrm{II}}(\tilde{x}) = \frac{d\tilde{U}}{d\tilde{x}}$,

$$\begin{aligned} \frac{d\tilde{U}_{\mathrm{I}}}{d\tilde{x}} &= \tilde{U}_{\mathrm{II}}, \\ \frac{d\tilde{U}_{\mathrm{II}}}{d\tilde{x}} &= \tilde{\beta}^2\tilde{U}_{\mathrm{I}} - 4\tilde{\beta}\, H(\tilde{x};\tilde{a})\, \tilde{U}_{\mathrm{I}}^2 + \tilde{U}_{\mathrm{I}}^3. \end{aligned} \tag{7.30}$$

The infinite interval $\tilde{x} \in (-\infty, \infty)$ must also once again be replaced with a finite one $\tilde{x} \in [-\tilde{B}, \tilde{B}+1\,]$ for large enough $\tilde{B}$. The boundary conditions (7.29) can thus be approximated as

$$\tilde{U}_{\mathrm{I}}(\tilde{x} = -\tilde{B}) = \tilde{U}_{\mathrm{I}}(\tilde{x} = \tilde{B}+1) = 0. \tag{7.31}$$

Initial guesses $\tilde{U}_{\mathrm{I}\,G_U}(\tilde{x})$, $\tilde{U}_{\mathrm{II}\,G_U}(\tilde{x})$, and $\tilde{U}_{\mathrm{I}\,G_S}(\tilde{x})$, $\tilde{U}_{\mathrm{II}\,G_S}(\tilde{x})$ are defined to compute the non-zero solutions $\tilde{U}_{\mathrm{I}\,U}(\tilde{x})$, $\tilde{U}_{\mathrm{II}\,U}(\tilde{x})$, and $\tilde{U}_{\mathrm{I}\,S}(\tilde{x})$, $\tilde{U}_{\mathrm{II}\,S}(\tilde{x})$ of (7.30)–(7.31) respectively. The first initial guess $\tilde{U}_{\mathrm{I}\,G_U}(\tilde{x})$ (solid orange line in Figure 7.2(a)) requires a specific Gaussian function to obtain the smaller of the two solutions. This function has a peak close to the centre of the solution's corresponding unstable equilibrium $\tilde{U}_2^*(\tilde{x})$ from (4.8)

$$\tilde{U}_{\mathrm{I}\,G_U}(\tilde{x}) = \begin{cases} 0 & \tilde{x} < -1 \text{ and } \tilde{x} > 2 \\ \frac{3}{2}\left(\tilde{U}_2^*(\tilde{x}=0.5)\right) e^{-\frac{(\tilde{x}-0.5)^2}{2D}} & -1 \le \tilde{x} \le 2, \end{cases} \tag{7.32}$$

where the value for D is taken from Table 3.2, and $\tilde{U}_{\mathrm{II}\,G_U}(\tilde{x})$ is defined as its derivative

$$\tilde{U}_{\mathrm{II}\,G_U}(\tilde{x}) = \frac{d}{d\tilde{x}}\tilde{U}_{\mathrm{I}\,G_U}(\tilde{x}). \tag{7.33}$$

The second initial guess $\tilde{U}_{\mathrm{I}\,G_S}(\tilde{x})$ (solid green line in Figure 7.2(a)) uses a simpler rectangular function constructed with a plateau at the level of the centre of its corresponding stable equilibrium $\tilde{U}_3^*(\tilde{x})$ from (4.8)

$$\tilde{U}_{\mathrm{I}\,G_S}(\tilde{x}) = \begin{cases} 0 & \tilde{x} < 0 \text{ and } \tilde{x} > 1 \\ \tilde{U}_3^*(\tilde{x}=0.5) & 0 \le \tilde{x} \le 1, \end{cases} \tag{7.34}$$

and again $\tilde{U}_{\mathrm{II}\,G_S}(\tilde{x})$ is defined as its derivative

$$\tilde{U}_{\mathrm{II}\,G_S}(\tilde{x}) = \frac{d}{d\tilde{x}}\tilde{U}_{\mathrm{I}\,G_S}(\tilde{x}). \tag{7.35}$$

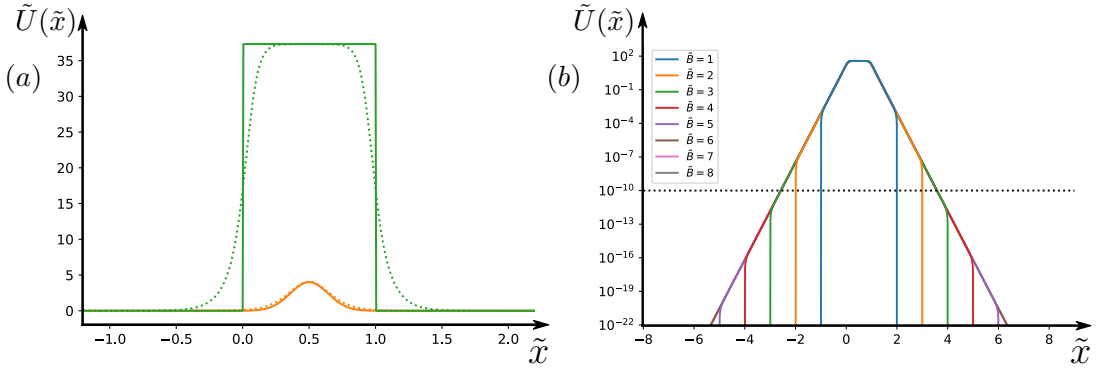


Figure 7.2: (a) Initial guesses for the unstable solution (7.32) (solid orange line) and stable solution (7.34) (solid green line) in the static habitat, with their respective final stationary solutions (dotted orange and green lines) of the IBVP (7.24)–(7.26), computed by solving the BVP (7.30)–(7.31) using the collocation method. (b) Solutions $\tilde{U}_{\mathrm{I}}(\tilde{x})$ of the BVP (7.30)–(7.31) computed using collocation with initial guess (7.34) and plotted logarithmically for various values of $\tilde{B}$. The dotted black line represents the threshold of $\varepsilon = 10^{-10}$ below which the value of $\tilde{U}_{\mathrm{I}}(\tilde{x})$ can jump to zero. The remaining parameters are set at $\tilde{\beta} = 10$, $\tilde{a} = 12$, and $k = 0.005$.

To calculate a suitable value for $\tilde{B}$ in the Allee Model, SciPy's "solve_bvp" function is used to solve the BVP (7.30)–(7.31) using $k = 0.005$ and the initial guesses $\tilde{U}_{\mathrm{I}\,G_U}(\tilde{x})$, $\tilde{U}_{\mathrm{II}\,G_U}(\tilde{x})$, and $\tilde{U}_{\mathrm{I}\,G_S}(\tilde{x})$, $\tilde{U}_{\mathrm{II}\,G_S}(\tilde{x})$ for a range of values of $\tilde{B}$.

These results can be seen in Figure 7.2(b) in logarithmic plots. It's clear that for $\tilde{B} \gtrsim 2.5$ the solutions naturally fall below the threshold $\varepsilon = 10^{-10}$ as $\tilde{x}$ tends towards the imposed zero boundary values. Therefore, the lowest integer value $\tilde{B} = 3$ is chosen for the static habitat Allee Model.

7.2.2 Computing Travelling Pulse Solutions

To compute the travelling pulse solutions the same collocation method introduced in Section 7.2.1.2 is used to solve the BVP given by the general travelling wave ODE (5.12)

$$\frac{d^2V}{d\xi^2} + \tilde{c}\,\frac{dV}{d\xi} + \tilde{f}(V,\xi) = 0, \tag{7.36}$$

and its Dirichlet boundary conditions (5.13)

$$\lim_{\xi \to \pm\infty} V(\xi) = 0, \tag{7.37}$$

for each model.

An infinite interval $\xi \in (-\infty, \infty)$ in the boundary conditions must once again be replaced by a finite one. This finite domain will be asymmetric, owing to the addition of the convective term, as a steep front forms in the direction of motion of the travelling pulses and a tail forms in their wake. Therefore, a finite interval $\xi \in [-\Omega_L, \Omega_R + 1\,]$ is introduced for sufficiently large Ω_L and Ω_R, such that the boundary conditions are approximated as

$$V(-\Omega_L) = V(\Omega_R + 1) = 0. \tag{7.38}$$

7.2.2.1 The Logistic Model

For the Logistic Model the ODE (7.36) becomes (6.11)

$$\frac{d^2V}{d\xi^2} + \tilde{c}\,\frac{dV}{d\xi} + \tilde{\alpha}\left(H(\xi;\tilde{a}) - \frac{1}{2}\right)V - V^2 = 0, \tag{7.39}$$

which, to be solved in Python, must once again be expressed as an equivalent system of first-order coupled ODEs,

$$\begin{aligned} \frac{dV}{d\xi} &= W, \\ \frac{dW}{d\xi} &= -\tilde{c}\,W - \tilde{\alpha}\left(H(\xi;\tilde{a}) - \frac{1}{2}\right)V + V^2, \end{aligned} \tag{7.40}$$

with the boundary conditions (7.37)

$$\lim_{\xi\to\pm\infty} V(\xi) = 0, \tag{7.41}$$

approximated by (7.38) for the numerical calculations,

$$V(-\Omega_L) = V(\Omega_R + 1) = 0. \tag{7.42}$$

Initial guesses $V_G(\xi;\tilde{c})$ and $W_G(\xi;\tilde{c})$ are defined to solve for the solutions $V(\xi;\tilde{c})$ and $W(\xi;\tilde{c})$ respectively. Initial guesses for the standing wave solution at $\tilde{c} = 0$ are defined using the stationary solution $\tilde{U}(\tilde{x})$ to the IBVP (7.18)–(7.21), (7.23) found in Section 7.2.1.1,

$$V_G(\xi;\tilde{c}=0) = \tilde{U}(\tilde{x}), \tag{7.43}$$

and its derivative

$$W_G(\xi;\tilde{c}=0) = \frac{d}{d\tilde{x}}\tilde{U}(\tilde{x}). \tag{7.44}$$

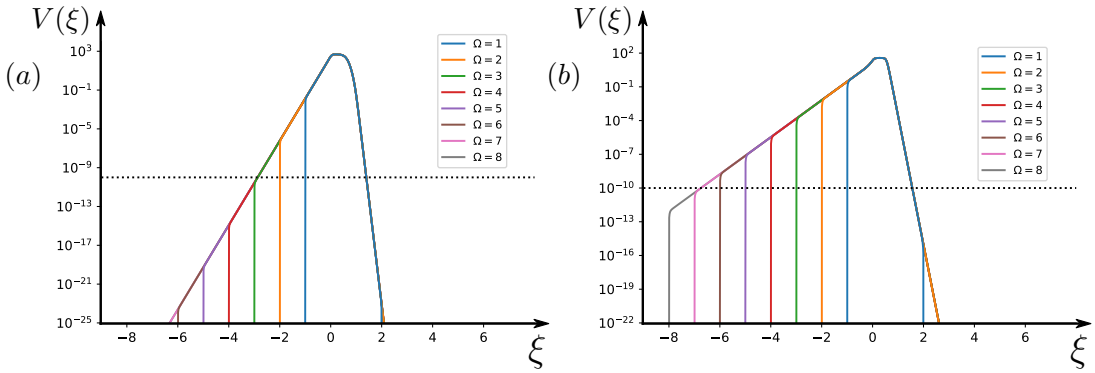


Figure 7.3: Solutions to (a) the BVP (7.40)–(7.42) for $\tilde{c} = 40$ using initial guess $V_G(\xi; \tilde{c}_j)$ from (7.46) and (b) the BVP (7.49)–(7.51) for $\tilde{c} = 22.599$ using initial guess $V_{G_S}(\xi; \tilde{c}_j)$ from (7.52), computed using collocation and plotted logarithmically for various values of Ω. The dotted black line represents the threshold of $\varepsilon = 10^{-10}$ below which the value of $V(\xi)$ can jump to zero. The remaining parameters are set at $\tilde{\alpha} = 1000$, $\tilde{\beta} = 10$, $\tilde{a} = 12$, and $\kappa = 0.005$.

The speed $\tilde{c}$ is then arbitrarily discretised

$$\tilde{c} = \tilde{c}_j \, (j = 0, 1, 2, ...), \tag{7.45}$$

with $\tilde{c}_0 = 0$, and an iterative process is created whereby every subsequent initial guess $V_G(\xi; \tilde{c}_j)$ is dependent on the solution $V(\xi; \tilde{c}_{j-1})$ found with the previous initial guess

$$V_G(\xi; \tilde{c}_j) = V(\xi; \tilde{c}_{j-1}), \tag{7.46}$$

for $j = 1, 2, 3, ...$, and again with $W_G(\xi; \tilde{c}_i)$

$$W_G(\xi; \tilde{c}_j) = W(\xi; \tilde{c}_{j-1}), \tag{7.47}$$

for $j = 1, 2, 3, ...$, until the critical speed $\tilde{c}_{crit}$ is reached and non-zero solutions can no longer be found.

For the purposes of plotting, a fixed value of $\Omega = \Omega_L = \Omega_R$ is considered and SciPy's "solve_bvp" function is used to solve the BVP (7.40)–(7.42) using stepsize $\kappa = 0.005$, a speed of $\tilde{c} = 40$, and the initial guesses $V_G(\xi; \tilde{c})$, $W_G(\xi; \tilde{c})$ for a range of values of Ω.

Solutions are plotted logarithmically in Figure 7.3(a) using a value of $\tilde{c} = 40$ near the Logistic Model's critical speed $\tilde{c}_{crit} = 44.1370$. The right side of the solutions clearly fall below the threshold $\varepsilon = 10^{-10}$ regardless of the value of $\Omega \geq 1$. Therefore, the optimal value for Ω_R is chosen where the right side of the solution is instead at its most diffuse, i.e. at $\tilde{c} = 0$ where $\tilde{B} = 2$ and thus

$\Omega_R = \tilde{B} = 2$. The left side of the solutions naturally fall below the threshold if $\Omega_L \gtrsim 3$ near the critical speed. A safe integer value of $\Omega_L = 4$ is therefore chosen for all speeds in the Logistic Model.

7.2.2.2 The Allee Model

For the Allee Model the ODE (7.36) becomes (6.26)

$$\frac{d^2V}{d\xi^2} + \tilde{c}\,\frac{dV}{d\xi} - \tilde{\beta}^2 V + 4\tilde{\beta}\,H(\xi;\tilde{a})\,V^2 - V^3 = 0, \tag{7.48}$$

which, to be solved in Python, must once again be expressed as an equivalent system of first-order coupled ODEs,

$$\begin{aligned} \frac{dV}{d\xi} &= W, \\ \frac{dW}{d\xi} &= -\tilde{c}\,W + \tilde{\beta}^2 V - 4\tilde{\beta}\,H(\xi;\tilde{a})\,V^2 + V^3, \end{aligned} \tag{7.49}$$

with the boundary conditions (7.37)

$$\lim_{\xi\to\pm\infty} V(\xi) = 0, \tag{7.50}$$

approximated by (7.38) for the numerical calculations,

$$V(-\Omega_L) = V(\Omega_R + 1) = 0. \tag{7.51}$$

The same method used in Section 7.2.2.1 is employed for both non-zero solutions in the Allee Model. The initial guesses $V_{G_U}(\xi;\tilde{c}_j)$,$V_{G_S}(\xi;\tilde{c}_j)$, and $W_{G_U}(\xi;\tilde{c}_j)$, $W_{G_S}(\xi;\tilde{c}_j)$ are defined to find the solutions $V_U(\xi;\tilde{c}_j)$,$V_S(\xi;\tilde{c}_j)$, and $W_U(\xi;\tilde{c}_j)$, $W_S(\xi;\tilde{c}_j)$ respectively using the solutions of the previous iteration in j:

$$\begin{aligned} V_{G_U}(\xi;\tilde{c}_j) = V_U(\xi;\tilde{c}_{j-1}), \quad W_{G_U}(\xi;\tilde{c}_j) = W_U(\xi;\tilde{c}_{j-1}), \\ V_{G_S}(\xi;\tilde{c}_j) = V_S(\xi;\tilde{c}_{j-1}), \quad W_{G_S}(\xi;\tilde{c}_j) = W_S(\xi;\tilde{c}_{j-1}), \end{aligned} \tag{7.52}$$

with $V_{G_U}(\xi;\tilde{c}_0 = 0) = \tilde{U}_{1U}(\tilde{x})$ from the BVP (7.30)–(7.31) etc..

To calculate a suitable value for Ω_L and Ω_R in the Allee Model, SciPy's "solve_bvp" function is used once again to solve the BVP (7.49)–(7.51) using stepsize $\kappa = 0.005$, a speed of $\tilde{c} = 22.5995$, and the initial guesses $V_{G_U}(\xi;\tilde{c})$,$V_{G_S}(\xi;\tilde{c})$, and $W_{G_U}(\xi;\tilde{c})$, $W_{G_S}(\xi;\tilde{c})$ for a range of values of

$\Omega = \Omega_L = \Omega_R$.

Solutions are plotted logarithmically in Figure 7.3(b) using a value of $\tilde{c} = 22.599$ near the Allee Model's critical speed $\tilde{c}_{crit} = 22.5995$. The optimal value of Ω_R is selected once again as the equivalent value at $\tilde{c} = 0$ in the Allee Model: $\Omega_R = \tilde{B} = 3$. The left side of the solutions naturally fall below the threshold $V = 10^{-10}$ if $\Omega_L \gtrsim 7$ near the critical speed. A safe integer value of $\Omega_L = 8$ is therefore chosen for all speeds.

7.3 Stability Analysis of Solutions

7.3.1 Time Evolution and Stability Analysis of Stationary Solutions

7.3.1.1 The Logistic Model

No analytical stability analysis was performed on the stationary solutions to the IBVP (7.1)–(7.3) but the results of the MOL (7.18)–(7.21) in Section 7.2.1.1 are used to study the time evolution of the time-dependent solutions to (7.1)–(7.3) and analyse the stability of its stationary solutions numerically. The MOL numerical integration initiated near each stationary solution is used to obtain long-term solutions which correspond to stable stationary solutions. Stationary solutions that are not detected using the MOL are classified as unstable.

7.3.1.2 The Allee Model

No analytical stability analysis was performed on the stationary solutions to the IBVP (7.24)–(7.26) but the approach taken in Section 7.2.1.1 with the MOL (using the value of $\tilde{B} = 3$ found in Section 7.2.1.2) and the methodology from Section 7.3.1.1 can be repeated for the Allee Model to study the time evolution of the time-dependent solutions of (7.24)–(7.26) and analyse the stability of its stationary solutions numerically.

7.3.2 Stability Analysis of Travelling Pulses

No analytical stability analysis can be performed on the travelling pulse solutions as before but the MOL can again be used to analyse the stability numerically.

Table 7.1: Upper: Numerical parameter values for both models.
Middle: Numerical parameters for the Logistic Model alone.
Lower: Numerical parameters for the Allee Model alone.

Symbol	Description	Inserted value
k	Spatial stepsize	0.005
κ	Spatio-temporal stepsize	0.005
	Logistic Model	
$\tilde{B}$	$\Delta\tilde{x}$ from static habitat to domain boundary	2.0
Ω_L	$\Delta\xi$ from moving habitat to left domain boundary	4.0
Ω_R	$\Delta\xi$ from moving habitat to right domain boundary	2.0
	Allee Model	
$\tilde{B}$	$\Delta\tilde{x}$ from static habitat to domain boundary	3.0
Ω_L	$\Delta\xi$ from moving habitat to left domain boundary	8.0
Ω_R	$\Delta\xi$ from moving habitat to right domain boundary	3.0

The RCDE is reintroduced (5.8)

$$\frac{\partial V}{\partial s} = \frac{\partial^2 V}{\partial \xi^2} + \tilde{c}\,\frac{\partial V}{\partial \xi} + \tilde{f}(V, \xi), \tag{7.53}$$

with initial condition (5.9)

$$V(\xi, 0) = V_0(\xi), \tag{7.54}$$

and Dirichlet boundary conditions (5.10)

$$\lim_{\xi \to \pm\infty} V(\xi, s) = 0. \tag{7.55}$$

The MOL is used once again as in Section 7.2.1.1 for both models except instead of the spatial increment a fixed spatio-temporal increment is utilised

$$\kappa = \Delta\xi, \tag{7.56}$$

and the central difference approximation for $\tilde{U}_{\tilde{x}}$ in (7.9) is translated for V_ξ

$$\frac{\partial V}{\partial \xi} = \frac{1}{2\kappa}\Big(V(\xi + \kappa) - V(\xi - \kappa)\Big) + O(\kappa^2). \tag{7.57}$$

along with the central difference approximation $\tilde{U}_{\tilde{x}\tilde{x}}$ from (7.11). ξ is discretised as follows

$$\xi_i = i\kappa - \Omega_L \quad (i = 0, 1, 2, ...N), \tag{7.58}$$

and the full set of N-1 IVPs approximating the IBVP (7.53)–(7.55) become:

for $i = 1$

$$\frac{dV_i}{ds} = \frac{V_{i+1} - 2V_i}{\kappa^2} + \tilde{c}\,\frac{V_{i+1}}{2\kappa} + \tilde{f}(V_i(s), \xi_i), \tag{7.59}$$

for $i = N-1$

$$\frac{dV_i}{ds} = \frac{-2V_i + V_{i-1}}{\kappa^2} - \tilde{c}\,\frac{V_{i-1}}{2\kappa} + \tilde{f}(V_i(s), \xi_i), \tag{7.60}$$

and for $i = 2, 3, ..., N-2$

$$\frac{dV_i}{ds} = \frac{V_{i+1} - 2V_i + V_{i-1}}{\kappa^2} + \tilde{c}\,\frac{V_{i+1} - V_{i-1}}{2\kappa} + \tilde{f}(V_i(s), \xi_i), \tag{7.61}$$

with initial condition

$$V_i(0) = V_{i\,0} = V_0(\xi_i), \tag{7.62}$$

defined in the form of a rectangular function once again with a constant v

$$V_{i\,0} = V_0(\xi_i) = \begin{cases} 0 & \xi_i < -1 \text{ and } \xi_i > 2 \\ v & -1 \leq \xi_i \leq 2. \end{cases} \tag{7.63}$$

Chapter 8

Conclusion

This research project sought to investigate the behaviour and persistence of a species in a drifting habitat when pushed to its limits. This work was primarily motivated by the symbiotic forces of earth's climate and biodiversity crises. The shifting isotherms of climate change are forcing ecosystems to move to climates more suited to their thermal niches and many species are struggling to keep pace with and adapt to these shifts [21]. How would the population growth of a species be affected by this change in environment? To address this question a combination of numerical and bifurcation analysis was used to study travelling pulse solutions of nonlinear non-autonomous one-dimensional reaction-diffusion equations (RDEs) representing the population dynamics and migration of this species in a moving habitat for two population models: our Logistic Model and our Allee Model.

This thesis began with the review of a paper by Berestycki et al. [3], which described the dynamics of a single species in an optimal static habitat with an RDE, and defined the location of the species's habitat using the discontinuities in a piecewise growth model. This model comprised of a logistic growth function in the "good habitat" and a linear death function outside of it in the "bad habitat". This paper, and other previously published work on the topic of a species in a moving habitat [2, 4], have been restricted by their use of just one discontinuous monostable population model based primarily on logistic growth. In this project, however, a smooth habitat function was constructed and added to the population models, which allowed the boundaries between the good and bad habitats to be defined using bifurcations of equilibria for two distinct growth models. A smooth monostable Logistic Model (2.19) was initially introduced,

and a further step was taken by incorporating the Allee effect into the Logistic Model to create the smooth bistable Allee Model (2.32). This allowed two robust models to be compared and contrasted throughout the thesis.

In the static habitat, an initial-boundary value problem (IBVP) consisting of an RDE with initial and boundary conditions was defined for each model. Direct numerical integration was used for the Logistic Model to find its stable stationary solution. An alternative approach was taken to compute both stable and unstable non-zero stationary solutions of the Allee Model. This was achieved by setting the time derivative in its IBVP to zero, and working instead with a boundary value problem (BVP). This method was used to find the stable stationary solution as well as an unstable stationary solution, which gave a crucial insight into the dynamics of the population for the Allee Model once its habitat begins to drift.

A co-moving frame transformation allowed the moving habitat to be studied more easily. To find travelling pulse solutions in each model, their IBVPs (consisting now of reaction-convection-diffusion equations (RCDEs), and initial and boundary conditions) were once again converted into BVPs and solved for stationary solutions of the co-moving frame, which translate to travelling pulse solutions in the original frame. These travelling pulses were computed for both models up to their respective critical speeds, where bifurcations occur.

For the Logistic Model, the critical speed was found at a transcritical bifurcation (shown in Figure 6.5), which corresponds to the point at which the stable travelling pulse solution collides with the unstable zero solution. For the Allee Model, the critical speed was found at a saddle-node bifurcation (shown in Figure 6.10), where the unstable travelling pulse rises up to collide with the stable pulse as the habitat speed increases, as illustrated in Figure 6.6. The models' non-autonomous bifurcation points are in fact R-tipping points as the rate at which the habitat changes location causes a collapse for the population contained within from a non-zero stable state to the stable extinction state. This result contributes to the limited literature on R-tipping points in partial differential equations, while providing crucial real-world information.

The R-tipping point of the Logistic Model can always be reversed. In ecological terms, this means that a species in a moving habitat with population dynamics following that of the Logistic Model could come close to extinction at a speed greater than its critical speed but would always come back from the brink of collapse if its habitat speed is reduced below the critical speed again. This could

occur in nature if, for example, a habitat shifting in latitude on flat land approached a steady incline, which would force a slower shift than on flat ground to satisfy the colder thermal niche requirements of the species due to its increased elevation. It is also theoretically possible to reverse the R-tipping in the Allee Model. However, this would require a very quick reversal in speed below its critical speed to return to the basin of attraction of the non-zero stable state. Typically, R-tipping will not be reversed under decreasing habitat speed in the Allee Model and the system will remain in the basin of attraction of the extinction state if its critical rate is exceeded. Ecologically, this implies that a species in a habitat following the Allee Model would likely be doomed to extirpation once its critical speed was exceeded.

The length of the habitat L, slope of the habitat a, and the diffusion D were kept constant throughout this project for both models. This project could be extended to find a critical length and create a two-parameter bifurcation diagram along with the critical speed for different combinations of values of the habitat slope and diffusion. This may give a more complete picture of the tipping in the Allee Model, for example. It is also expected that if c is fixed and L is decreased the same transcritical bifurcation shown in Section 6.1.4 would occur for the Logistic Model. Due to the systems of both models being non-autonomous, there were no equilibria present in the phase portraits of the comoving frame ODEs shown in Figure 6.2 and Figure 6.7. There would therefore also be further research possibilities in the compactification of the spatio-temporal domain, and the study of these travelling pulse solutions as heteroclinic orbits in phase space of the compactified co-moving ODE. A nonlinear drift term $g(ct)$, such as a periodic forcing function to represent the seasonal variations in climate change-induced drift, could also be substituted in place of ct from the beginning in (2.1). The introduction of a second species, such as a predator, to study inter-species dynamics and coexistence in a moving habitat, is another interesting question for future research.

Chapter 9

Appendix

9.1 Code

A few example snippets of code are presented from both Python and Mathematica.

9.1.1 Python Code

Preamble of libraries and functions.

```
%matplotlib inline
import numpy as np
import sympy as sym
import matplotlib.pyplot as plt
from scipy.integrate import solve_bvp
from scipy.integrate import solve_ivp
```

Parameter preamble from Table 3.2.

```
a0 = 6
be0 = 0.5
D = 0.02
ga = 1
L = 2


be = L * (be0 / D)**0.5
a = a0 * L
```

9.1.1.1 Collocation Code for the Allee Model in the Static Habitat

Defining the ODE (7.30) for the "solve_bvp" function.

```
def AlleeBVP(x, U):
    return np.vstack((U[1], be**2 * U[0] \
    - 4*be*((np.tanh(a*(x))-np.tanh(a*(x-1))) \
    / (2*np.tanh(a))) * U[0]**2 + U[0]**3))
```

Defining the boundary conditions (7.31) for the "solve_bvp" function.

```
def BC(Ua,Ub):
    return np.array([Ua[0],Ub[0]])
```

Defining the Allee Model's non-zero equilibria (4.8).

```
def equilibria(x, a, be):

    H = (np.tanh(a*x) - np.tanh(a*(x-1))) / (2*np.tanh(a))

    if(4*H**2 - 1 >= 0):
        ue2 = be * ( 2*H - np.sqrt(4*H**2 - 1) )
        ue3 = be * ( 2*H + np.sqrt(4*H**2 - 1) )
    else:
        ue2=0
        ue3=0

    return ue2,ue3
```

Defining the numerical parameters from Table 7.1, the spatial domain, and the initial guesses for the static Allee Model (7.32)–(7.35).

```
B,k = 3,0.005
x = np.arange(-B,B+1+k/2,k)

U_2 = np.zeros((2, x.size))
U_3 = np.zeros((2, x.size))

Ue_2 = equilibria(0.5,a,be)[0]
Ue_3 = equilibria(0.5,a,be)[1]

for i in range(x.size):
```

```
    if(x[i]>=-1 and x[i]<=2):
        U_2[0,i] = Ue_2*1.5*np.exp(-(x[i]-0.5)**2/(2*D))
        U_2[1,i] = Ue_2*1.5*(0.5 - x[i])/D \
        * np.exp(-(x[i]-0.5)**2/(2*D))
    else:
        U_2[0,i] = 0
        U_2[1,i] = 0

for i in range(x.size):
    if(x[i]>=0 and x[i]<=1):
        U_3[0,i] = Ue_3
    else:
        U_3[0,i] = 0
```

Executing the "solve_bvp" function to the two non-trivial numerical solutions to the static habitat Allee Model BVP (4.15)–(4.16).

```
res_2 = solve_bvp(AlleeBVP, BC, x, U_2, max_nodes=100000)
res_3 = solve_bvp(AlleeBVP, BC, x, U_3, max_nodes=100000)
```

9.1.1.2 MOL Code for the Allee Model in the Static Habitat

Defining the initial solution (7.23) for any value of $\tilde{u}$.

```
def initsol(x,u):
    x = np.round(x,5)
    U = np.zeros(x.size)
    for i in range(x.size):
        if(x[i]<-1 or x[i]>2):
            U[i] = 0
        elif(x[i]>=-1 and x[i]<=2):
            U[i] = u
        else:
            print("error")
    return U
```

Defining the system of ODEs (7.18)–(7.20) converted to the Allee Model, with `x.size` $= N+1$.

```
def AlleeIVP(t, u, x):
```

```
    dudt = np.zeros(x.size)
    k = x[1]-x[0]

    for i in range(1,x.size-1):
        if(i==1):
            dudt[i] = (u[i+1] - 2*u[i]) / k**2 \
            - be**2 * u[i] + 4*be*( (np.tanh(a*x[i]) \
            - np.tanh(a*(x[i]-1))) / (2*np.tanh(a)) ) * u[i]**2 \
            - u[i]**3
        elif(i==x.size-2):
            dudt[i] = (-2*u[i] + u[i-1]) / k**2 \
            - be**2 * u[i] + 4*be*( (np.tanh(a*x[i]) \
            - np.tanh(a*(x[i]-1))) / (2*np.tanh(a)) ) * u[i]**2 \
            - u[i]**3
        else:
            dudt[i] = (u[i+1] - 2*u[i] + u[i-1]) / k**2 \
            - be**2 * u[i] + 4*be*( (np.tanh(a*x[i]) \
            - np.tanh(a*(x[i]-1))) / (2*np.tanh(a)) ) * u[i]**2 \
            - u[i]**3

    return dudt
```

Defining the numerical parameters from Table 7.1, the spatial domain, the timeframe `tint`, and the initial conditions.

```
B,k = 3,0.005
x = np.arange(-B,B+1+k/2,k)
tint = (0,1)

u0a = initsol(x,3)
u0b = initsol(x,2)
```

Executing the "solve_ivp" function to find numerical solutions to the static habitat Allee Model IBVP (4.3)–(4.5), representing the time evolution of the population in the habitat, using the BDF method.

```
allivp_a = solve_ivp(AlleeIVP,tint,u0a, args=(x,),method='BDF')
allivp_b = solve_ivp(AlleeIVP,tint,u0b, args=(x,),method='BDF')
```

9.1.2 Mathematica Code

9.1.2.1 MOL Code for the Allee Model in the Moving Habitat

Defining the differential equation (7.53).

```
dVds = D[V[xi, s], {xi, 2}] + c*D[V[xi, s], xi] - be^2*V[xi, s] +
   4*be*(Tanh[a*xi] - Tanh[a*(xi - 1)])/(2 Tanh[a])*V[xi, s]^2 -
   V[xi, s]^3;
```

Defining the initial solution (7.63) for any value of v and the finite boundary conditions (7.51).

```
initsol = V[xi, 0] == v*(UnitStep[1 + xi] + UnitStep[2 - xi] - 1);
bc = {V[OmL, s] == 0, V[OmR+1, s] == 0};
```

Subbing in Allee Model parameter values from Table 3.2, numerical parameter values from Table 7.1, a speed of $\tilde{c} = 22.599$ and $v = 5$.

```
sub = {v -> 5, c -> 22599/1000, be -> 10, a -> 12, OmL -> -8,
  OmR -> 3}; cth = N[c /. sub, 8];
```

Executing the "NDSolve" function from $s = 0$ to $s = 1000$ to analyse the stability of the non-trivial stationary solutions of the co-moving frame Allee Model IBVP (6.21)–(6.23) (i.e. the travelling wave solutions of the IBVP (6.2)–(6.4)) near the critical speed $\tilde{c}_{crit} = 22.5995$ using the BDF method.

```
pde = {D[V[xi, s], s] == dVds /. sub, initsol /. sub, bc /. sub};
OmLeft = OmL /. sub;
OmRight = OmR /. sub;
(* ,PrecisionGoal\[Rule]\[Infinity] *)
pdesol = V /.
  NDSolve[pde, V, {xi, OmLeft, OmRight+1}, {s, 0, 1000},
    Method -> "BDF"][[1, 1]]
```

References

[1] IPCC AR5 WGII (2014) Synthesis Report. Climate Change 2014: Impacts, Adaption and Vulnerability (Report).

[2] Potapov, A. B., Lewis, M. A., 2004. Climate and Competition: The Effect of Moving Range Boundaries on Habitat Invasibility. *Bull. Math. Bio. 66, 975*

[3] Berestycki, H., Diekmann, O., Nagelkerke, C. J., Zegeling, P. A., 2009. Can a Species Keep Pace with a Shifting Climate?. *Bull. Math. Bio. 71, 399*

[4] MacDonald, J. S., Lutscher, F., 2018. Individual Behavior at Habitat Edges May Help Populations Persist in Moving Habitats. *J. Math. Biol. 77, 2049*

[5] Hoegh-Guldberg, O., Poloczanska, E. S., Skirving, W., Dove, S., 2017. Coral Reef Ecosystems under Climate Change and Ocean Acidification. *Front. Mar. Sci. 4, 158*

[6] Thomas, C. D, Cameron, A., Green, R. E., et al., 2004. Extinction risk from climate change. *Nature 427, 145*

[7] Sala, O. E., Chapin, F. S., Armesto, J. J., et al., 2000. Global Biodiversity Scenarios for the Year 2100. *Science 287 (5459), 1770*

[8] Pounds, J., Fogden, M., Campbell, J., et al., 1999. Biological response to climate change on a tropical mountain. *Nature 398, 611*

[9] Williams, S. E, Bolitho, E. E., Fox, S., 2003. Climate change in Australian tropical rainforests: an impending environmental catastrophe. *Proc. R. Soc. Lond. B 270, 1887*

[10] Pecl, G. T., Araújo, M. B., Bell, J. D., et al., 2012. Biodiversity redistribution under climate change: Impacts on ecosystems and human well-being. *Science 355 (6332), 1*

[11] Sahney, S., Benton, M. J., Ferry, P. A., 2010. Links between global taxonomic diversity, ecological diversity and the expansion of vertebrates on land. *Biol. Lett. 6, 544*

[12] Parmesan, C., Ryrholm, N., Stefanescu, C., et al., 1999. Poleward shifts in geographical ranges of butterfly species associated with regional warming. *Nature 399, 579*

[13] Walther, G. -R., Post, E., Convey, P., et al., 2002. Ecological responses to recent climate change. *Nature 416, 389*

[14] Chen, I. -C., Hill, J. K., Ohlemüller, R., et al., 2011. Rapid Range Shifts of Species Associated with High Levels of Climate Warming. *Science 333, 1024*

[15] Burrows, M. T., et al., 2011. The pace of shifting climate in marine and terrestrial ecosystems. *Science 334, 652*

[16] Pinsky, M. L., Worm, B., Fogarty, M. J., et al., 2013. Marine Taxa Track Local Climate Velocities. *Science 341, 1239*

[17] Poloczanska, E. S., Brown, C. J., Sydeman, W. J., et al., 2013. Global imprint of climate change on marine life. *Nat. Clim. Chang. 3, 919*

[18] Lenoir, J., Svenning, J. -C., 2015. Climate-related range shifts – a global multidimensional synthesis and new research directions. *Ecography 38, 15*

[19] Schloss, C. A., Nuñez, T. A., Lawler, J. J., 2012. Dispersal will limit ability of mammals to track climate change in the Western Hemisphere. *PNAS 109, 8606*

[20] Parmesan, C., Yohe, G., 2003. A globally coherent fingerprint of climate change impacts across natural systems. *Nature 421, 37*

[21] Lenoir, J., Bertrand, R., Comte, L., et al., 2020. Species better track climate warming in the oceans than on land. *Nat. Ecol. Evol. 4, 1044*

[22] Ashwin, P., Wieczorek, S., Vitolo, R., Cox, P., 2012. Tipping points in open systems: bifurcation, noise-induced and rate-dependent examples in the climate system. *Phil. Trans. R. Soc. A 370, 1166*

[23] Thompson, J. M. T., Stewart, H., Ueda, Y., 1994. Safe, explosive, and dangerous bifurcations in dissipative dynamical systems. *Phys. Rev. E. 49, 1019*

J. M. T. Thompson, H. Stewart, and Y. Ueda, Safe, explosive, and dangerous bifurcations in dissipative dynamical systems, Phys. Rev. E, 49 (1994), 1019.

[24] O'Keeffe, P., Wieczorek, S., 2020. Tipping Phenomena and Points of No Return in Ecosystems: Beyond Classical Bifurcations. *SIAM J. App. Dyn. Sys. 19, 2371*

[25] Kuehn, C., 2011. A mathematical framework for critical transitions: Bifurcations, fast–slow systems and stochastic dynamics. *Phys. D. 240, 1020*

[26] Scheffer, M., Carpenter, S., Foley, J. A., et al., 2001. Catastrophic shifts in ecosystems. *Nature 413, 591*

[27] Leemans, R., Eickhout, B., 2004. Another reason for concern: Regional and global impacts on ecosystems for different levels of climate change. *Global Environmental Change 14, 219*

[28] Siteur, K., Eppinga, M. B., Doelman, A., et al., 2016. Ecosystems off track: rate-induced critical transitions in ecological models. *Oikos 125, 1689*

[29] Wieczorek, S., Ashwin, P., Luke, C. M., Cox, P. M., 2011. Excitability in ramped systems: The compost-bomb instability. *Proc. A. 467, 1243*

[30] Biggs, R., Carpenter, S. R., Brock, W. A., 2009. Turning back from the brink: Detecting an impending regime shift in time to avert it. *PNAS 106, 826*

[31] Strogatz, S. H., 1994. Nonlinear Dynamics and Chaos: Chapter 1. *Perseus Books Publishing, L.L.C., New York*

[32] Krebs, C. J., 1972. Ecology: The Experimental Analysis of Distribution and Abundance. *Harper and Row, New York*

[33] Kramer, A. M., Dennis, B., Liebhold, A. M., Drake, J. M., 2009. The evidence for Allee effects. *Popul. Ecol. Evol. 51, 341*

[34] Courchamp, F., Clutton-Brock, T., Grenfell, B., 1999. Inverse density dependence and the Allee effect. *Trends Ecol. Evol. 14, 406*

[35] Allee, W. C., et al., 1972. Principles of Animal Ecology. *W. B. Saunders Company, Philidelphia and London*

[36] May, R., McLean, A., 1972. Theoretical Ecology (3rd ed.). *Oxford University Press Inc., New York*

[37] Taylor, C. M., Hastings, A., 2005. Allee effects in biological invasions. *Eco. Lett. 8, 895*

[38] Cushing, J. M., Hudson, J. T., 2012. Evolutionary dynamics and strong Allee effects. *J. Biol. Dyn. 6, 941*

[39] Dennis, B., 1989. Allee Effects: Population Growth, Critical Density, and the Chance of Extinction. *Nat. Res. Model. 3, 481*

[40] Volterra, V., 1938. Population growth, equilibria, and extinction under specified breeding condiions: a development and extension of the logistic curve. *Hum. Biol. 3, 1*

[41] Sandstede, B., Scheel, A., 2001. On the Stability of Periodic Travelling Waves with Large Spatial Period. *J. Differen. Equat. 172, 134*

[42] Cornwell, P., Jones, C. K., 2017. On the Existence and Stability of Fast Traveling Waves in a Doubly Diffusive FitzHugh-Nagumo System. *SIAM J. Applied Dynamical Systems 17(1), 754*

[43] Kuehn, C., 2019. PDE Dynamics: An Introduction. *Society for Industrial and Applied Mathematics, Philadelphia*

[44] Roache, P. J., 1972. Computational Fluid Mechanics. *Hermosa, Albuquerque*

[45] Smith, G. D., 1985. Numerical Solution of Partial Differential Equations: Finite Difference Methods. *Oxford University Press Inc., New York*

[46] Crank, J., Nicolson, P., 1947. A practical method for numerical evaluation of solutions of partial differential equations of the heat-conduction type. *Proc. Cambridge Philos. Soc. 43, 50*

[47] SciPy, 2016. scipy.integrate.solve_ivp, SciPy Python function. *https://docs.scipy.org/doc/scipy/reference/generated/scipy.integrate.solve_ivp.html (updated 2020)*

[48] Ascher, U. M., Petzold, L. R., 1998. Computer Methods for Ordinary Differential Equations and Differential-Algebraic Equations. *Society for Industrial and Applied Mathematics, Philadelphia*

[49] Wolfram Research, 1991. NDSolve, Wolfram Language function. *https://reference.wolfram.com/language/ref/NDSolve.html (updated 2019)*

[50] SciPy, 2016. scipy.integrate.solve_bvp, SciPy Python function. *https://docs.scipy.org/doc/scipy/reference/generated/scipy.integrate.solve_bvp.html (updated 2020)*

[51] Kierzenka, J., Shampine, L. F., 2001. A BVP Solver Based on Residual Control and the Maltab PSE. *ACM Trans. Math. Softw. 27, 299*